PERFORMANCE EVALUATION OF GREEN CORROSION INHIBITORS FOR X60 MILD STEEL IN SWEET OILFIELD CONDITIONS

BY

BASHIR JELANI USMAN

A Thesis Presented to the
DEANSHIP OF GRADUATE STUDIES

KING FAHD UNIVERSITY OF PETROLEUM & MINERALS

DHAHRAN, SAUDI ARABIA

In Partial Fulfillment of the
Requirements for the Degree of

MASTER OF SCIENCE

In

MATERIALS SCIENCE AND ENGINEERING

MAY, 2016

KING FAHD UNIVERSITY OF PETROLEUM & MINERALS

DHAHRAN- 31261, SAUDI ARABIA

DEANSHIP OF GRADUATE STUDIES

This thesis, written by [**BASHIR JELANI USMAN**] under the direction his thesis advisor and approved by his thesis committee, has been presented and accepted by the Dean of Graduate Studies, in partial fulfillment of the requirements for the degree of [**MASTER OF SCIENCE IN MATERIALS SCIENCE & ENGINEERING**.

Dr. ZUHAIR M. GASEM
Department Chairman

Dr. [ZUHAIR M. GASEM]
(Advisor)

Dr. Salam A. Zummo
Dean of Graduate Studies

5/29/2016

Dr. [IHSANUL-HAQ TOOR]
(Member)

23/6/16

Date

5/29/2016

Dr. [IME BASSEY OBOT]
(Member)

Dedication

This work is dedicated to Alhaji Jelani Usman (My father), Hajiya Khadijatu Dankoko (My mother), Hajiya Safiyatu Dankoko (Grandmother) and all my family members for their support, caring and prayers.

ACKNOWLEDGMENTS

I wish to first of all acknowledge the Deanship of Graduate Studies, King Fahd University of Petroleum and Minerals for approving my admission and in particular the department of mechanical engineering, for accepting my application into the department. I am very grateful to Saudi Ministry of Higher Education for financial support throughout my stay in Saudi Arabia. The study leave fellowship given by my work organization, Kebbi State University of Science and Technology is also highly appreciated.

My deep appreciation goes to my amiable advisor, Dr. Zuhair M. Gasem who also is the incumbent chairman of mechanical engineering department for supervising this work in spite of his tight schedules. I also wish to acknowledge the support and contribution of my thesis committee members; Dr. Ihsanul-haq Toor and Dr. Ime Bassey Obot. The chief technician of Materials Science Laboratory, Mr. Lateef has also contributed to the progress of this work.

Finally I want to mention the help of my brothers from my country's national organization in the kingdom for their rigorous orientation on how to succeed in KFUPM. In particular, I recognize the assistance of Mohammad Suleiman, Sagir Adamu, Nasiru Ibrahim, to mention but few. Thank you all.

TABLE OF CONTENTS

LIST OF TABLES

LIST OF FIGURES

LIST OF ABBREVIATIONS

AC	:	Alternating Current
AFM	:	Atomic Frequency Modulation
C_R	:	Corrosion Rate
CS	:	Carbon Steel
EDX	:	Energy Dispersive X-ray
EIS	:	Electrochemical Impedance Spectroscopy
FTIR	:	Fourier Transform Infrared spectroscopy
HF	:	Higher Frequency
IE	:	Inhibitor Efficiency
KI	:	Potassium Iodide
LF	:	Lower Frequency
LPR	:	Linear Polarization Measurements
MF	:	Medium Frequency
MS	:	Mild Steel
PDP	:	Potentiodynamic Polarization
RDE	:	Rotating Disc Electrode

Rp	:	Polarization Resistance
SCE	:	Saturated Calomel Electrode
SEM	:	Scanning Electron Microscopy
ST	:	Scaling Tendency
TA	:	Tannic Acid
TBA	:	Thiobarbituric Acid
WL	:	Weight Loss
XPS	:	X – ray Photoelectron Spectroscopy

ABSTRACT

Full Name : [Bashir Jelani Usman]

Thesis Title : [Performance Evaluation of Green Corrosion Inhibitors for X60 Mild Steel in Sweet Oilfield Conditions]

Major Field : [Materials Science and Engineering]

Date of Degree : [May, 2016]

The inhibition performance of 2-Thiobarbituric Acid (TBA) and Tannic Acid (TA) on X60 mild steel in CO_2-saturated 3.5 % NaCl solution was investigated using electrochemical measurements: Linear Polarization Resistance (LPR), Electrochemical Impedance Spectroscopy (EIS) and Potentiodynamic Polarization (PDP). The effects of concentration, pH, temperature and duration of immersion were investigated. Surface characterization techniques: Scanning Electron Microscopy (SEM), X-ray Photoelectron Spectroscopy (XPS) and Fourier Transformation Infrared (FTIR) spectroscopy were employed to examine the mechanism of the inhibition. TBA exhibited excellent inhibition beyond 90 % efficiencies in all experimental conditions studied. The excellent inhibition behavior of TBA persisted even after long immersion time of three days. Tannic acid, on the other hand, was more efficient at higher concentration and the inhibition efficiency increased with immersion time. The addition of Potassium Iodide (KI) has synergistically improved TA inhibition effect. However, TA inhibition efficiency decreased at higher temperatures. Both inhibitors obeyed Langmuir adsorption isotherm. EIS results have shown that the thickness of the double layer increased as a result of adsorption of the inhibitors. Thermodynamics analysis have shown that the compounds adsorbed on the steel surface

by both physical and chemical adsorption modes. This was further confirmed by surface analysis using FTIR and XPS.

ملخص الرسالة

الاسم الكامل: بشير جيلاني عثمان

عنوان الرسالة: تقييم أداء مثبطات التآكل الخضراء للفولاذ الطري (X60) في الظروف البيئية لحقول النفط الحلوة

التخصص: هندسة وعلوم المواد

تاريخ الدرجة العلمية: أيار من عام 2016

تم دراسة حمض الثيوباربيتريك (2-Thiobarbituric Acid) وحمض التانيك (Tannic Acid) كمثبطات لتآكل الفولاذ الطري في محلول ملحي مشبع بغاز ثاني أكسيد الكربون وذلك باستخدام الطرق الكهروكيميائية: مقاومة الاستقطاب الخطي (Linear Polarization Resistance) والاستقطاب الطيفي (Electrochemical Impedance Spectroscopy) و الجهد الديناميكي (Potentiodynamic Polarization) تحت تأثيرمتغيرات تركيز المثبط ، مستوى الحموضة ، درجة الحرارة ، ووقت الغمر. كما تم توظيف أدوات توصيف السطح مثل المجهر الإلكتروني الماسح والأشعة السينية الضوئية الطيفي وتحويل فوريه الطيفي بالأشعة تحت الحمراء للتحقق من آلية التثبيط. كانت كفاءة الثبيط لحمض الثيوباربيتريك أعلى من 90% في جميع الظروف الإختبارية ، كما تم الحفاظ على مستوى أداء المثبط بشكل ممتاز حتى بعد تعرض الفولاذ لفترة طويلة تصل إلى ثلاثة أيام. وتشير قياسات الاستقطاب عند الجهد الديناميكي أن المثبط يعمل أساساً من نوع المثبطات المختلطة. كان حمض التانيك في المقابل ذو فعالية أكبر عند ارتفاع تركيز المثبط ومع زيادة وقت الغمر. إضافة يوديد البوتاسيوم كان قد حسّن من أداء حمض التانيك كمثبط ، لكن أنخفضت الكفاءة مع إرتفاع درجة الحرارة. المثبطان كلاهما متوافقان مع لانجميرأيزوثيرم للإدمصاص. كما اظهرت النتائج أن سماكة الطبقة المزدوجة زادت نتيجة امتصاص المثبطات. وقد أظهرت دراسة الديناميكا الحرارية للتآكل أن إمتصاص المثبطات على سطح الفولاذ يكون بطريقة فيزيائية بالإضافة إلى الادمصاص.

CHAPTER 1

INTRODUCTION

About 60% of all global energy demands is oil and natural gas [1]. In spite of the current need for other alternative sources, it is anticipated to remain for many years the major source of energy [2]. Mild steel even though has low resistance to corrosion, is immensely used in oil and gas industries mainly because of its availability, strength and cost effectiveness [3]. The role of mild steel in this environment is to transport gases and liquids through pipelines from their sources to the consumers over a long distance[4]. These liquids and gases are often inherently combined with impurities like CO_2, hydrogen sulfide (H_2S), water, nitrogen, oxygen and trace elements[4] which can cause severe corrosion problems to the pipelines [5]. Risers transport oil and natural gas together with the impurities from downhole to wellhead platforms. These fluids are then transported by flowlines from the wellhead platform to central gathering platforms (or treatment platform) where oil and gas from different wells are mixed and treated. After treatment which merely involves separation of the mixtures with separators, the oil and gas are conveyed in pipelines separately to treatment facilities, storage facilities and refining plants. Small percentage (0.5-2%) of water is yet unavoidable even after the separation. In addition to its natural existence, it becomes a normal practice recently the technique of injecting back the formation water (and sometimes seawater or fresh water and CO_2) into the downhole to maintain or increase the pressure and stability of the reservoir for better oilfield recovery of deep reservoirs [6,7]. This leads to the growing quantity of CO_2 and produced water up to 95% water/oil or higher as field ages. The increase in CO_2 and water content results in the rise in corrosion problems [7].

As noted from above, corrosion problems in oil and gas can occur at every stage of production starting from the initial extraction, treatment to storage [1,8]. Internal corrosion of steel pipelines and flowlines is one of the serious problems caused by the produced water. The dangers of internal corrosion include; loss of production as a result of pipeline failure, and consequently plant shutdown and probably environmental disaster[9]. Crude oil may leak as a result of CO_2 corrosion and cause environmental and water pollution or even fire accidents [10]. The most prevalent form of corrosion found in oilfield are those caused by CO_2 (sweet) corrosion and H_2S (sour) corrosion in the produced water and corrosion caused by oxygen dissolved in the formation water [8,11, 12].

CO_2 corrosion, first reported in early 1940s has been a long-standing challenge in the oil and gas production and transportation [13]. It is considered to be the most potential and predominant type of attack encountered in oil and gas industries [7,11,14–17]. In addition to general corrosion, it causes a localized corrosion which is difficult to detect, predict and protect [7]. About 60% of the failures in oilfields are related to corrosion and majority of these problems are due to CO_2 corrosion mainly because of insufficient knowledge or inability to predict it and to low resistance of mild steel to the corrosion [7,11,18]. Investigations have shown that up to 10-30% of maintenance budget is linked to the oil refining plants and corrosion of natural gas sweetening (CO_2 corrosion) [19].

Despite its limited corrosion resistance to the environment in which it is used, mild steel is often used in oil and gas pipelines due mainly to its availability, strength and cost effectiveness [20,21]. Among the different methods [22,23] available to combat the problems arising from CO_2 corrosion, the use of corrosion inhibitors appears to be the most practical and economically wise [1,7,22,23,26,27]. Application of suitable corrosion

inhibitor incorporated with lower grade steels is of better capital economy in comparison to the use of expensive high grade alloys in the same condition [28].

Organic compounds are mostly in use today having replaced the previously used toxic inorganic chemicals like chromates, arsenates, nitrates etc [29]. Organic inhibitors typically, are heterocyclic with structures that contain pi-electrons and electronegative heteroatoms like Nitrogen (N_2), Oxygen (O) and Sulphur (S) which adsorb on the surface of the steel substrates. Unfortunately, most of these synthetic compounds are environmentally hazardous [30,31]. In the last two decades, the approach towards selection of inhibitors changed to using compounds that have low environmental risks because of the world increased consciousness towards environmental problems and need to protect the environment against hazardous chemicals, [26,30-32].

The aim of this work is to assess 'green' corrosion inhibitors with good inhibition efficiency and above all environmentally compatible. To achieve this objective, the interest is in naturally occurring biological compounds that are biodegradable and do not contain heavy metals or other toxic species. The work seeks to investigate the performance of tannic and 2-thiobarbituric acids as corrosion inhibitors in CO_2-environment.

CHAPTER 2

LITERATURE REVIEW

2.1. Mechanism of CO_2 Corrosion

The underlying mechanism of CO_2 corrosion is complex as it is affected by a number of factors including physical, environmental and metallurgical parameters [33]. As a result of chemical and electrochemical processes, the corrosion product which is mainly *iron carbonate layer/film ($FeCO_3$)* is precipitated on the metal surface (because of its low solubility k_{sp} = 10.54 at 25^0C) [34]. This layer also known as Siderite or Chalbyte [35] protects the metal from further corrosion. This reaction is favored at higher temperature, pH and CO_2 partial pressure among other factors. Apart from the $FeCO_3$, this corrosion product may also contains cementite (Fe_3C) and alloying elements [11]. This film protects the metal from further attack and therefore its formation or depletion determines the corrosion rate[17,36,37]. The protectiveness of this surface layer which determines the corrosion rate depends on the environment and the metal (microstructure and composition) [7, 37–39]. Therefore the characteristics of the film and its effect on the corrosion rate are very useful factors to be considered when studying the corrosion of steel in CO_2 aqueous solution[7].

Dry CO_2 is not itself corrosive to mild steel pipeline however, in the presence of produced brine-water, CO_2 dissolves in the water to give aqueous carbonic acid (H_2CO_3) which promotes the rate of corrosion of steel by enhancing the reaction rate of hydrogen evolution. Carbonic acid is a weak type of acid and does not completely dissociate in water. It was established experimentally that at a given pH, the acid causes higher corrosion rate

than strong acids like hydrochloric acid (HCl) and sulfuric acid (H_2SO_4) which dissociate in water completely. This is because, in strong acids, the rate at which hydrogen is evolved cannot exceed the rate of transfer of H^+ from the bulk of the solution to the metal surface. However, when solutions pH > 4, the mass transfer of H^+ from bulk of the solution to the metal surface is small and therefore the presence of H_2CO_3 causes hydrogen evolution at a much faster rate [40].

The chemical reactions involved are the dissolution of CO_2 to produce carbonic acid (H_2CO_3). Further, the produced carbonic acid being diprotic dissociates in two steps to give bicarbonate and carbonate ions (HCO_3^- and CO_3^{2-}) [17,41–44]

$$CO_2(g) + H_2O(l) \rightarrow H_2CO_3(aq) \quad 2.1$$

$$H_2CO_3(aq) \rightarrow H^+(aq) + HCO_3^-(aq) \quad 2.2$$

$$HCO_3^-(aq) \rightarrow H^+(aq) + CO_3^{2-}(aq) \quad 2.3$$

The electrochemical processes which give rise to the CO_2 corrosion involve three cathodic reduction reactions;

$$2H^+(aq) + 2e^- \rightarrow H_2(g) \quad 2.4$$

$$2H_2CO_3(aq) + 2e^- \rightarrow H_2(g) + 2HCO_3^-(aq) \quad 2.5$$

$$2HCO_3^{2-}(aq) + 2e^- \rightarrow H_2(g) + 2CO_3^{2-}(aq) \quad 2.6$$

The anodic reaction in CO_2-corrosion is the oxidation of iron into ferrous ion as shown below.

$$Fe(s) \rightarrow Fe^{2+}(aq) + 2e^- \quad 2.7$$

This reaction provides the electrons required to keep the process going [15,45,46].

As a result of these processes, the corrosion layer is precipitated on the surface of the metal [36,47]

$$Fe^{2+}(aq) + CO_3^{2-}(aq) \rightarrow FeCO_3(s) \quad 2.8$$

$$Fe^{2+}(aq) + 2HCO_3^{-}(aq) \rightarrow Fe(HCO_3)_2(s) \quad 2.9$$

$$Fe(HCO_3)_2(s) \rightarrow FeCO_3(s) + CO_2(g) + H_2O(l) \quad 2.10$$

The rate of precipitation (R_{FeCO3}) is the determining factor of the formation of the layer [48]. The value of "Scaling Tendency" (ST) which is a non-dimensional parameter gives tendency of formation of this layer and is given by:

$$ST = R_{FeCO3}/CR \quad 2.11$$

Where CR = corrosion rate. When ST << 1, the layer is non-adherent and non-protective and can result in localized corrosion. On the other hand, if ST > 1, the layer is compact and protective and decreases the rate of corrosion both in experimental and empirical conditions. Prior to the precipitation of the film, the corrosion attack is usually considered as uniform [47].

2.2. Factors affecting CO_2 Corrosion

There are a number of parameters that influence the rate of corrosion in CO_2 environment. The factors are listed and briefly explained below:

2.2.1. PH of the Environment:

This is the concentration of hydrogen ions (H^+) in a given solution which in no exception, is regarded as one the most significant variable in CO_2 corrosion [42]. When the pH of the solution is < 4, then the dominant of the three cathodic reactions is hydrogen reduction (eq. 2.4) because of more H^+ available. However if the pH range is 4 - 6, the superior cathodic reaction is the reduction of carbonic acid (eq. 2.5). When the pH of the solution > 6, research has shown that the cathodic reaction is dominantly due to reduction of bicarbonate (eq. 2.6) [40,49,50].

Both computational and experimental studies have shown that any change in the pH of the solution has a strong influence of changing the rate of CO_2 corrosion. This effect can either be in a direct or an indirect way. Directly, increase in pH decreases the rate of CO_2 corrosion because of the limited concentration of H^+ which means less of cathodic reaction hence less corrosion. In other words, at pH < 4, particularly when the partial pressure of CO_2 is low, the direct reduction of H^+ ions causes an increased corrosion rate. In an indirect way, increase in pH lowers the solubility of $FeCO_3$ thereby promoting the precipitation of the layer and scaling tendency at a faster rate and ultimately corrosion rate is decreased In other words when the pH is higher, the solubility of $FeCO_3$ decreases, and consequently carbonated is precipitated at a faster rate on metal surface which protects it [40,48,49].

2.2.2. Oxygen Concentration

Passive films usually form in the absence of oxygen because $FeCO_3$ is not stable in the aerobic condition. Oxygen may interfere with the production equipment as a result of injecting water or inhibitors. Ferrous ions (Fe^{2+}) can oxidize to ferric ions (Fe^{3+}), if the

oxygen content is higher than 40ppb since high level of oxygen interrupts the stability of the layer. Furthermore, oxygen increases the rate of cathodic reaction since it is a strong oxidizer as would be seen in equation (2.12). Both of these phenomena increase the corrosion rate[7,51,52].

$$O_2 + 2H_2O + 4e^- \rightarrow 4OH^- \qquad 2.12$$

The electrons required for this reduction reaction are generated from equation (2.7), the oxidation of iron

2.2.3. Iron content

Precipitation of ferrous ion (Fe^{2+}) and carbonate ion (CO_3^{2-}) determines the rate of formation of $FeCO_3$. The solubility limit of these ions must be exceeded for the film to form. In other terms, the degree of supersaturation which is the ratio of the product of Fe^{2+} and CO_3^{2-} concentration to the solubility limit (K_{sp}) must be greater than unity.

$$\text{Supersaturation} = [Fe^{2+}][CO_3^{2-}]/K_{sp} \qquad 2.13$$

Thus, higher concentration of Fe^{2+} leads to the higher the degree of supersaturation and faster growth of $FeCO_3$ film and consequently the corrosion rate is minimized [7,17,43].

2.2.4. Effect of CO_2 Partial Pressure

At film forming conditions, when there is high temperature and high pH (> 6), increasing CO_2 partial pressure decreases the corrosion process. When the pH is high, higher CO_2 partial pressure yields more concentration of bicarbonate and carbonate ions and a higher supersaturation which ultimately promote precipitation and scale formation. Film forming conditions have the favorable tendency of facilitating the rate of carbonate layer formation

which lowers the corrosion rate as opposed to the effect of high CO_2 partial pressure. However, when the condition is scale-free, according to Henry's law, higher CO_2 partial pressure produces more dissolved CO_2 and consequently the carbonic acid concentration in the solution is increased. Therefore, as a result of the increase in the concentration of carbonic acid, pH of the solution decreases, which accelerates H_2CO_3 cathodic reduction and in turn corrosion rate is raised [7,17,39,43].

2.2.5. Temperature Effect

All the processes that affect the rate of $FeCO_3$ formation like chemistry of the bulk of the solution, mass transport between bulk of the solution and metal surface, chemical reactions and electrochemical reactions at the metal surface are greatly influenced by temperature[40]. Temperature can be said to have two conflicting effects. With rise in temperature, corrosion rate can either increase or decrease depending on whether the solubility limit of $FeCO_3$ layer is exceeded or not [53]. At non-film forming conditions (at low pH), increasing the temperature increases the corrosion rate. However at film forming conditions (at high pH), increase in temperature accelerates the kinetics of precipitation and protective $FeCO_3$ layer formation thereby decreasing the corrosion rate.

Generally, corrosion rate increases as the temperature increases up to 60 - 80^oC depending on flow conditions and water chemistry [40,43]. When temperature is high, protective film is formed with less difficulty which tends to decrease the corrosion process [43,54].

2.2.6. Effect of Flow

Flow velocity usually affects corrosion rate depending on whether other conditions are favoring protective scale formation or not. When the conditions are non-film forming (at

low solution pH or in the absence of inhibitor film), turbulent flow velocity usually increase corrosion rate as a result of increased mass transfer of species to and from the metal surface. On the other hand when the conditions are film favorable (at higher pH or when inhibitor films are present), increased mass transfer process is insignificant since the metal in this case is protected by the film(s). The effect of the turbulent flow is due to interference with protective layer precipitation or damaging the existing films thereby increasing the corrosion rate in both situations [40,53].

2.3. Corrosion Inhibitors

Corrosion can be controlled by using an appropriate technique, however it is nearly impossible to be prevented completely [55]. Corrosion inhibitors are substances which when added to a corroding system in small amount, reduces the corrosion rate of a metal exposed to that system. Among the different ways of combating corrosion, the use of corrosion inhibitors appears to be the most considered. The role of inhibitors in the oil extraction and processing industries is of paramount importance, in fact, they are given first consideration for protection against corrosion [27]. The use of corrosion inhibitors is regarded as one of the most economical and practical technique for corrosion protection [1,57]. Application of suitable corrosion inhibitors can be incorporated with the use of lower grade steels and it is of better capital economy in comparison with the use of expensive high grade alloys in the same condition [28].

Based on the way they function, inhibitors used can be any of the following types [57]: Anodic, cathodic passivating, neutralizing and active, vapor phase, and film forming inhibitors

The mode of action of these compounds is either by adsorbing on the metal surface or by reacting with some impurities in the system that may cause corrosion [57]. Adsorption is an adhesive process where a substance (ions, atoms or molecules of a gas, liquid or dissolved solid) called adsorbate adheres to a surface (adsorbent). The efficiency of an organic inhibitor is dependent on its adsorption property on the metal surface [24]. Further, the adsorption of a particular inhibitor is dependent on its physical and chemical properties; functional groups, aromaticity, steric effect, electronic arrangement of its molecules, density of electrons at the donor atoms and character of the π orbital of the donating electrons [58-60]. It is also established that nature of the metal, composition, microstructure, temperature and electrochemical potential between metal-solution interface affects adsorption hence the efficiency of the inhibitor [46,61].

According to the type of forces involved adsorption phenomenon can either be; (a) physisorption (b) chemisorption or combination of both

(a) Physisorption involves electrostatic interaction between the electric charge at the surface of the metal (adsorbent) and ionic charges or dipoles of the inhibitor (adsorbate). In physisorption, heat of absorption is low and therefore this type of adsorption is unstable at high temperature [62,63]. Physisorption may also arise as a result of electrostatic attraction between the adsorbed chlorides on the metal surface and the protonated inhibitor molecules [64].

(b) Chemisorption involves charge sharing or electron transfer between the inhibitor molecules and metal surface. A coordinate type of bond is formed as a result of this interaction between the d-orbital of the metal adsorbent and the π-electrons or unshared

electron pairs of the inhibitor adsorbate. In this mode of adsorption, either the anodic or the cathodic reaction or both are reduced from the adsorption of inhibitor on the corresponding active sites [61]. Unlike physisorption which is characterized by low bond energy, chemisorption energy is higher and is therefore stable at higher temperatures[62,63].

This adsorption whether physical or chemical results in the formation of protective hydrophobic surface film which involves removal of water molecule at the metal solution interface by the inhibitor molecules. This serves as a barrier to the metal dissolution in the electrolyte as represented in equation 2.14 [59].

$$Org(sol) + nH_2O(ads) \rightarrow Org(ads) + nH_2O(sol) \qquad 2.14$$

When inhibitor molecules get adsorbed to the surface of the metal, they retard or stifle the corrosion process by:

- Adsorption of molecules on the metal surface
- Changing the rate of anodic cathodic reaction
- Retarding the rate of diffusion from reactants to the surface of the metal
- Decreasing the electrical resistance of the metal surface

There are several factors to be considered for choosing an appropriate corrosion inhibitor Availability, cost effectiveness, toxicity and above all environmental friendliness [59,60,65-68].

The use of organic inhibitors gained interest of corrosion scientists in the mid of 1970s. They replaced the previous use of inorganic acids and salts such as arsenic acid or arsenate, chromates, dichromates, nitrates e.t.c which are rather toxic and poisonous to the environment [1]. In his review, Sanyal [69] have reported the classification and mechanism of action of organic corrosion inhibitors. He ascribed the potential of an inhibitor as its ability to donate lone pair of electrons. This is usually due to the presence of an electronegative elements- heteroatoms like N_2, O_2 and S in the structure or pi-electron which serve as active centers for the adsorption on the metal surface. Azoles (Pyrazole, Thiazole, Oxazole, Isoxazole and Imidazole) have long been investigated as inhibitors for the corrosion of many metals and alloys [70]. Other organic inhibitors that are usually found in industrial formulations are condensation products of amines and carbonyls compounds, quaternary salts, acetylenic alcohols, aromatic aldehydes, and alkenyl phenones [1,8]. However, these synthetic compounds are reported to have a number of drawbacks. They pose threat to the environment due to their toxicity and some of them are effective only at higher concentrations [71].

2.3.1. Inhibitors used in CO_2 environment.

Since steels widely used in oil and gas transportation are plagued by sweet corrosion, researchers worldwide have come up with different formulations of compounds and various techniques to tackle this problem. This section gives a summary of the corrosion inhibitors used in CO_2 environment. Experimental condition, various techniques used for inhibitor assessment and behavior of the inhibitor under investigation are reviewed.

Wang et. al. [72] studied the performance of thioureido imidazoline inhibitor on Q235 mild steel using EIS, Atomic Force Microscopy (AFM) and XPS in 2% NaCl saturated with

CO_2. The concentration range of 0.08 – 0.31 mmol was employed however the peak efficiency of about 92.2% was at 0.15 mmol. The electrostatic forces between AFM tip and the charged steel surface were studied for the potential of zero charge at the surface as well as the reduction of the surface charge. XPS studies have shown that the inhibitor has chemically adsorbed because of the coordination bond formation with metal substrate.

The inhibition performance of amido imidazoline derivative was investigated on American Petroleum Institute (API) 5L X52 mild steel grade using EIS and PDP in 3% NaCl at pH 4. The synergistic effect of this inhibitor with iodide solution was also studied in the same condition. Concentration range of 25 – 150 mmol was used and the efficiency increases with concentration increase reaching the maximum efficiency of 95% noted at 150mmol using EIS. Addition of potassium iodide has raised the efficiency of just 50 mmol from 76.7-90.1%. There is no much significant change in efficiency at higher inhibitor concentration with the addition of the iodide. There is a strong agreement between EIS and PDP results [73].

Chemisorption type of adsorption was proposed by Okafor et. al when they used 2-undecyl -1- ethyl amino imidazoline (2UEI) on N80 mild steel in 3% NaCl saturated CO_2 at pH 4 using EIS and PDP. The performance was investigated at the concentration range of 20 – 100mgL-1 and temperature range of 25 – 50^oC. The inhibition was found to increase with increase of both concentration and temperature. Synergistic study with 830 – 2000mgL-1 potassium iodide improved the efficiency of the inhibitor. The maximum inhibition of 97.3% was reported for 80mgL-1 2UEI + 2000mgL-1 KI at 25oC after 3hrs [74]. A Temkin isotherm was employed to approximate the adsorption characteristics of the inhibitor in the presence of iodide ions. Study of activation energy changes in the absence and presence of

inhibitor (as well as in iodide synergism) was made to propose the chemisorption mechanism. A correlation was made between EIS and PDP results. SEM images were used to study the surface of the samples after immersion.

The corrosion inhibition of amphilic- amido amine was investigated in 5% NaCl CO_2 saturated solution at 25^{o}C using EIS, PDP and Polarization Modulation – Infrared Reflection Absorption Spectroscopy (PM- IRRS) electrochemical measurements. The concentration range of $0.07 \times 10^{-5} – 5.44 \times 10^{-5}$ mol was employed. The efficiency increases with increase in concentration reaching the maximum performance of about 99% at 5.44×10^{-5} mol [75]. The authors further reported that at lower concentration up to $2.7 \text{ X } 10^{-5}$ mol, the inhibitor performance decreases with increase in temperature which indicates physisorption. However at higher concentrations, the inhibition efficiency increases with temperature increase which suggest chemisorption. The Frumkin adsorption isotherm was approximated for the inhibitor on the steel surface [76].

In CO_2 saturated 0.5M hydrochloric acid, the performance of 12- aminododecanoic acid on carbon steel was assessed using EIS, PDP and WL methods. The compound acts as a mixed type inhibitor with up to 98.1% efficacy after 3 days of immersion at 3 mmol concentration. The physical adsorption mechanism was proposed by the researchers [32]. Furthermore, the authors reported the effect of electrolyte velocity and pattern of the inhibitor by using jet impingement to compliment the RDE and square duct methods. At lower concentrations, high velocity decreases the inhibitor efficacy because of desorption of inhibitor molecules from the metal surface. At higher concentrations however, not much change in its performance was observed with increase of flow [77].

Using EIS and PDP, the anticorrosive behavior of praseodymium 4-hydroxycinnamate on mild steel was investigated in both NaCl CO_2 saturated solution (pH 4 at 25^oC) and naturally aerated systems (pH 5.5-8 at 25^oC). In naturally aerated solutions, continuous protective film on the metal surface was believed to protect it against corrosion as revealed by SEM. In CO_2 containing system, the protection of the metal was believed to be as a result of inhibiting layer at active electrochemical corrosion site in addition to the inner film [78].

The effect of flow entrained sand concentration on the N80 mild steel by quaternary alkonoxy methyl amine IMC-80 and imidazoline CO_2 saturated 3 % NaCl solution was reported using EIS, LPR, SEM and weight loss techniques. The efficiency of quaternary alkonoxy methyl amine IMC-80 increased with increase in concentration up to 150mgL^{-1} beyond which the performance decreases. The maximum concentration for both static and flow condition of up to 5 m/s was reported at 150mgL^{-1}. For imidazoline, the peak efficiency was at 100mgL^{-1} under static mode. However, the peak efficiency increase at 200mgL^{-1} at 5m/s. Under static mode, the imidazoline shows better performance than quaternary alkonoxy methyl amine IMC-80 while the reverse was observed at higher flow velocity of 5m/s. Langmuir and Freudlich adsorption isotherms were approximated for concentrations below and above 150mgL^{-1} respectively [77].

The effect of Talloil Diethylenetriamine (TOFA/DETA) imidazoline was investigated in 3% NaCl saturated with CO_2 at 20 and 70^oC and pH 5 for API X65 mild steel using EIS, LPR and Potentiodynamic Sweep Measurements (PDS). At 70^oC, the corrosion rate reduced from 1 mmy-1 for blank to 0.1 mmy^{-1} with addition of 70ppm of the inhibitor (a novel). Quartz Crystal Microbalance (QCM) was used to study the adsorption mechanism

and kinetics of self-assembled MOFA/DETA formation of monolayers onto the gold. Weight loss measurements and AFM studies have confirmed the effective (95%) inhibition of the steel surface due to the addition of the inhibitor Langmuir adsorption isotherm was proposed [79].

In 0.01M NaCl solution at pH 4 and 25^{o}C the EIS and PDP based study of 0.12 – 2.41 mmol concentration of 4 – carboxyphenylboronic acid (CPBA) as a corrosion inhibitor was made on mil steel. The formation of organic-inorganic film was believed to arrest corrosion with up to 95.36 % efficiency at 2.41 mmol [80].

For the first time, the comparison of the anticorrosive property of DETA derived imidazolines, tetraethylenepentaamine (TEPA) derived imidazoline and bis imidazoline was made in 0.5 M NaCl saturated with CO^2 at 30 – 60^{o}C. The performance increases with increase of both temperature and concentration. At 100ppm and 40^{o}C, the performances of the mono imidazolines (DETA and TEPA) and bis imidazoline were 84, 95 and 96 respectively. They all responded mainly as anodic corrosion inhibitors and the protection was through the formation of a film adsorbed on the metal surface which hinders the access of the corrosive chloride/CO_2 specie from attacking the metal surface [81].

In CO_2 saturated 5% NaCl, solution at 40^{o}C and pH 6, the performance Aminopropylimidazole (API) and two commercial imidazoline based products (PC and QB) on two microstructures of carbon steel (annealed and quenched & tempered) was studied using EIS and LPR. The fixed amount of 100, 20 and 50ppm for API, PC and QB respectively. The inhibition was more on annealed sample than quenched and tempered when API and PC were used even though there was not observed any formation of

protective film and the corrosion process continued through time. When QB was used, the corrosion process was arrested as a result of formation of a protective film. The presence of QB presented an excellent efficiencies of nearly 100% in both microstructures even though the annealed samples seemed to be a little bit more protected. API is not a good inhibitor under the conditions studied. On the other hand PC was effective for both microstructures [82].

EIS and PDP based studies were made to investigate anticorrosive behavior of five ammonium salt of O,O'- dialkyl dithiophosphoric acid on mild steel in CO_2 saturated brine at 15 – 70^{o}C and pH 5.3. The concentration range of 0.25 – 5mgL^{-1} was used. For all compounds, effective inhibition of about 70 -99% was achieved. The compounds were mixed type with more influence on the anodic reaction. For some compounds efficiency was increased with temperature increase [83].

The inhibition of water base acrylic terpolymer (ATP) on SAE 1018 mild steel in CO_2 saturaated 3.5% NaCl, 0.305 CaCl2 and 0.186 MgCl2.6H2O at pH 4.7 was investigated in both stagnant and flow conditions (500, 1000 , 1500 and 2000 rpm). The inhibitor is believed to act as mixed type and its efficiency increases with increase in concentration (0.1 – 0.8ppm) and flow speed. The maximum performance of 93.3% was achieved at 0.8ppm and 2000rpm using PDP and 90.8 using EIS [84].

Using weight loss, XPS, EIS and PDP, the synergistic study of oleic imidazoline (OIM) and sodium benzoate was made on mild steel in CO_2 saturated china oilfield standard produced water. The protection of about 78.62% with addition of 10mgL^{-1} OIM was achieved. The inhibition was strengthened when 10mL-1 of Sodium Benzoate was added

which raises the efficiency to 91.45%. The inhibitor acts as the mixed type but predominantly affected anodic process [85].

EIS and LPR based study of the inhibition of (1-(2-hydroxyethyl)-2heptadec-8enyl) imidazoline and 1-(2-aminoethyl)-2(heptadec-8-enyl)-bis imidazoline on API 5L X65 mild steel in 3% NaCl saturated with CO_2 at 80^{o}C and pH 4 was verified. The concentration range of 5- 50ppm was employed. There was effective inhibition of up to 98.9% at 50ppm after 24 hours of exposure [86].

The inhibition performance of 5 heterocyclic compounds; 2 amino benzotraizole (ABA), 5-tollyl 1,3,4 triazole (TTA), 3-amino 1,2,4 triazole (ATA), 3-amino 5-methyl mercapto 1,2,4 triazole (AMTA) and 2-amino 1,3,4 thiadiazole (ADTA) was investigated using PDP and LPR on mild steel at 55^{o}C in 3.5 and 2.5% NaCl solution saturated with CO_2. ABA was shown to be the best of the studied compounds with maximum efficiency of about 95% in 3.5 NaCl.

The inhibition of undecyl sodium ethanoate imidazoline salt (2M2) and thiourea (TU) was investigated on N80 mild steel in 3% NaCl CO2-saturated at pH 4 and 25^{o}C using EIS, LPR and PDP. The efficiency of 2M2 (41.8 -93.2%) increase with increase in concentration (20 – 800mgL-1). However, TU performance decrease (91.7-77.9) as the concentration increases (20 – 100mgL^{-1}). Both the compounds behaved as mixed type inhibitors and the protection was due to the film formation on the metal surface. 2M2 obeyed Langmuir adsorption isotherm.

The table below presents a summary of the corrosion inhibitors used against sweet corrosion.

Table 2.1: Inhibitors for CO_2 Corrosion

Table 2.1 lists some of the corrosion inhibitors used for CO_2 corrosion protection

Inhibitor Compounds	**Medium, pH and temperature**	**Material Used**	**Inhibitor concentration**	**Methods of Assessment**	**% IE**	**References**
Undecyl sodium ethanoate (2M2)	3.0 NaCl at 25^{o}C and pH 4	N80 MS	20 – 800mgL-1	EIS, PDP and LPR.	41.8 – 93.2	[87]
Thiourea (TU)	3.0 NaCl at 25oC and pH 4	N80 MS	20 – 100mgL-1	EIS, PDP and LPR.	77.9 – 91.7	[87]
Thioureido Imidazoline	2.0 NaCl at 20^{o}C and saturated pH.	Q235 MS	0.08 – 0.31mmol	EIS XPS, and AFM	88.6 – 93.2	[72]
2 undecyl -1-ethylamino imidazoline (2UEI)	3.0 % NaCl at 25 – 50oC and pH 4.0	N80 MS	20 – 100mgL-1	EIS and PDP	After 3h, the % IE was 90.89 at 80mgL^{-1}. Addition of 2g of KI has synergistically raised the performance to 97.3%.	[74]
N-[2-[(2-aminoethyl) amino] ethyl]-9-octadecenamide	5.0 NaCl, at 25^{o}C and pH = 6	MS	0.7-54.4 10^{-6}	PDP, EIS and PM-IRRAS	28 – 99	[75]
N-[2-[(2-aminoethyl) amino] ethyl]-9-octadecenamide	5.0 NaCl, at 25 - 45^{o}C and pH = 6	MS	1.4-54.4 10^{-6}	PDP, EIS and PM-IRRAS	45 – 99	[76]
Amido imidazoline derivative	3.0 % NaCl at 25^{o}C and pH 4	API 5L X52 MS	25 – 150mmol	EIS and PDP	76.7 – 90.1	[73]
Benzimidazole	5.0%NaCl at 40^{o}C, pH = 6	MS	100ppm	EIS and LPR	27.5	[88]
(1-(2-hydroxyethyl)-	3.0%NaCl at 80^{o}C and pH = 4	CS	5 - 50ppm	EIS and LPR	91.21 to 98.90	[86]

Inhibitor Compounds	Medium, pH and temperature	Material Used	Inhibitor concentration	Methods of Assessment	% IE	References
2(heptadec-8-enyl)-imidazoline						
12-aminododecanoic acid	CO_2 saturated 0.5M HCl at 25-50^oC. Under static conditions.pH = 0.38-3.5	CS	0.5 - 4mM	EIS, PDP and WL	98.1% after 3 days	[32]
12-aminododecanoic acid	CO_2 saturated 0.5M HCl at 25-50^oC. Under flow conditions. pH = 0.38-3.5.	CS	1 - 3Mm	EIS, PDP and WL	77% at 3mM and 350 cm^3 min^{-1}	[77]
1-(2-aminoethyl)-2(heptadec-8-enyl)-bis-imidazoline	3.0%NaCl at 80^oC and pH = 4	CS	5 - 50ppm	EIS and LPR at 80^oC and pH = 4	91.51 to 99.51	[86]
Carboxymertyl imidazoline	3.0%NaCl at RT, pH = saturated with CO_2.	MS	100ppm	EIS and LPR	97.8	[89]
hydroxyethyl imidazoline	3.0% NaCl at RT, pH = saturated with CO2.	MS	100ppm	EIS and LPR	96.5	[89]
Praseodymium 4-hydroxycinnate	0.01M NaCl CO_2 saturated and Naturally aerated systems at 25^oC	MS	0.02 – 0.63mM	EIS, and PDP	Excellent in both conditions	[78]
Quartenary alkynoxy methyl amine IMC 80 Q	3% NaCl CO_2 saturated under flow with entrained sand	N80 mild steel	50 – 300mgL^{-1}	EIS, LPR and SEM	78.2 % at 150mgL^{-1} under static conditions. At high flow velocity the efficiency improves.	[77]

Inhibitor Compounds	Medium, pH and temperature	Material Used	Inhibitor concentration	Methods of Assessment	% IE	References
Imidazoline	3% NaCl CO2 saturated under flow with entrained sand	N80 mild steel	25 – 150mgL^{-1}	EIS, LPR and SEM	84.2 % at 100mgL^{-1} under static conditions. At high velocity the efficiency decreases	[77]
Talloildiethylenetriamine (TOFA/DETA) imidazoline	3% NaCl saturated with CO2 at 20 and 70oC and pH 5	API X65	70ppm	EIS, LPR and PDS	95 % at 20oC and 90% at 70^{o}C	[90]
Talloildiethylenetriamine (TOFA/DETA) imidazoline	3% NaCl saturated with CO2 at 20 and 70oC and pH 5	API X65	70ppm	WL and AFM	98.4 % at 20oC and 94.3 at 70^{o}C	[79]
Diethylenetetramine (DETA) derived imidazoline	0.5M NaCl saturated with CO2 at 30-60oC	AISI C 1018	0.5 – 100ppm	EIS, LPR and PDP	84 % at 100ppm and 40oC	[81]
Tetraethylene pentamine (TEPA) derived imidazoline	0.5M NaCl saturated with CO2 at 30-60oC	AISI C 1018	0.5 – 100ppm	EIS, LPR and PDP	95 % at 100ppm and 40oC	[81]
Bis-imidazoline	0.5M NaCl saturated with CO2 at 30-60oC	AISI C 1018	0.5 – 100ppm	EIS, LPR and PDP	96% at 100ppm and 40oC	[81]
4-carboxymethyl boronic acid (CPBA)	0.01 M NaCl saturated with CO2at 25^{o}C and pH 4	MS	0.12 – 2.41mM	EIS and PDP	95.36 at 2.41mM	[80]
aminoethyl imidazoline	3.0%NaCl at RT, pH = saturated with CO_2.	MS	100ppm	EIS and LPR	96.1	[89]
Imidazoline	3.0%NaCl at RT, pH =	MS	100ppm	EIS and LPR	88.4	[89]

Inhibitor Compounds	Medium, pH and temperature	Material Used	Inhibitor concentration	Methods of Assessment	% IE	References
	saturated with CO_2.					
carboxyamido imidazoline	3.0%NaCl at 50°C, pH = saturated with CO2	MS	0.0161 – 0.332 mmol	EIS, LPR and PDP	88 – 96	[91]
imidazoline amide	3.0%NaCl at 25 – 45°C, pH = 3.6	Armco Steel	5 – 20ppm	EIS and LPR	64 – 97	[92]
Synthesized sulfated fatty acid sodium salt	1.0%NaCl at 50°C, pH = saturated CO_2.	CS	10 – 100ppm	WL, EIS and LPR	80.90 - 99.5	[93]
Imidazoline	Saltwater at 25 - 55°C, pH = 4.86	CS	100-8000ppm	WL, EIS, LPR and PDP	81.3 – 95.3	[94]

2.3.2. Need for green corrosion Inhibitors

It is important to note that chemical structural pre-requisite is not only consideration for the selection of corrosion inhibitor but also its harmlessness. The obvious disastrous impact of most synthetic organic inhibitors and the recent need for cheap, eco-friendly and non-toxic processes have necessitated the need to focus on the inhibitors with natural origin [95]. It is on this regard that the inorganic and many organic hazardous inhibitors although many of them effective even at lower concentrations have to be replaced by benign ones [96,97].

There is an increased environmental restrictions for the use of unfriendly chemicals on ecological balance as a result of world's growing interest and attention towards environmental problems and towards the environmental protection and the hazards [30].

To comply with these restrictions, the approach for the selection of corrosion inhibitor has changed gradually. The search for the effective replacement of the traditional organic and inorganic inhibitors has started and the direction seems to be towards biodegradable compounds with natural origin [98]. In the past decade, efforts were considerably made in search for suitable corrosion inhibitors with natural origin in different media corrosive environments [95]. The focus is therefore more on the use of natural, non-toxic, eco-friendly or green corrosion inhibitors[99]. Natural polymers, amino acids, expired drugs, plant extracts and medicinal products have so far been suggested by researchers[98].

As the study of green corrosion inhibitors becomes an area of active research due mainly to the environmental problems caused by the use of harmful chemicals, tannins and barbiturates will not remain untested as anticorrosion compounds, since these chemicals have natural origin, biodegradable, water soluble and above all environmentally friendly. In this research, our interest is tilted specifically towards the use of tannic acid and barbituric acid as corrosion inhibitors for mild steel in CO_2-brine environment.

Thiobarbituric acid

Thiobarbituric acid (2-thioxodihydropyrimidine-4,6 (1H, 5H)-dione as represented by Figure 2 [100]., is a derivative of barbibituric acid which is an organic heterocyclic compound belonging to pyrimidine group with chemical formula $C_4H_4N_2O_3$. Barbiturates generally are non-toxic and due to their pharmacological activity, they found several applications in medicine and biological chemistry. They are also frequently used in manufacturing industries such as plastics, textiles and polymers industries [101]. Due to its simplicity and speed, 2-thiobarbituric acid test is the most popular and currently used

assay to determine the level of rancidity of fats and oils caused by peroxidation. It is based on the reactivity of the TBA with the end product of lipid autoxidation, malondialdehyde (MDA) [102].

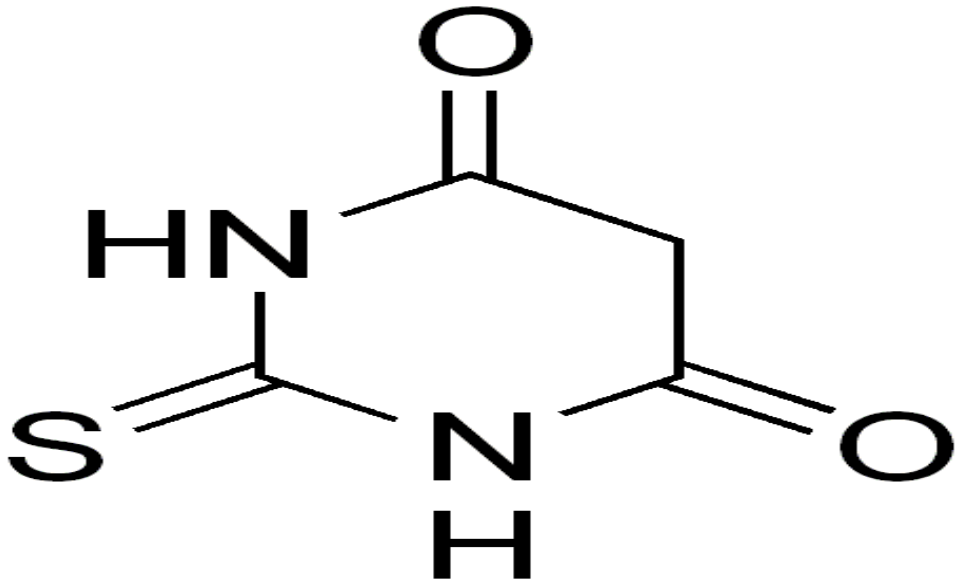

Figure 2.1: Structure of 2- thiobarbituric acid

There is a meagre available literature on the use of barbiturates in corrosion inhibition. Some barbiturates; 5-benzlidenepyrimidine-2,4,6-trione (BPT), 5-(2-hydroxybenzylidene) pyrimidine-2,4,6-trione (HPT), 5-(4-nitrobenzylidene) pyrimidine-2,4,6-trione (NPT), and 5-(3-phenylallylidene) pyrimidine-2,4,6-trione (PPT), have already shown good inhibition efficiency (89-97%) as mixed type inhibitors on mild steel in 1M HCl solutions at 350mg/L[103]. Barbituric acid (BA), TBA, and 5,5-dietylbarbituric acid sodium salt (DEBA) were investigated as corrosion inhibitors for mild steel in 1 M H_3PO_4 solution[30]. TBA, BA and Ethyl Barbituric Acid (EBA) were studied as inhibitors for mild steel corrosion in 0.5M HCl solution [104]. Furthermore, TBA was reported to have been tested as corrosion inhibitor for mild steel in 0.5M HCl solution [101]. However no available published work to date for the use of barbiturates against mild steel corrosion

in CO_2 environment. In this research, our interest is specifically towards the use of TBA as corrosion inhibitor for mild steel in sweet oilfield conditions.

The choice of TBA among other barbiturates is because:

- TBA has an interesting chemical structure with regards corrosion inhibition. In addition to N_2 and O_2 active centers possessed by all barbiturates for donating or sharing lone pair of electrons, TBA has S functional group. S group is believed to be more important for corrosion inhibition than N_2 and O_2 because it is stronger electron donating group [69].
- TBA can be produced in a pure state.
- It is ecofriendly.

Tannic acid

Tannins or sometimes simply referred as tannic acids [105,106] are spread widely in the plant kingdom[107]. They are type of natural, non-toxic, biodegradable and water soluble polyphenols[108]. Any mixture of polygalloyl glucose or polygalloyl quinic acid esters with 2 - 12 galloyl moieties per molecule can be described as tannins[105]. In a broader sense, these compounds can be divided into two;

a. Hydrolysable Tannins – gallotannins containing glucose esters of carboxylic acids and
b. Condensed tannins – which are derived from flavonoids.

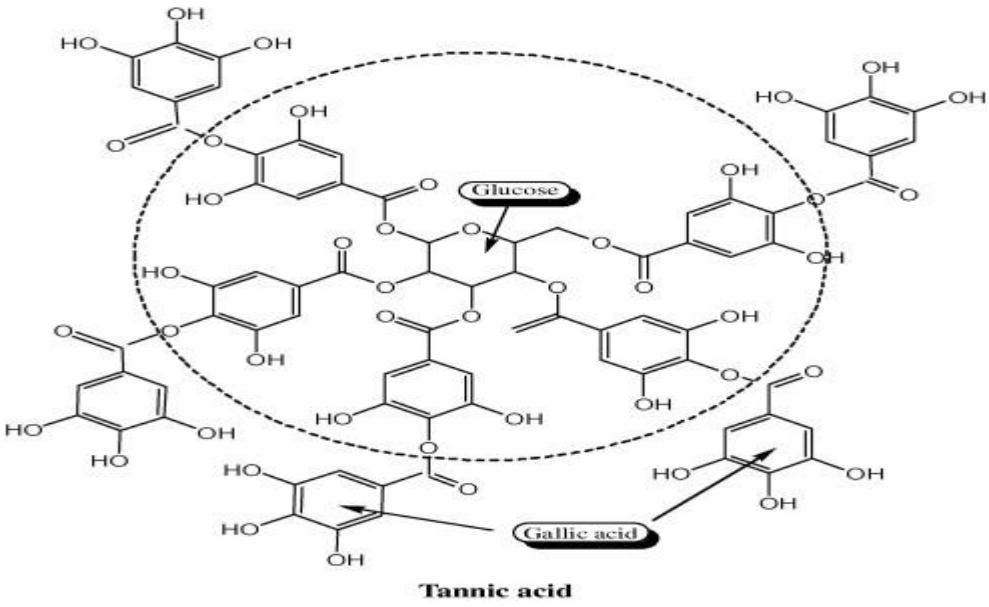

Figure 2.2: Structure of tannic acid

Tannic acid (penta-*m*-digallolyl glucose) is the principal member of a specific group of hydrolysable tannins. The chemical formula for commercial tannic acid $C_{76}H_{52}O_{46}$, whose structure is represented by Figure 2.2 [106], corresponds to a deca-galloyl glucose which comprises of a central glucose molecule esterified at all five hydroxyl functional groups with two gallic acid molecules. It appears in form of yellow or pale brown amorphous powder [105]. Tannic acid is available in the barks and fruits of many plants especially bananas, sorghum, grapes, chocholate, coffe, red wine, spinach, resins and tea [106]. The compound has found enormous number of applications in pharmacology [109-111] food and beverages [112,113] and in dye manufacturing industries[114,115].

Even though tannins are already in use as corrosion alleviators in aqueous media and in reinforcing steel in concrete, ingredients of rust converters, pigments in paint coatings, chemical cleaning agents for removing iron-based deposits and oxygen scavengers for boiler water treatment system[108], there is however no universal agreement in the use of

tannins as iron anticorrosion compounds [116]. It is therefore controversial whether tannins are efficient corrosion inhibitors for iron or not.

Corrosion products from iron surface (Iron oxides and hydroxides) react with the polyphenolic moieties from tannins to form a blue-black ferric-tannate complex as a major product which forms as coating layer on the metal surface[108], [116]. Some works that examined the corrosion of metals in solid wood state that tannins accelerate corrosion rates [117,118], whereas many studies on corrosion in the pulp and paper industry reported that tannins are corrosion inhibitors [119-123]. Studies by Winkelmann et. al [117] has shown the tannins as corrosion accelerators both by lowering the pH of the solution and formation of the ferric-tannate complex with iron which is not protective to the metal surface. In the same vein, report by Pugsley et. al [118] has shown the effect of 8.5g/L (5mM) tannins in the corrosion of sawblades. The strength of the steel decreased with exposure time and stress corrosion cracking was observed from the alloys. Contrary to the above studies, tannins are often reported as corrosion decelerators in the broader sense of literature [108,124,125]. Report from matamala et. al[124] shows there is about 250% increase in time to failure when tannins extracted from black acacia (*Acacia melanoxylon*) and radiata pine (*Pinus radiata*) are used as anticorrosive compounds in paint system as compared to the tannins-free paint system. Similarly, researchers have reported corrosion inhibition in sodium chlorides and acidic media when tannins are used [108,125,126]. In the end, the different behavior of tannins in these papers can be described due to the nature of the studied application. In sawblade corrosion for example, it is possible that the iron-tannates complex which passivates the metal from further corrosion are removed from the surface due to friction or heat and the chelation results in a more active surface than normal

corrosion processes, whereas in other situations, iron protects the surface. Regardless, the effect of tannins on the corrosion of metals in wood remains unclear [123].

X60 mild steel was used in this research which is the typical pipeline material used in Saudi Aramco. The inhibitor was tested by varying key parameters affecting CO_2 corrosion such as temperature, flow velocity and pH. Effect of inhibitor concentration and time of exposure to the corrosive environment was also taken into scrutiny.

2.4. Objectives

From the literature so far, little or no work was done on the electrochemical assessment of tannic and thiobarbituric acids as eco-friendly inhibitors in CO_2 environment. Hence it is the objective of this work to:

(1) Assess the corrosion inhibition performance of two green inhibitors namely tannic and barbituric acid in sweet oilfield conditions using electrochemical techniques.

(2) Evaluate the effect of concentrations, temperature, pH and immersion time on the corrosion inhibition performances of the two green inhibitors.

CHAPTER 3

METHODOLOGY

3.1. Sample Preparation

Three electrodes set up was used. An X60 mild steel whose elemental composition is given in Table 3.1 was used as the working electrode. The other two electrodes were graphite and saturated calomel which served as counter and reference electrodes, respectively.

The sample of dimension 1 x 1 cm^2 was cut and mounted on epoxy resins. The electrical connection was achieved by soldering the sample with a copper wire. The surface to be exposed for investigation was polished with SiC paper up to 600 grit and then washed with ethanol and distilled water.

The surface area exposed for the analysis was 1 cm^2. The equivalent weight of the X60 steel is 27.92g/mol and its density is 7.87g/cm^3. Only when the experiment is about to be conducted the polishing and cleaning was done to avoid atmospheric corrosion of the specimen.

Table 3.1: Chemical composition of X60 Mild Steel.

C	Si	Mn	P	S	Cr	Mo	Ni
0.195%	0.356%	1.16%	0.0103%	0.0029%	0.0824%	0.0925%	0.0975%
Al	Co	Cu	Nb	Ti	V	W	Fe
0.0176%	0.0128%	0.176%	0.0177	<0.001%	0.0569%	<0.0150	97.7%

3.2. Electrolyte Preparation

3.5 wt% (0.6M) NaCl prepared by dissolving 35g of American Chemical Standard (ACS) grade NaCl in 1L of double deionized water was used as a reference solution. Where inhibitor is needed, stock solution of 1000ppm was prepared by dissolving 1g of the compound (TBA or TA) in 1L of the reference solution. In each experiment, 0.8L of the solution was used in a four neck round bottom glass cell.

To simulate the oxygen free oilfield condition, the solution was bubbled first with N_2 (99.99%) for 30 minutes. This ensures low concentration of dissolved oxygen required to mimic the produced oilfield fluid [41]. Immediately after deoxygenation, CO_2 gas was bubbled to saturate the environment for 2 hours before taking the measurement. The theoretical saturation pH was reached which is approximately 4.0 at room temperature. The CO_2 gas was bubbled continuously throughout the experiment. For pH adjustment, sodium bicarbonate (Na_2CO_3) and hydrochloric acid (HCl) were used to raise and lower the pH, respectively.

3.3. Equipment

Gamry Potentiostat Reference 3000 was used in the electrochemical measurements. To set up three electrode assembly, a four neck round bottom pyrex glass whose capacity is 1 L was used. Saturated Calomel Electrode (SCE) and graphite were used as reference and counter electrodes, respectively. SCT BEN-pH-6 was used for measuring the pH and temperature of the solution. Figure 3.1 presents the experimental set up for this work.

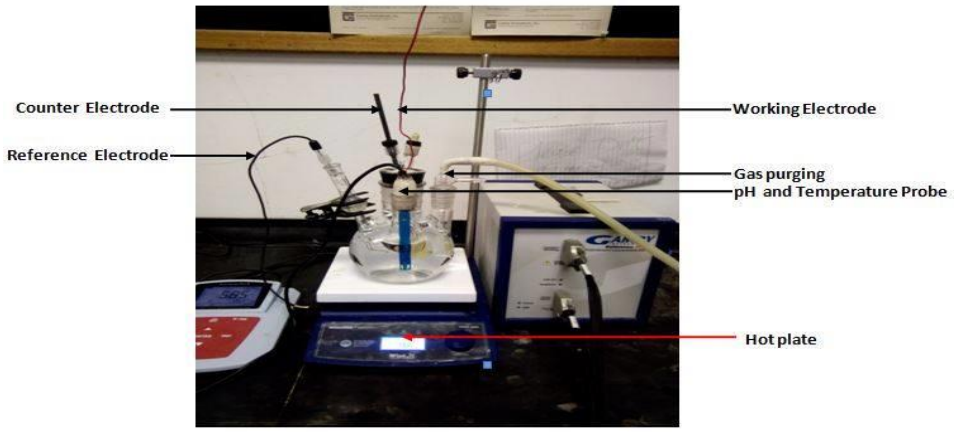

Figure 3.1: Experimental set up

3.4. Electrochemical Measurements

Several techniques have been used over time by researchers to determine corrosion rates. Some of these methods include; weight loss, chemical analysis of solution, thickness measurements and inert marker methods. Whether in field or laboratory, each one of these techniques can be used [20]. However, the process of corrosion being an electrochemical process, its kinetics is more conveniently understood by electrochemical measurements. Through this technique, it is possible to understand the corrosion reaction taking place and its mechanism by controlling electrode potential. Above all, electrochemical measurements are faster, more accurate and multiple analysis can be done on one sample under same condition. By electrochemical techniques, corrosion rate can be determined through various methods either by using a direct current (DC) or those using an alternating current (AC).

3.4.1. Linear Polarization Resistance (LPR)

LPR is based on the fact that there is a linear relationship between the applied potential and the measured current in cathodic and anodic region near the open circuit potential. It involves a step wise polarization from small potential below OCP (-20mV) to a potential above OCP (+20mV). The graph of potential versus current is linear and its slope ΔE/ΔI is the polarization resistance, Rp. Open Circuit Potential (OCP) is the potential at which there is no current flow through the electrode. It is sometimes referred to as or Free Corrosion Potential or simply Corrosion Potential and is denoted by symbol Ecorr. LPR was first reported theoretically in 1957 by Stern-Geary [127], based on the derivation of their well-known Stern-Geary equation from Butler-Volmer equation. Since then, many works were carried out to investigate the corrosion rate using this method. One of the early works include that of Skold and Larson [128]. They have empirically correlated the slope of ΔE/ΔI near the region of linear polarization with the corrosion rate determined from weight loss measurement. There exists an inverse relationship between the value of ΔE/ΔI and the corrosion rate.

The small applied potential which is at most 50mV removed from Ecorr may not have any effect on the electrode surface. This makes the linear polarization a non-destructive method and hence allows the linearly polarized specimen (test coupons) to continuously be used to give the corrosion rate as a function of immersion time. It allows the calculation of Rp from which calculation of corrosion rate is possible using Stern-Geary approximation in equation 4.1.

The method has been successfully used in various applications some of which include: monitoring atmospheric corrosion, assessment of corrosion inhibitors, corrosion study of biomedical alloys, water treatment etc. Despite these applications, some of the draw backs of this method are that it is inaccurate when: Butler-Volmer equation does not apply, Stern-Geary equation is not under steady state conditions, there is non-linearity near the $E_{corr,}$ anodic and cathodic half-cell reactions equilibrium potentials are close to E_{corr} and Tafel slope changes with time.

All electrochemical measurements were performed using Gamry Reference 3000. Open Circuit Potential was carried out an hour after the sample was immersed in the test solution before EIS LPR and PDP measurements. LPR measurements were performed by polarizing the working electrode at ± 15mV with scan rate of 0.2 mVs^{-1}.

3.4.2. Electrochemical Impedance Spectroscopy (EIS)

EIS is also known as AC impedance because of the small AC voltage (1 – 10mV) that is applied to the working electrode. The use of small AC voltage amplitude which exerts a very small perturbation on the system, makes the EIS advantageous over other techniques. It is one of the powerful tools used in electrochemistry and corrosion studies to investigate the formation of films on the surface of either pure metals or alloys [129]. The wide application of this technique in the study of corrosion inhibitors is because of its ability to indicate the mechanism of film formation on the metal surface and the persistency of the film. Other corrosion studies where EIS is used include; corrosion coatings, formation of films on metals and corrosion product analysis [10]. Information like interfacial properties where basic microscopic reactions take place and electrochemical properties of electrically

conducting electrode and electrode/solution interface can be extracted from the technique. As such, kinetic and mechanism of electrochemical properties of a system can be studied. EIS was performed at a sinusoidal excitation ac voltage of + 10mV (rms) and the response was determined in the frequency range of 100 kHz – 10 mHz with 10 points per decade.

3.4.3. Potentiodynamic Polarization

Polarization methods involves the use of current – potential relationship to investigate the corrosion behavior of a metal. PDP is one of the most widely used polarization method.

PDP measurement as a destructive test, comes at the end of the experiment. It was performed by polarizing working electrode at a potential range of $\pm$ 250mv versus OCP (E_{ocp}) at $1mVs^{-1}$. Tafel extrapolation was used to analyze graphically the corrosion rate (i_{corr}).

3.5. Surface Characterization Techniques.

Surface characterization is widely used by researchers to study the mechanism of corrosion inhibition [64,72,82,86,93,94,130,131]. Surface morphology and corrosion products analysis are paramount in understanding the corrosion behavior from which corrosion mechanism can be well stated. In order to investigate the mechanism of inhibition, surface characterization methods namely; Scanning Electron Microscopy/Energy Dispersive Xray (SEM/EDX), X-ray Photoelectron Spectroscopy (XPS) and Fourier Transform Infrared spectroscopy, were employed.

The mild steel specimen, mechanically polished up to 600 grit size SiC paper were immersed for 24 hours at 25^{o}C in 3.5% NaCl saturated with CO_2 with and without

inhibitors. After removal from the solution, the samples were rinsed with distilled water and ethanol and dried at room temperature. Coupons were stored in desiccator until the time for the characterization.

3.5.1. Scanning Electron Microscopy

SEM was taken to observe the change in surface feature of samples before and after immersion in the corrosive environment in the presence and absence of the inhibitors. JOEL JSM-6610LV Scanning Electron Microscope was used

3.5.2. X-ray Photoelectron Spectroscopy

Since XPS is a surface sensitive quantitative method, it is widely employed to give surface chemistry and elemental composition of steel before and after corrosion. XPS furnishes the respective binding energies of the corrosion products as a result of interaction of photoelectron with the metal substrate. Since binding energy is an intrinsic property of a material, a particular binding energy gives an identity of the type of chemical component present and its chemical state. We used ESCALAB 250Xi XPS from Thermo Scientific Company for this investigation.

3.5.3. Fourier Transform Infrared Spectroscopy

Infrared spectra for absorption/emission can be obtained for all organic substances since most of molecules absorb light in the infrared region of the electromagnetic spectrum. We employed NICOLET 6700 FTIR from Thermo-electron Corporation.

CHAPTER 4

RESULTS

4.1. Inhibition by Thiobarbituric acid

4.1.1. Effect of concentration at pH = 4

Typical representation of LPR curves are shown in Figure 4.1. The slope of ΔE/ΔI is a measure of polarization resistance (Rp) of the metal to corrosion. The higher the value of ΔE/ΔI, the higher is the resistance of the metal to corrosion attack and hence the lower the corrosion rate (C_R). Stern-Geary approximation can then be used to calculate the actual corrosion rate according to equation 4.1:

$$\frac{\Delta E}{\Delta I} = Rp = \frac{ba \times bc}{2.303(ba+bc) * i_{corr}} \qquad 4.1$$

Where, i_{corr} is the corrosion current density, b_a and b_c are the anodic and cathodic Tafel slopes respectively. The i_{corr} (A/cm^2) in equation 4.1 can be calculated by using:

$$i_{corr} = \frac{ba \times bc}{2.3(R_p)(ba+bc)} \qquad 4.2$$

Corrosion rate (C_R) in mil per year can finally be calculated under approximation that ba and bc are both equal to 0.1V/decade [23]:

$$C_R = \frac{0.129 \times i_{corr} \times (E.W.)}{n \times d} \qquad 4.3$$

Where, 0.129 is a conversion factor, (E.W.) is the equivalent weight, n is number of electrons and d is the density (g/cm^3).

For example, in fig 4.1 (a) the $\Delta E/\Delta I = R_p = 142.6\ \Omega cm^2$

$i_{corr} = 0.1x0.1/2.3\ (142.6)\ (0.1 + 0.1) = 1.52 \times 10^{-4}\ A/cm^2 = 152\ \mu A/cm^2$ by substituting this value in equation 4.3, we get $C_R = 69.6$ mpy, which is close to the value already calculated from the Gamry software automatically (69.5mpy).

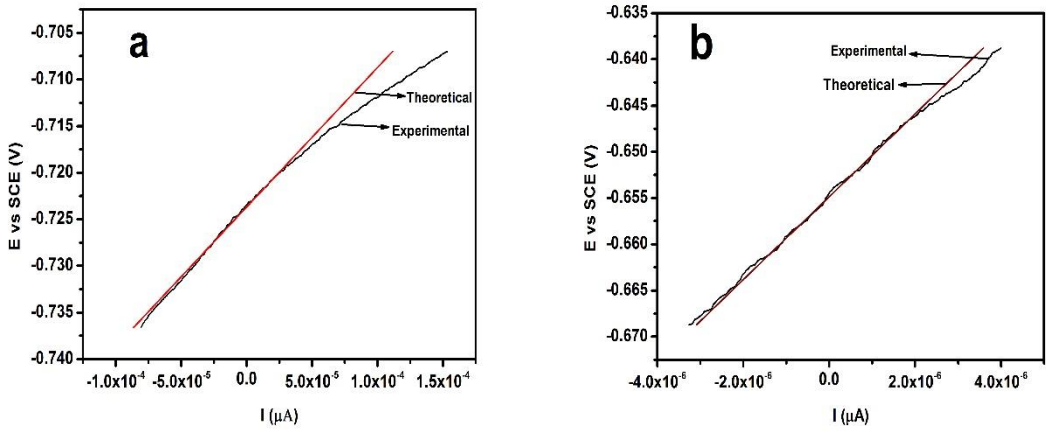

Figure 4.1:Potential-current variation for X60 mild steel at 25°C and pH 4 after 2 hours in (a) CO_2-saturated 3.5% NaCl and (b) CO_2-saturated.3.5 % NaCl + 50ppm TBA

Table 4.1 shows R_p values from LPR method for X60 mild steel electrode immersed in absence and presence of various concentrations of TBA inhibitor after 2 hours of immersion at 25°C and pH 4. To assess quantitatively the performance of an inhibitor, percentage inhibition efficiency was calculated using equation 4.4

$$\%\ \boldsymbol{IE} = \frac{\boldsymbol{Rp_i - Rp_b}}{\boldsymbol{Rp_b}}\ \boldsymbol{X\ 100} \qquad 4.4$$

Where R_{pi} and R_{pb} are polarization resistances in the presence and absence of the inhibitors respectively [132].

In the same way, the Inhibitor performance can be assessed in terms of corrosion rate using equation 4.5

$$\% \, \boldsymbol{IE} = \frac{\boldsymbol{C_{Rb} - C_{Ri}}}{\boldsymbol{C_{Rb}}} * \mathbf{100} \qquad 4.5$$

Where C_{Rb} and (C_{Ri}) are the blank and inhibited corrosion rates respectively.

Table 4.1: Effect of TBA concentration at pH 4 and 25 °C from LPR

Concentration (ppm)	R_p (Ω cm2)	C_R (mpy)	% IE
0	142.6	69.5	0
25	1717	5.8	91.7
50	4655	2.1	96.9
75	5697	1.7	97.5
100	1919	5.2	92.5

It can be seen clearly in Table 4.1 that TBA significantly reduced the corrosion rate of X60 steel in CO_2 saturated (sweet) environment in the employed concentration range of 25 – 100ppm ($5.9 \times 10^{-5} – 5.9 \times 10^{-4}$M). Corrosion rate decreases as the amount of TBA is added to the solution up to 75ppm. This leads to increase in efficiency reaching its peak at 75ppm. However, when the concentration was increased to 100ppm, the corrosion rate rises and the efficiency drops slightly. This behavior is plotted in Figure 4.2

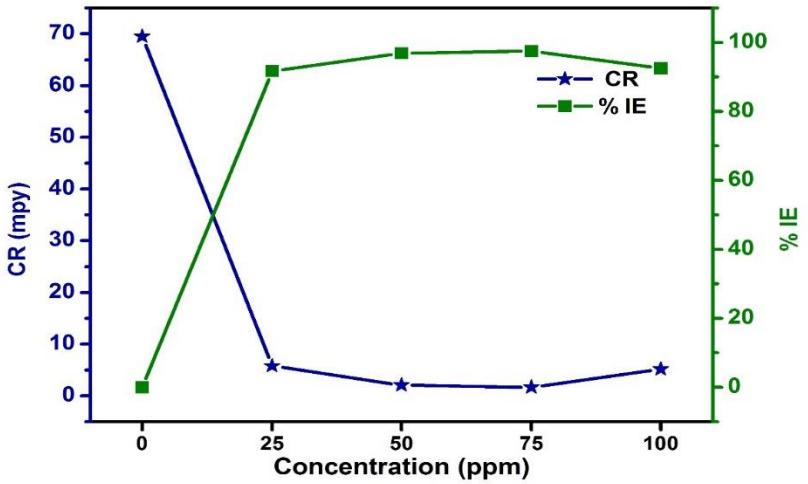

Figure 4.2: Inhibition efficiency of TBA at pH 4 and 25°C using LPR

The impedance spectra for X60 Mild steel in 3.5% NaCl with and without TBA concentration range of 25-100ppm at pH 4 are shown in Figure 4.3. Uninhibited solution exhibits Nyquist plot (Figure 4.3a) which is characterized by appearance of two time constants; a depressed capacitive semicircle from high frequencies (HF) to medium frequencies (MF) and an inductive loop at low frequencies (LF). In Bode plot (Figure 4.3b), there is a much significant increase in absolute impedance which indicates maximum protection at lower frequencies with addition of TBA compared to the blank solution. The impedance was observed to have increased with increase in concentration reaching its peak at 75ppm and then dropped at 100ppm. The more negative value of the phase angle at high frequency was observed with increasing inhibitor concentrations. Furthermore, the phase angle depression at relaxation frequency occurs with decrease in concentrations.

There is a capacitive semicircle from higher to medium frequencies just like in the blank solution. It is however obvious that TBA addition has significantly changed the mode of behavior of uninhibited steel in two ways:

1. The semicircle diameter which is ascribed to charge transfer resistance and double layer capacitance, increases with increase in concentration up to 75ppm. At 100ppm, the semicircle decreases which signifies a drop in inhibition efficiency compared to 50 and 75ppm.
2. The inductive loop noted in the uninhibited solution was observed to have disappeared in the TBA containing solutions.

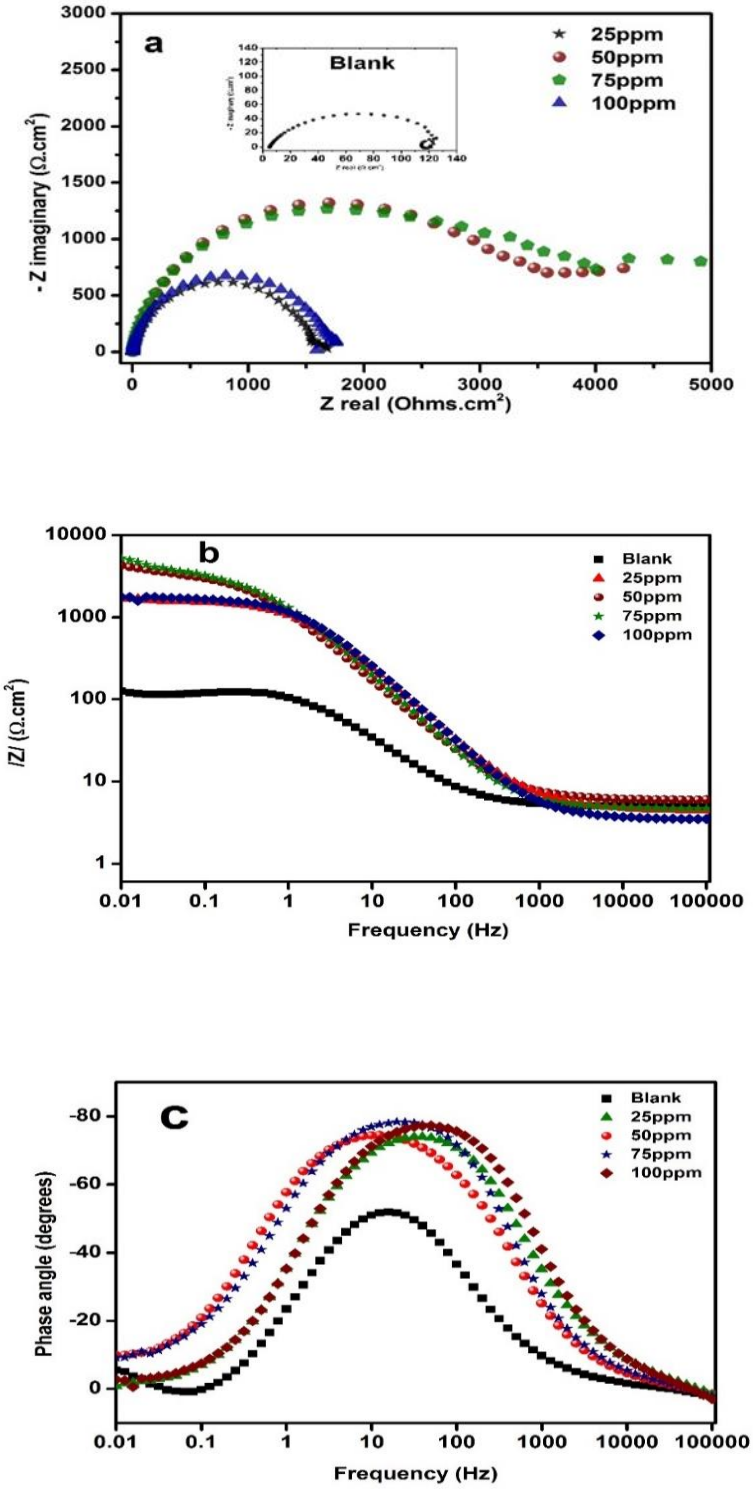

Figure 4.3: EIS Spectra for X60 Mild Steel in 3.5% CO_2 saturated NaCl with and without TBA at pH 4 and 25°C (a) Nyquist (b) Bode and (c) Phase angle plots.

The equivalent circuits used for the fitting of the EIS spectra are shown in Figure 4.4 and the extracted parameters are presented in Table 4.2. In the equivalent circuits, Parameters such as resistance of the solution (R_s) charge transfer resistance (R_{ct}) and electrical double layer capacitance are obtained. It is generally accepted to use a distributed circuit element in an electrical circuit since there is a non-ideal frequency response. The most widely used of such elements is the Constant Phase Element (CPE) since it has a non-integer dependence on frequency. Usually the double layer assumes a characteristics of a CPE rather than a pure capacitor. To fit the semicircle more accurately, CPE is substituted for a pure capacitor. The impedance of CPE is described by the following equation:

$$\boldsymbol{Z_{CPE}} = \frac{\mathbf{1}}{\boldsymbol{Y_o\,(j\omega)^n}} \qquad 4.6$$

Where Y_o is a proportional factor, j is an imaginary unit = $\sqrt{-1}$, $\omega = 2\pi f$ and n has a meaning of phase shift between 0 and 1 [88]. In fact, n can be a gauge for assessing surface heterogeneity and furnish information about the degree of roughness depending on its magnitude. CPE is a pure capacitance when n = 1 (Y =C), resistance when n = 0 (Y= R), inductance when n = -1 (Y = L) or Warburg impedance when n = 0.5 (Y = W) [64],[88].

The value of C_{dl} can be obtained from the following equation:

$$\boldsymbol{C_{dl} = Y_0\,(2\pi f_{max})^{n-1}} \qquad 4.7$$

Similarly, C_{dl} can be extracted using this relationship;

$$\boldsymbol{C_{dl}} = \frac{\mathbf{1}}{\boldsymbol{2\pi f_{max} R_{ct}}} \qquad 4.8$$

Where f_{max} is the maximum frequency of the imaginary part of impedance (rad s^{-1}).

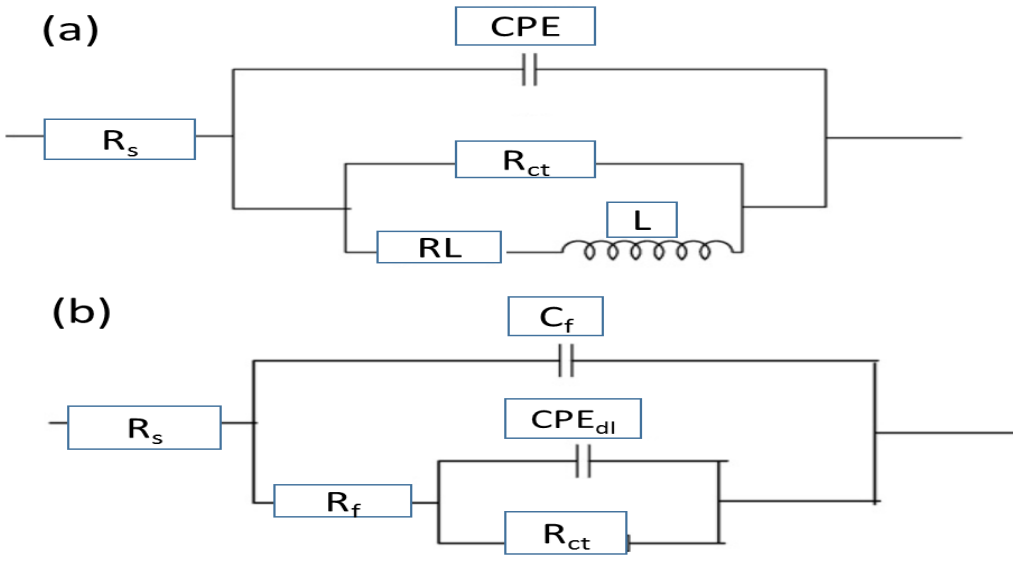

Figure 4.4: Equivalent Circuits used for fitting (a) Blank (b) Inhibited

Table 4.2 gives the parameters obtained from the fitting of the EIS spectra. We noted increase in charge transfer resistance from 25 -75ppm. However, the charge transfer resistance declined at 100 ppm. The C_{dl} although independent of the concentration, has decreased in the TBA containing solutions compared to the blank specimen. The EIS based inhibition efficiency fluctuation is presented in Figure 4.5.

Table 4.2 EIS parameters for the effect of TBA concentration at pH 4

Concentration (ppm)	R_s (Ω cm^2)	R_{ct} (Ω cm^2)	R_f (Ω cm^2)	C_{dl} ($\mu F/cm^2$)	C_f ($\mu F/cm^2$)	X^2 (10^{-4})	%IE
Blank	4.9	135.4	…	588	…	5.4	…
25	4.5	1580	2.8	101	19	5.0	91.2
50	4.6	3762	6.2	72	38	0.9	96.3
75	4.9	4748	8.8	83	60	0.4	97.1
100	3.6	1696	3.1	74	29	8.3	91.8

Figure 4.5 shows the effect of TBA addition in 3.5% CO_2-saturated NaCl using EIS. The result is in good agreement with that obtained from LPR.

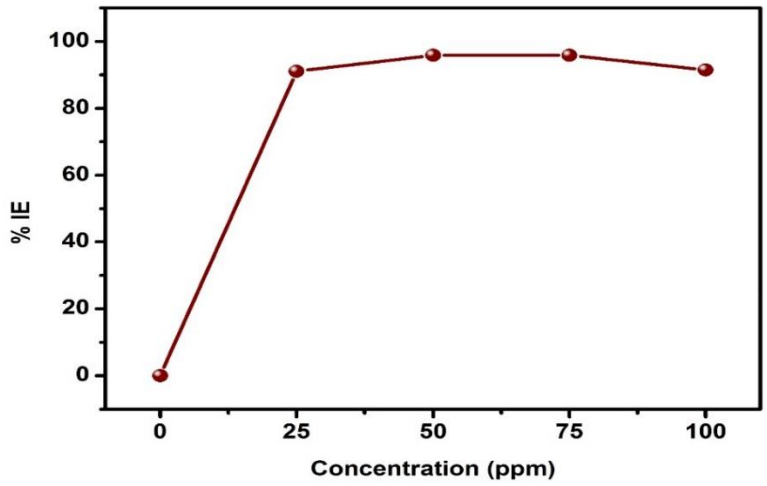

Figure 4.5: Behavior of X60 mild steel in CO_2 saturated 3.5% NaCl with and without TBA at pH 4 and 25°C for 2 hours from EIS

4.1.2. Effect of Concentration at pH 6

It is worthy to investigate the performance of a particular inhibitor in different pH as it is of the important parameters in CO_2 corrosion. In the sweet oilfield environment, pH varies between 4 and 6. Excellent performance of TBA was already observed at pH 4 in the last section of this chapter.

The linear polarization parameters for the X60 mild steel electrode in the absence and presence of TBA at pH 6 and 25°C after 2 hours are presented in Table 4.3 and plotted in Figure 4.6. Similar to the TBA behavior noted in pH 4, the 75ppm was noted as the peak concentration. As expected, it is also observed that the corrosion rate for X60 mild steel in the corrosive solution both in the presence and absence of TBA at pH 6 is lower than the similar experiments noted at pH 4, even though the efficiency generally remains the same.

Table 4.3: Behavior of X60 mild steel in CO_2 saturated 3.5% NaCl with and without TBA at pH 6 and 25°C for 2 hours from LPR

Concentration (ppm)	Rp (Ω cm^2)	C_R (mpy)	% IE
0	236.4	41.9	0
25	2291	4.3	89.7
50	4977	2.1	95.3
75	8297	1.1	97.1
100	3161	3.1	92.5

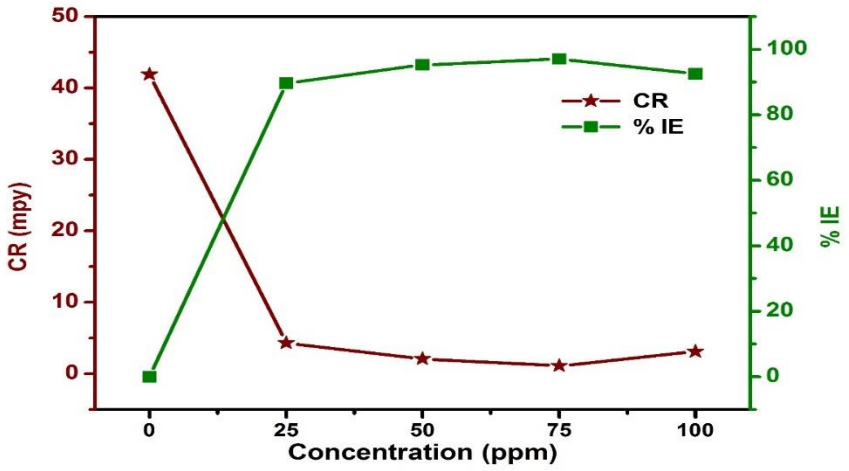

Figure 4.6: Behavior of X60 mild steel in CO_2 saturated 3.5% NaCl with and without TBA at pH 6 and 25°C using LPR

EIS spectra for X60 mild steel in CO_2 saturated 3.5%NaCl in the presence and absence of TBA at pH 6 and 25°C are shown in Figure 4.7. It is observed that the behavior of spectra in the Nyquist plot for the uninhibited solution has changed with TBA addition. There is an increase in semicircle diameter and disappearance of the inductive loop as noted

similarly in the case of pH 4 previously. For the inhibited samples, the overall behavior remains the same as in pH 4 except that the semicircles are wider which indicates lower corrosion rates. Consistent with polarization measurements, the overall performance was not much different.

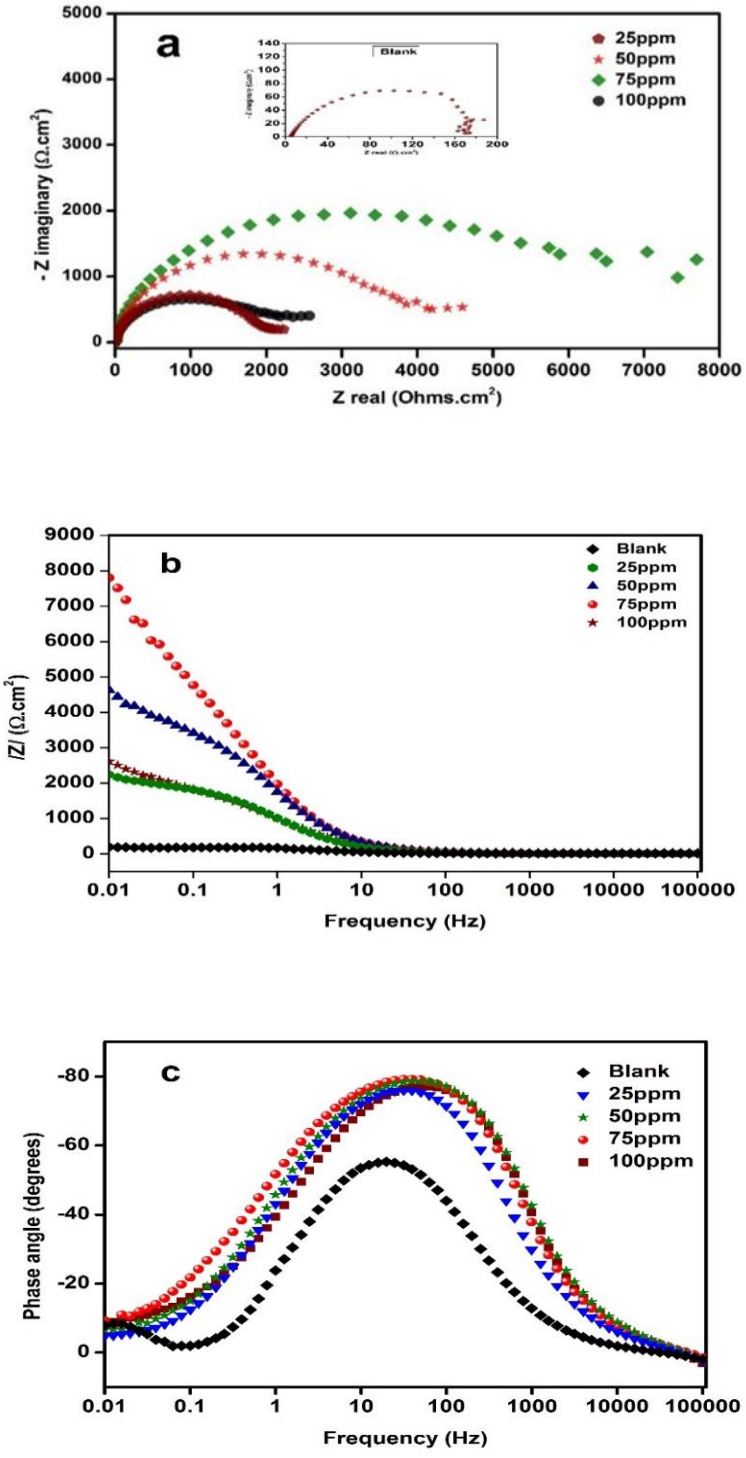

Figure 4.7: EIS Spectra for the behavior of X60 Mild Steel in 3.5% CO_2 saturated NaCl with and without TBA at pH 6 and 25°C (a) Nyquist (b) Bode and (c) Phase angle plots.

Table 4.4 presents the results obtained by fitting of the EIS spectra for the behavior of X60 mild steel in sweet oilfield conditions at pH 6. The charge transfer resistance has significantly increased with addition of TBA up to 75 ppm. At 100 ppm the resistance drops lower than 50 and 75ppm. The capacitance of the double layer which has an inverse relationship with its thickness reduces significantly in the presence of TBA.

Table 4.4: EIS parameters for the behavior of X60 mild steel in CO_2-saturated 3.5% NaCl at pH 6 and 25°C with and without TBA

Concentration (ppm)	Rs(Ω cm^2)	Rct(Ω cm^2)	Rf (Ω cm^2)	C_{dl} (µF/cm^2)	C_f (µF/cm^2)	X^2 (10^{-4})	%IE
Blank	5.3	166.7	…	478	…	23	…
25	4.6	2100	5.9	120	48	18	91.8
50	4.5	4342	9.3	73	33	19	96.0
75	5.3	7875	9.9	80	35	26	97.8
100	3.5	2716	4.4	92	48	18	93.7

Figure 4.8 presents the effect of TBA on X60 mild steel in CO_2saturated 3.5% NaCl in the absence and presence of TBA range of concentration from 25 – 100ppm. As noted in case of the behavior in pH 4, 75ppm remains as the peak concentration. There is a strong correlation between LPR and EIS results.

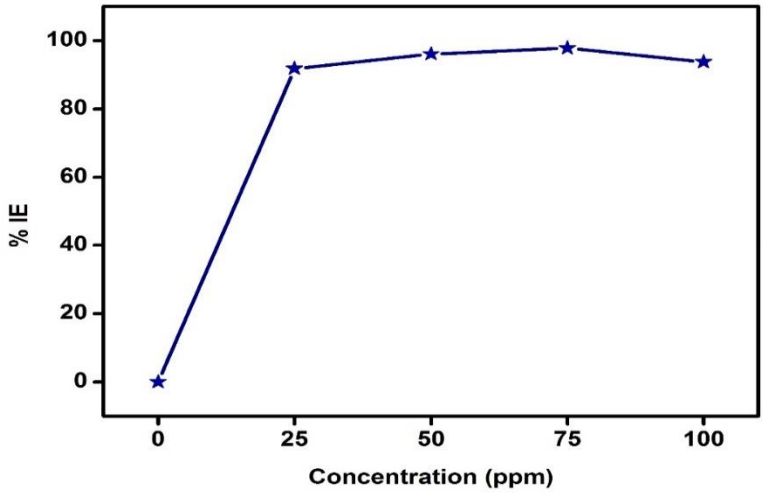

Figure 4.8: Behavior of X60 mild steel in CO_2 saturated 3.5% NaCl with and without TBA at pH 6 and 25°C using EIS

4.1.3. Comparison for TBA performance in pH 4 and 6

It was observed by comparing between pH 4 and 6 in the aforementioned tests that the corrosion rate for both blank and inhibited solutions at pH 4 is higher than that at pH 6. The overall performance of the inhibitor however remains the same. This is clearly illustrated in Figure 4.9

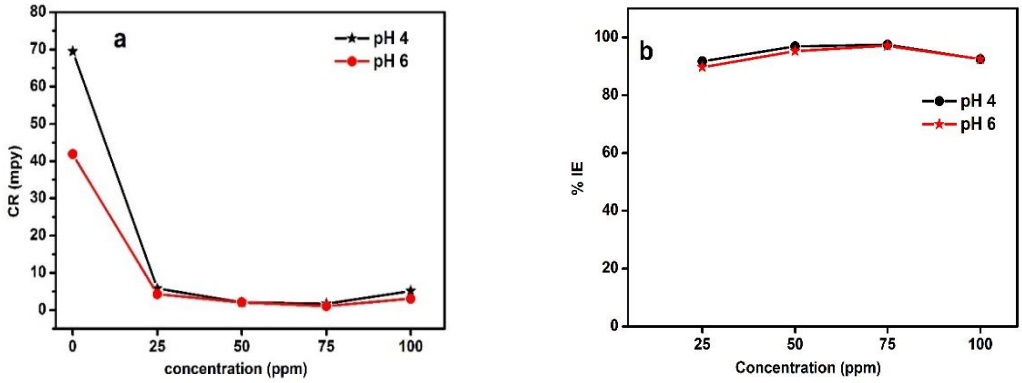

Figure 4.9: Comparison of behavior of X60 mild steel in CO_2 saturated 3.5% NaCl in the presence and absence TBA in pH 4 and 6 (a) Corrosion rate (b) % IE

4.1.4. Effect of Temperature

This section presents the temperature effect on corrosion behavior of X60 mild steel in the sweet environment with and without TBA addition. Because temperature affects almost all chemical and electrochemical reactions, some inhibitors as well are sensitive to temperature changes. The performance of a particular inhibitor may change depending on the temperature. Furthermore, inhibitor's response to a range of temperature is usually used as a criterion for assessing mode of adsorption taking place.

Table 4.5: Effect of Temperature on TBA at pH 4 for 2 hours

	Blank		50ppm		
Temperature(^{o}C)	R_p ($\Omega.cm^2$)	C_R (mpy)	R_p ($\Omega.cm^2$)	C_R (mpy)	%IE
25	142.6	69.5	4655	2.1	96.9
40	93.5	106.1	3952	2.5	97.6
60	64.5	153.7	3006	3.3	97.9
80	56.6	175.2	2801	3.5	98.0

Table 4.5 and Figure 4.10 show that the corrosion rate for the the inhibitor-free solutions increase significantly with temperature rise up to 60^{o}C and then slightly as temperature was raised to 80^{o}C. In the case of the TBA containing solutions, the corrosion rate slightly decreases with temperature increase. However, the overall inhibitor performance was found to show little increase as the temperature was increased from 25 – 80^{o}C.

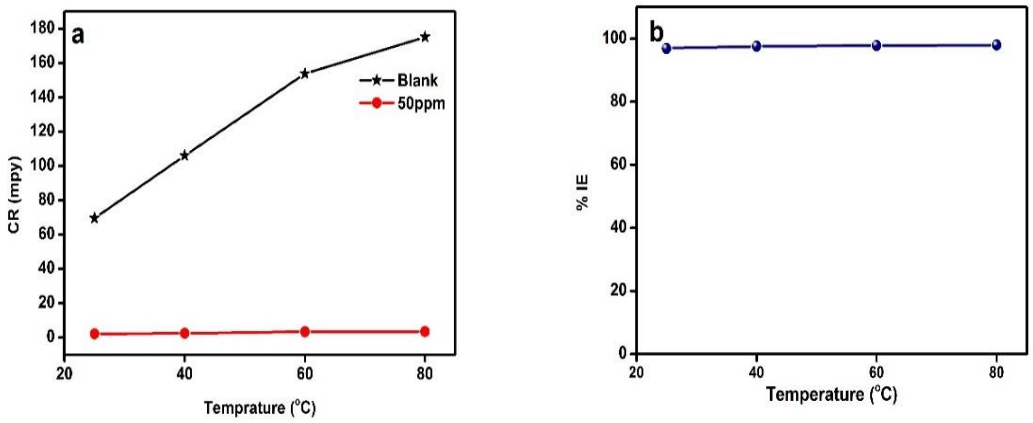

Figure 4.10: Effect of Temperature on Behavior of X60 mild steel in CO_2 saturated 3.5% NaCl with and without TBA (a) corrosion rate (b) % Efficiency

EIS results of the temperature effect on the performance of TBA on the corrosion inhibition of X60 mild steel in sweet oilfield conditions are presented in Table 4.6 as well as Figure 4.11. There is observed a strong agreement between the EIS and LPR results.

Table 4.6: EIS Results for the effect of temperature on corrosion of X60 mild steel in CO_2 saturated 3.5% NaCl with and without TBA at pH 4.

Solution	Temp. (°C)	Rs (Ω cm^2)	Rct (Ωcm^2)	Rf (Ωcm^2)	C_{dl} (μF/cm^2)	C_{dl} (μF/cm^2)	X^2 (10^{-4})	%IE
Blank	25	4.9	135.4	…	588	…	5.4	…
	40	4.2	65.3	1.6	617	130	0.2	…
	60	2.8	41.1	1.6	487	130	0.39	…
	80	2.1	40.4	…	496	0.16	0.37	…
50ppm	25	6.1	3762	6.1	73	0.35	0.19	96.2
	40	5.0	2697	4.9	65	0.44	0.4	97.4
	60	2.8	2228	2.7	56	0.22	0.45	98.0
	80	2.3	2005	2.4	32	0.50	0.56	97.9

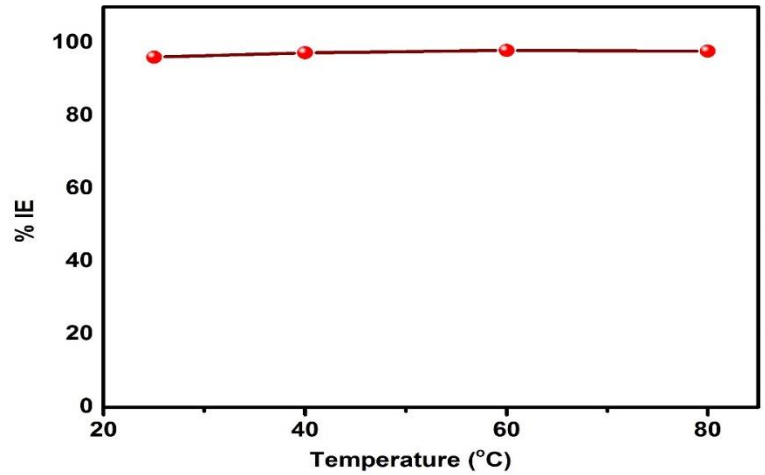

Figure 4.11: EIS Result for the effect of temperature on TBA at pH 4 for 2 hours

4.1.5. Effect of immersion time on TBA

Table 4.7 shows the LPR data for the time influence on sweet corrosion of X60 mild steel both in absence and presence of 50 ppm TBA.

Table 4.7: Effect of exposure time on TBA at 25°C and pH 4

	Blank		50ppm		%IE
Time(Hrs)	CR (mpy)	Rp(Ωcm^2)	CR (mpy)	Rp(Ωcm^2)	
2	69.5	142.6	2.1	4655	96.9
12	75.6	131.1	1.8	5469	97.6
24	81.5	121.7	1.6	6248	98.1
48	93.7	105.8	1.5	6701	98.4
72	95.8	103.4	1.4	7202	98.6

It can be observed that the corrosion rate for the uninhibited solution increases with time while that of the inhibited one decreases slightly with time. The overall efficiency increases slightly with time. This trend is shown by Figure 4.12.

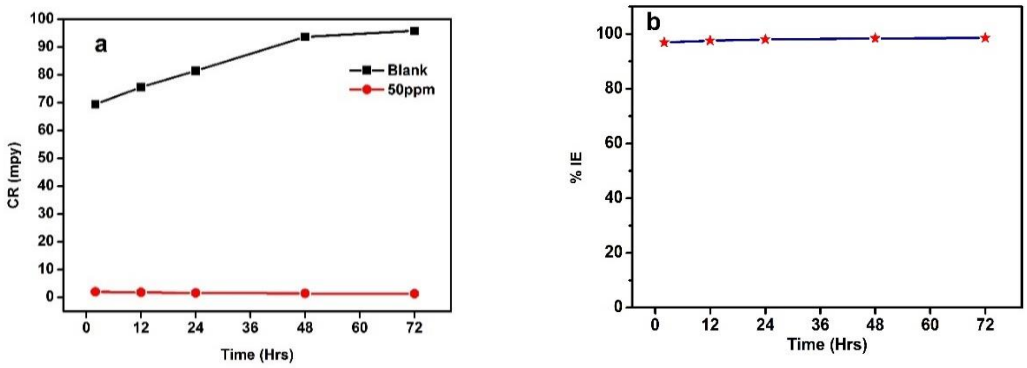

Figure 4.12: Effect of time on sweet corrosion inhibition of X60 mild steel in with 50ppm TBA at pH 4 (a) corrosion rate (b) % IE.

The EIS spectra for both blank and TBA-containing solution are presented respectively in Figures 4.13 and 4.14. According to EIS Nyquist results displayed in Figure 4.13a, all the spectra are characterized by appearance of a depressed semicircle with center under the real axis from higher to medium frequencies. At lower frequencies, the inductive loop appears. The magnitude of inductive loop however reduces with time. The diameter of semicircle which signifies charge transfer resistance becomes smaller with time. With TBA addition according to Figure 4.14, the mode behavior has changed. The inductive loop observed in uninhibited steel disappeared. Furthermore, the capacitive semicircle which indicates charge transfer resistance and hence corrosion inhibition has increased. As the time increases, the charge transfer resistance increases contrary for the uninhibited electrode which decreases with time. More so, we observed the appearance the second peak at the medium frequencies in the phase angle plot as time of immersion increases.

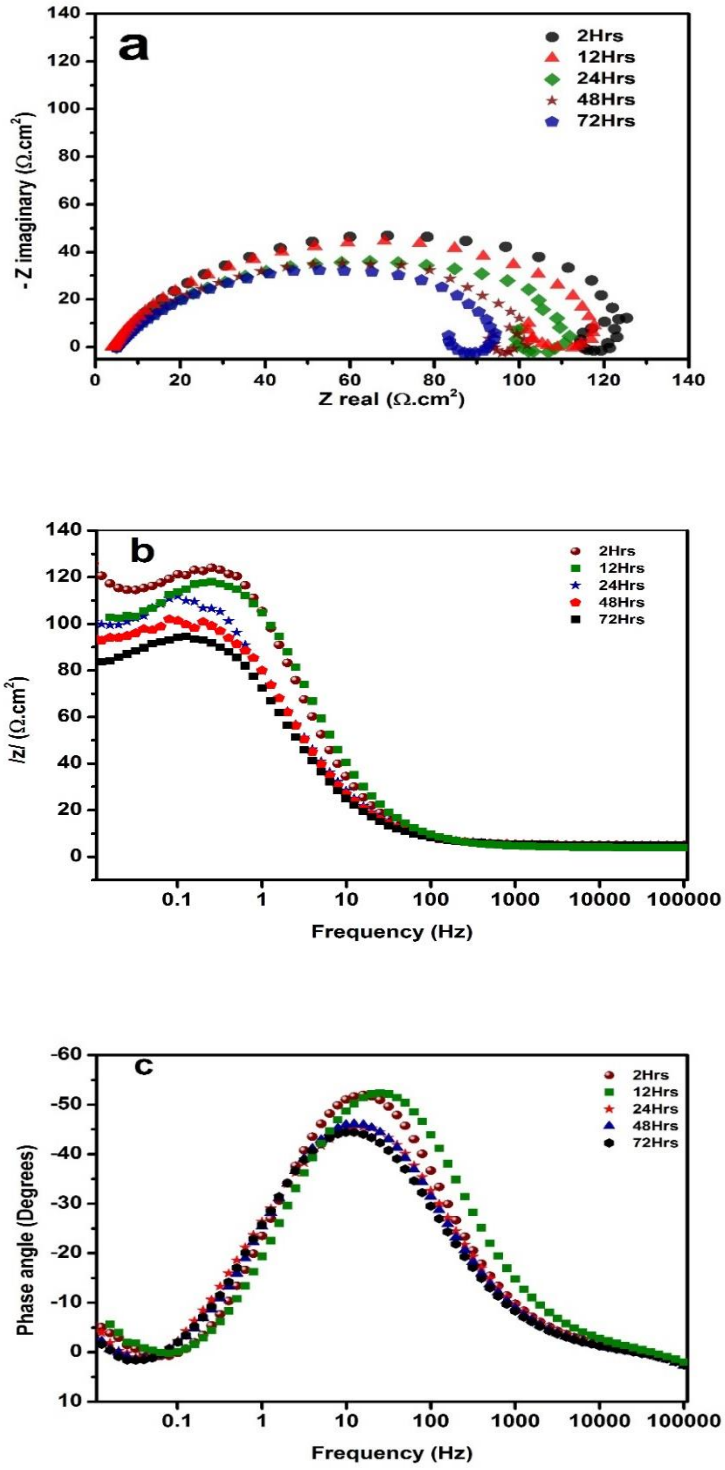

Figure 4.13: EIS results for the effect of time on corrosion of X60 mild steel in CO_2-saturated 3.5 % NaCl at 25°C and pH 4 (a) Nyquist (b) Bode and (c) Phase angle.

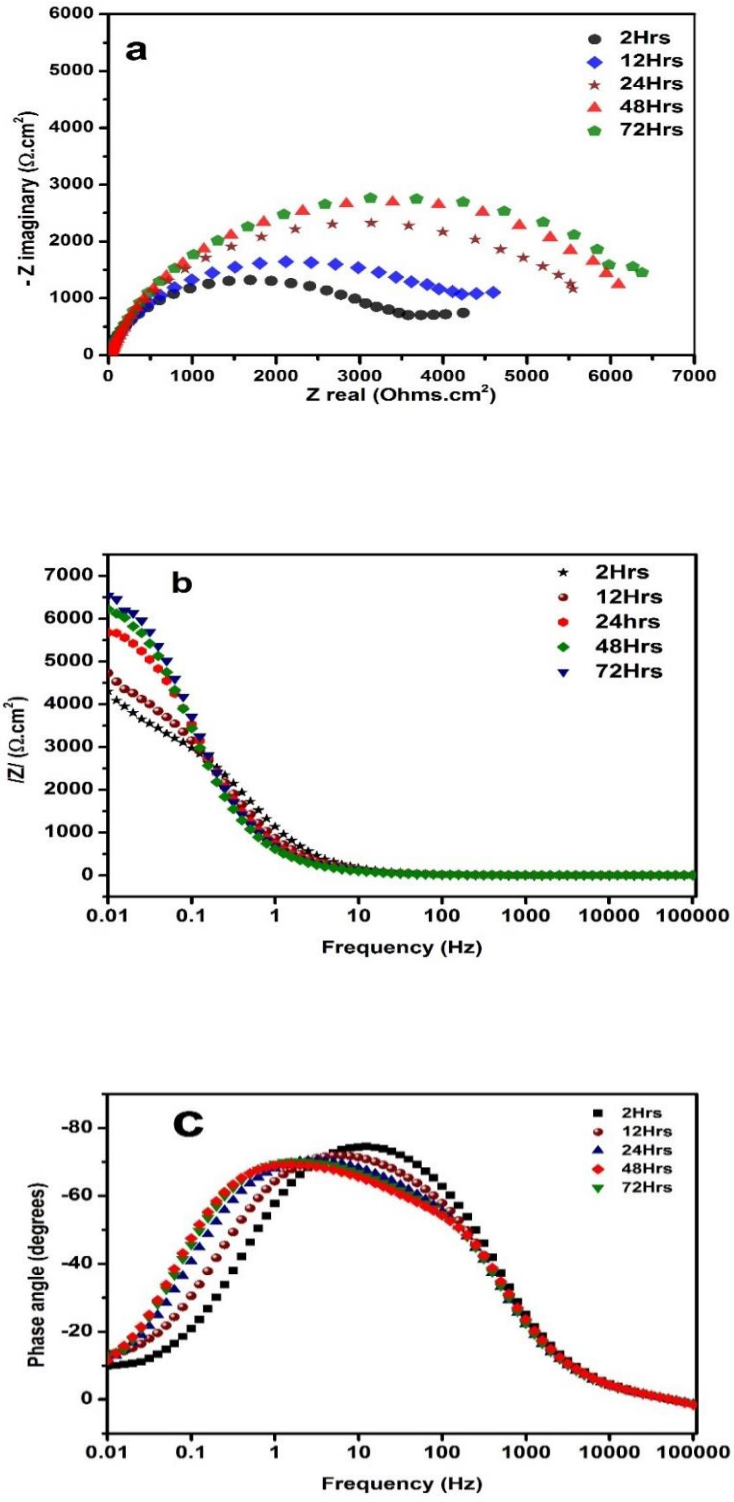

Figure 4.14: EIS results for the effect of time on corrosion of X60 mild steel in CO_2 saturated 3.5 % NaCl with and without 50ppm TBA at 25°C and pH 4 (a) Nyquist (b) Bode and (c) Phase angle.

Table 4.8 presents the fitting parameters of Figures 4.13 and 4.14. The charge transfer resistance has decreased continuously with time in the uninhibited solution. Moreover, in the presence of TBA, the charge transfer resistance has increased continuously with time. This joint effect, makes the inhibition efficiency also to increase with time and is plotted in Figure 4.15. On the other hand, the double layer capacitance of the inhibited solution which is higher than that of TBA containing formulation increased continuously while that of TBA decreased with time.

Table 4.8: EIS parameters on the effect of time on X60 mild steel sweet corrosion in the absence and presence of TBA

Solution	Time (Hrs)	Rs (Ω cm^2)	Rct (Ω cm^2)	Rf (Ω cm^2)	C_{dl} (µF.cm^2)	C_{dl} (µF.cm^2)	X^2 x 10^{-4}	%IE
Blank	2	4.9	135.4	…	588	…	5.4	…
	12	4.9	125.3	…	901	…	6.4	…
	24	4.9	117.1	…	1002	…	4.5	…
	48	4.9	107.7	…	932	…	2.7	…
	72	5.0	100.9	…	995	…	2.8	…
50ppm	2	6.1	3762	6.2	72	37.5	0.19	96.2
	12	6.1	4656	8.6	215	44.1	0.12	97.0
	24	6.2	6225	19.4	3.22	53.7	8.0	98.0
	48	6.2	7032	26.4	3.58	57.6	0.15	98.4
	72	6.2	7243	26.6	2.77	57.7	0.12	98.5

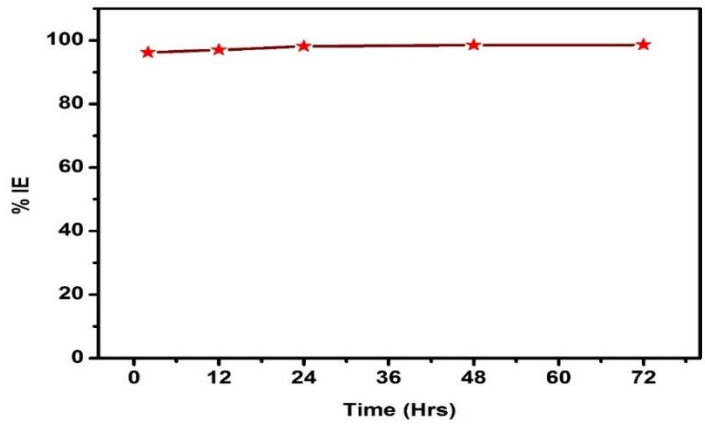

Figure 4.15: Effect of time on TBA at 25°C and pH = 4 obtained from EIS

4.1.6. Potentiodynamic Polarization behavior

In addition to EIS and LPR experiments, potentiodynamic polarization tests were conducted in order to investigate the inhibition mechanism.

Table 4.9: Tafel analysis for X60 mild steel in the absence and presence of TBA

Concentration (ppm)	E_{corr} (mV)	i_{corr} (µA/cm^2)	b_a (mV/decade)	b_c (mV/decade)	%IE
Blank	-707	231	55.5	306	
25	-680	7.42	37.7	46.4	96.8
50	-680	6.23	32.2	38.4	97.3
75	-672	2.69	26.9	26.6	98.9
100	-696	9.62	23.8	23.7	95.8

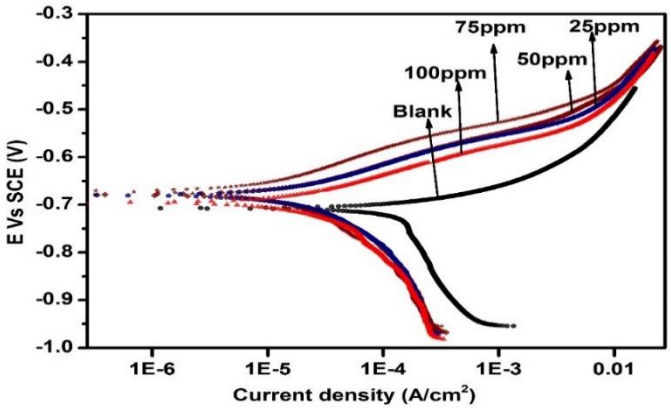

Figure 4.16: Potentiodyanamic polarization curves for blank and 50ppm TBA after at pH 4 and 25°C 2 hours.

Table 4.9 and Figure 4.16 show shifts in E_{corr} from a more negative value for blank specimen to a more noble value for the inhibited one. Also, the corrosion current density was significantly reduced from higher value for the uninhibited to a lower value for the inhibited sample.

4.1.7. Surface Characterization

In this section, the results for surface characterization namely; SEM, XPS and FTIR are presented.

SEM

The images in Figure 4.17 represent the specimens before immersion and after immersion CO_2-saturated 3.5% NaCl with and without 50ppm TBA addition at 25°C and pH = 4. We observed a serious damage for inhibitor-free sample compared to the sample inhibited with 50ppm of the inhibitor. There is no significant change in morphology for the sample inhibited with TBA compared to the sample before immersion.

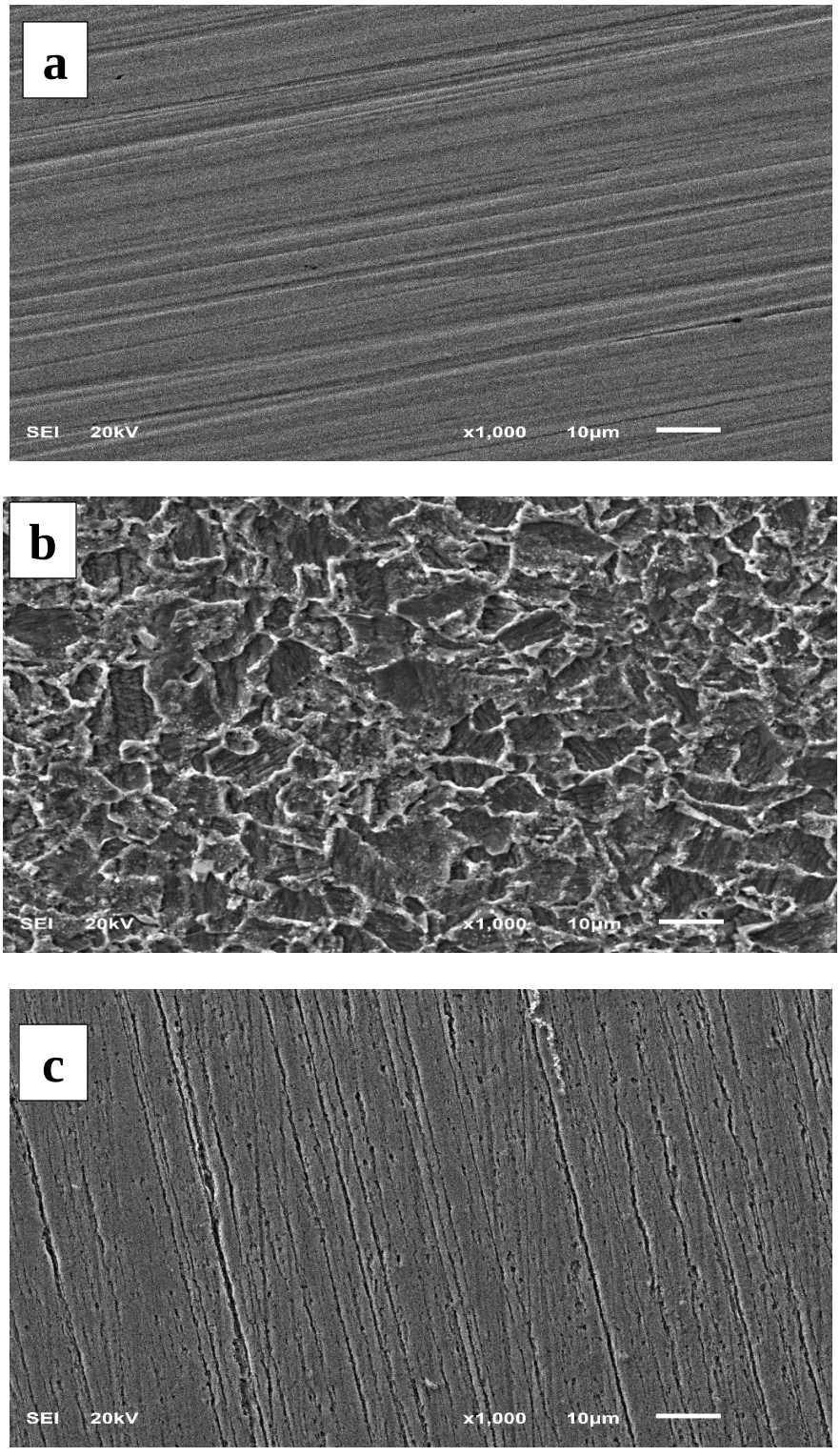

Figure 4.17: SEM images for X60 mild steel (a) before immersion and after immerstion in CO_2 –saturated 3.5% NaCl (b) without inhibitor (c) with 50 ppm TBA

XPS

XPS analysis for both wide and narrow scans were carried out in absence and presence of 50ppm TBA at 25^{o}C and pH = 4. In the wide scan, majorly peaks for C1s, O1s and Fe2p have been detected for both the inhibited and blank specimen according to Figure 4.18. Sulfur and nitrogen were not detected. However, in the narrow scan (Figure 4.19) for the blank and (Figure 4.20) for the inhibited, high resolution XPS analysis show the absence of sulfur in blank sample but present at 162 eV for the TBA contained sample. This is clearly seen by comparing Figure 4.19(e) and 4.20(e).

The binding energy of the XPS peaks, proportions (in atomic weight %) and their corresponding possible assignments are detailed in Table 4.10

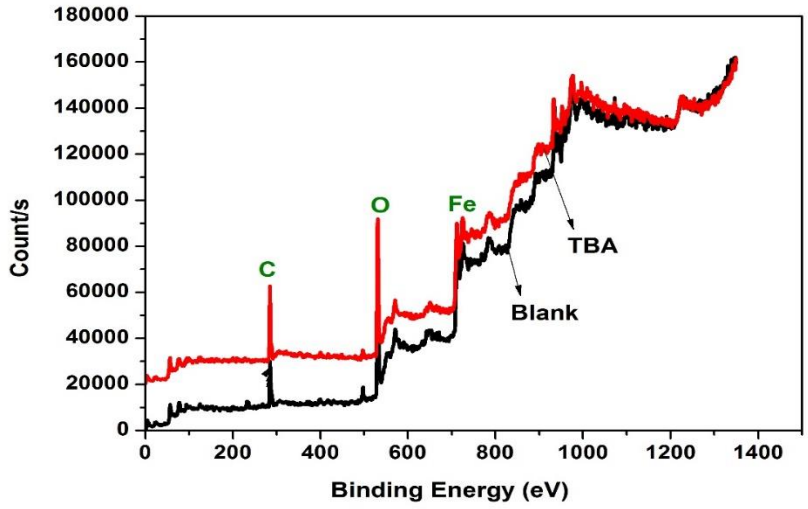

Figure 4.18: Survey scan spectra for mild steel surface product obtained after 24 hours immersion time in 3.5 % NaCl at 25^{o}C and pH = 4 with and without 50ppm TBA

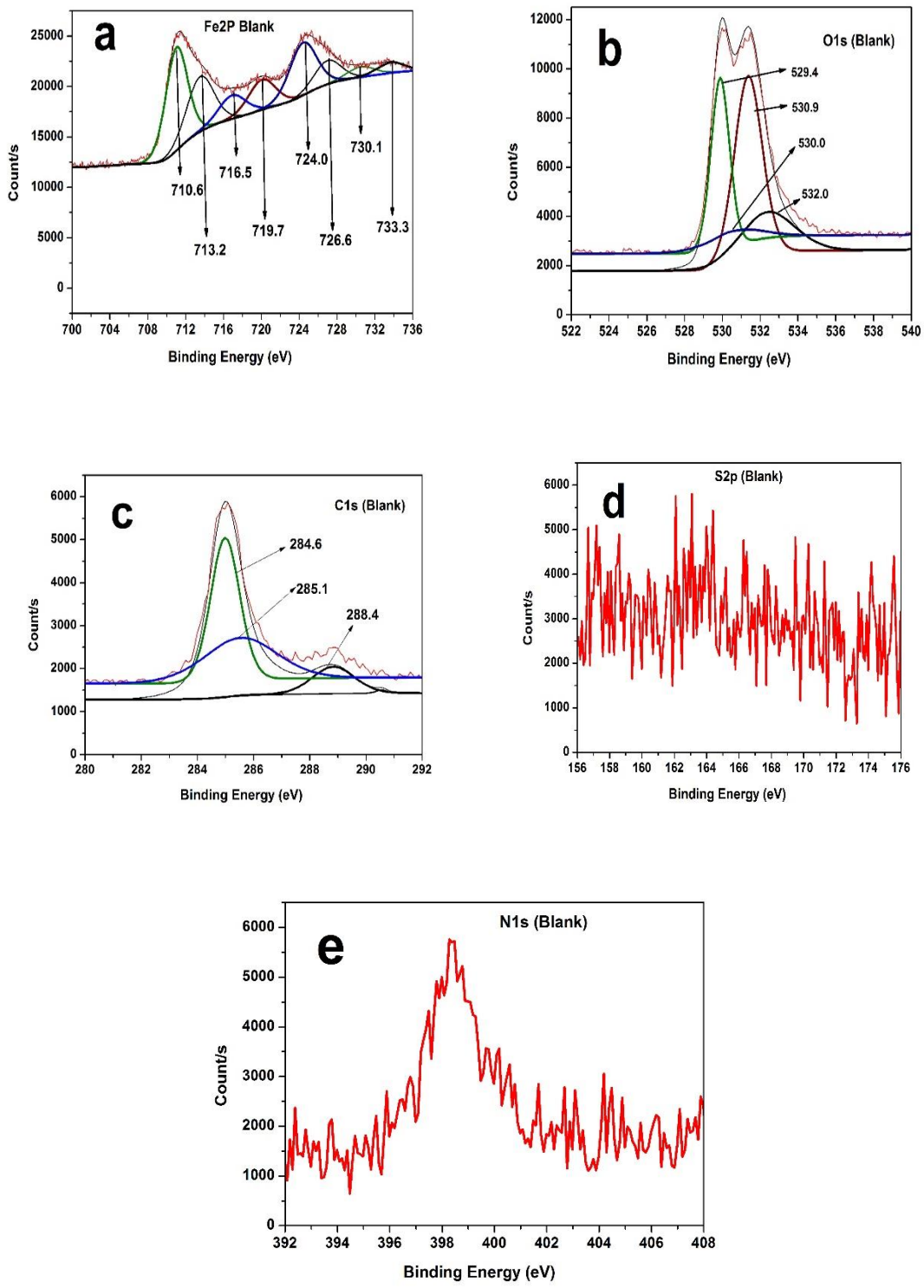

Figure 4.19: High Resolution XPS Spectra for mild steel after 24 hours immersion at 25^{o}C and pH = 4 in CO_2 - saturated 3.5 % NaCl: (a) Fe2p (b) O1s (c) C1s (d) S2p.

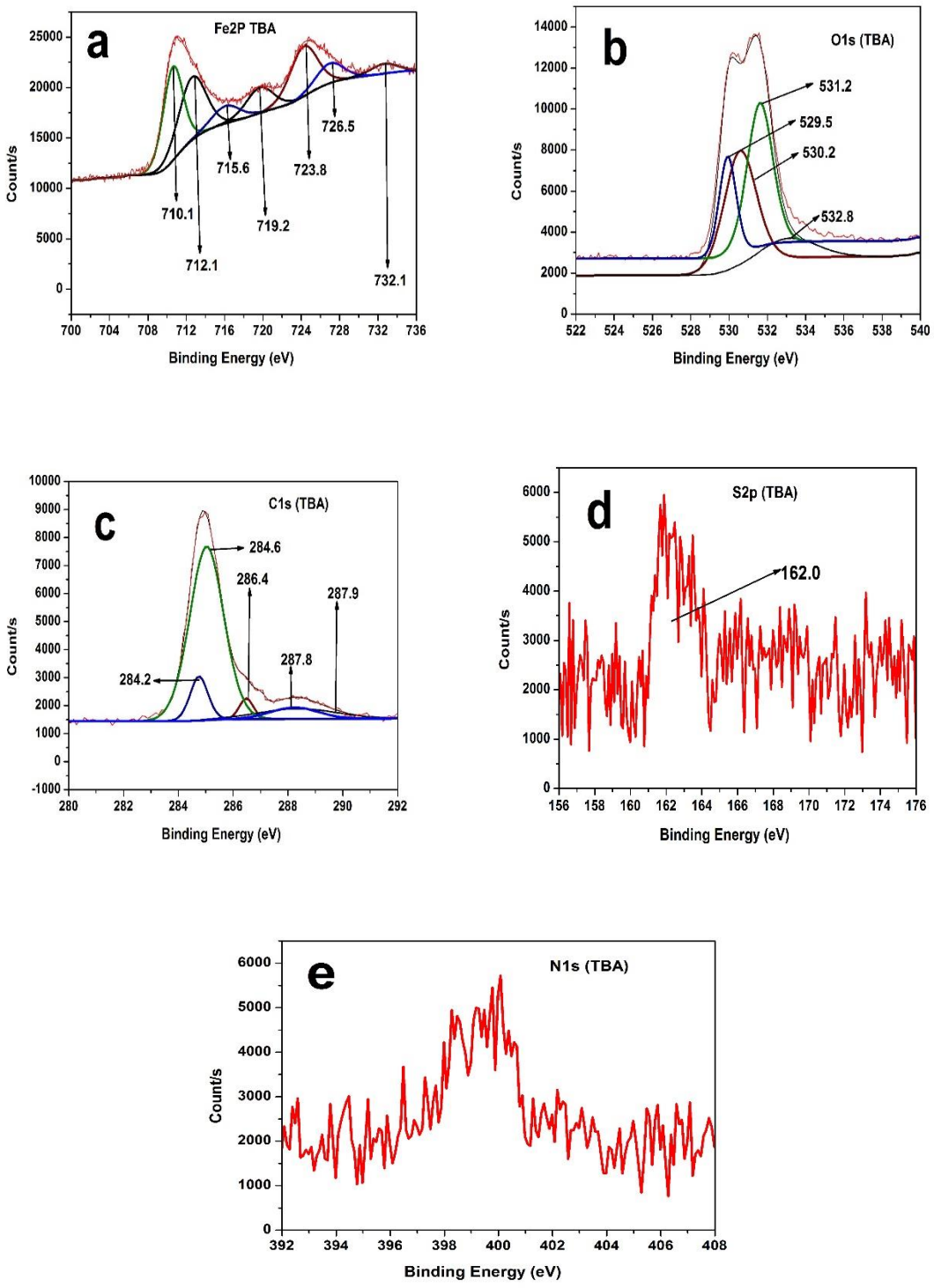

Figure 4.20: High Resolution XPS Spectra for mild steel after 24 hours immersion at 25°C and pH = 4 in CO_2 - saturated 3.5 % NaCl with 50ppm TBA: (a) Fe2p (b) O1s (c) C1s (d) S2p.

Table 4.10: XPS spectral analysis for the surface products on mild steel after 24-hours immersion in CO_2 -saturated 3.5 % NaCl in the absence and presence of 50ppm TBA

Concentration (ppm)	Peak	Energy (eV)	Atomic Weight (%)	Possible Assignment
Blank	Fe2p	710.6	28.84	FeO, $FeCO_3$, Fe_2O_3, $FeCl_2$
		713.2	18.92	Fe_2O_3, FeOOH
		724.0	18.26	$FeCO_3$, Fe_3O_4, Fe_2O_3
	O1s	529.4	30.29	Fe_2O_3, FeO
		530.0	7.74	Fe_2O_3, FeO
		530.9	42.97	FeOOH, $FeCO_3$
		531.9	18.99	C=O
	C1s	284.6	50.16	C-C
		285.1	37.08	C-O-C
		288.4	12.77	O-C=O or CO_3
50	Fe2p	710.1	26.89	FeO, $FeCO_3$, Fe_2O_3, $FeCl_2$
		712.1	24.73	FeS, $FeSO_2$, FeOOH,
		723.8	19.75	$FeCO_3$, Fe_3O_4, Fe_2O_3
	O1s	529.5	16.91	Fe_2O_3, FeO
		530.2	35.95	Fe_2O_3, FeO
		531.2	36.97	FeOOH, $FeCO_3$
		532.8	10.17	C=O
	C1s	284.2	9.50	C=C
		284.6	70.73	C-C
		286.0	3.56	C-O-C, C=N
		287.8	6.57	C=O, C-N
		287.9	9.65	C=O, C-N
	S2p	167.6	34.82	SO_2
		162.0	65.18	FeS

FTIR

Figure 4.21 represents FTIR peaks and their corresponding wavenumbers for X60 mild steel in 3.5% NaCl with and without 50ppm TBA inhibitor. Both inhibited and uninhibited specimen show peaks with almost same intensity at 3408 cm^{-1}. Contrary, peaks with numbers 679, 1410, 1545 and 3777 cm^{-1} were observed to be present in TBA-containing mild steel but absent in the TBA-free specimen.

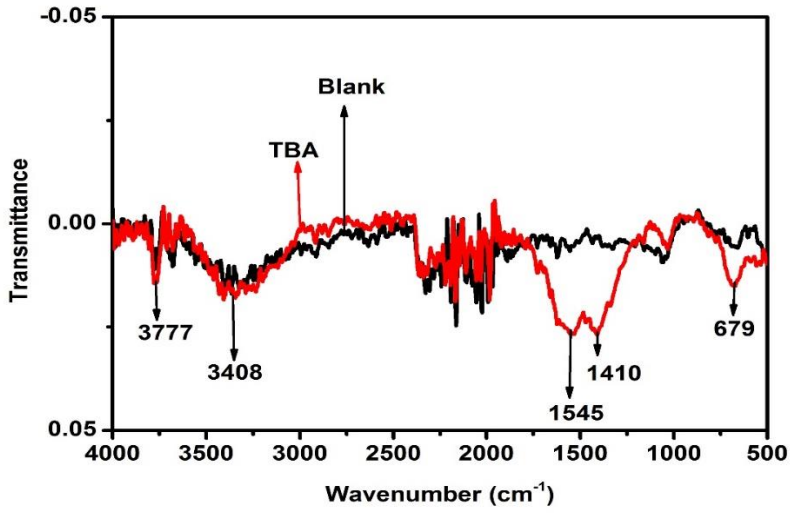

Figure 4.21: FTIR Spectra for the X60 Mild Steel immersed in CO_2-saturated 3.5% NaCl in the absence and presence of 50ppm TBA inhibitor at 25°C after 24 hours

Table 4.11 shows the noted FTIR bands with the possible functional groups responsible for such absorptions.

Table 4.11: FTIR Spectra analysis for the X60 Mild Steel in CO_2-saturated 3.5% NaCl in the absence and presence of 50ppm TBA inhibitor at 25°C after 24 hours

FTIR Band (cm^{-1})	Assignment
679	Adjacent H wagging or C=S
1410	Aromatic C=C Stretching
1545	C=N Stretching
3407	O-H Stretching
3777	N-H

4.2. Tannic Acid

4.2.1. Effect of concentration

The Rp values and corrosion rates obtained from LPR measurements for X60 mild steel both in the absence and presence of different concentrations of tannic acid are presented in Table 4.12.

Table 4.12: Effect of tannic acid concentration at 25°C and pH 4 after 2 hours

Concentration (ppm)	R_p (Ω cm^2)	C_R (mpy)	% IE
Blank	142.6	69.5	…
100	218.8	45.3	34.8
250	255.3	38.8	44.1
500	281.7	35.2	49.4
1000	212.5	46.6	32.9

Figure 4.17 presents the variation of corrosion rates and corresponding efficiencies with TA concentration.

It could be seen apparently that as the corrosion rate decreases with increase of TA dose, the efficiency rises to a higher value.

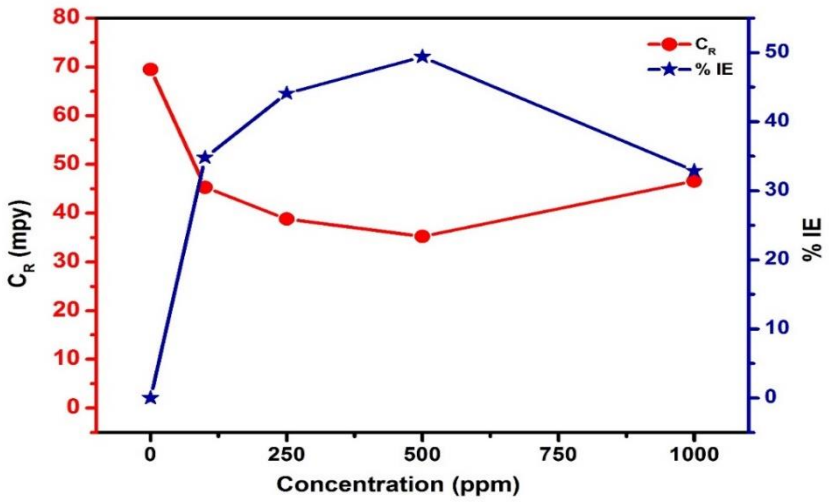

Figure 4.22: Effect of tannic acid concentration at 25°C and pH 4 from LPR

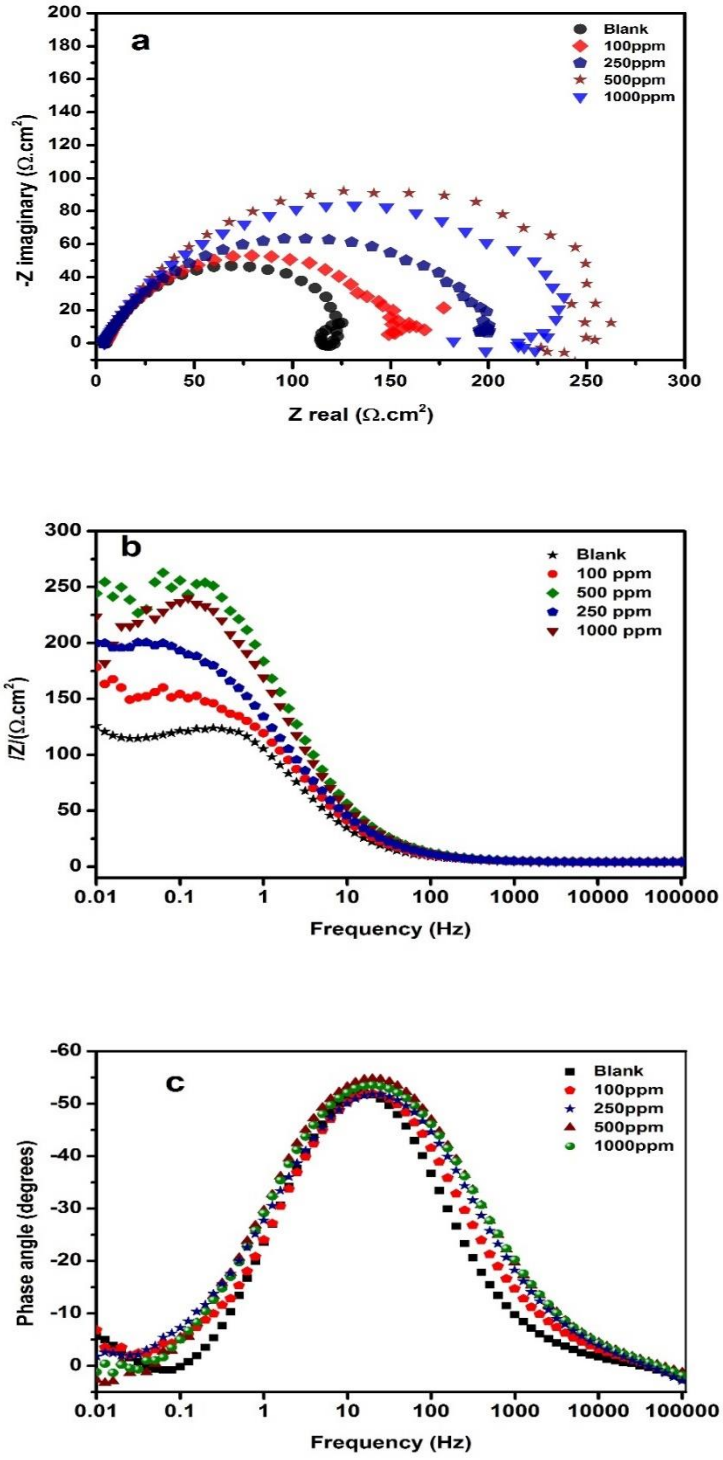

Figure 4.23: EIS Spectra for the effect of tannic acid concentration at 25°C and pH 4

The equivalent circuit used for fitting both blank and inhibited EIS results was already presented in Figure 4.4 (a). EIS results for the impact of TA concentration are presented in Figure 4.24 and the values extracted from the fitting are presented in Table 4.13. All the spectra exhibit a depressed semicircle with the center under the real axis. However, uninhibited electrode has an inductive loop at the lower frequencies. Apparently, with addition of tannic acid the inductive loop disappeared up to 500ppm. At 1000ppm, the inductive loop appears though smaller than the uninhibited one.

Table 4.13: EIS results for the effect of concentration on TA at 25°C and pH 4

Concentration (ppm)	Rs (Ω cm^2)	Rct (Ω cm^2)	Cdl (μF.cm^2)	X^2 x 10^{-4}	%IE
Blank	4.9	135.4	588	5.4	…
100.0	4.4	156.6	520	7.4	12.9
250.0	4.0	200.8	499	2.7	31.5
500.0	4.3	280.3	358	6.3	50.5
1000.0	4.1	255.1	393	8.9	45.7

Figure 4.24 presents the EIS based study of the behavior of X60 mild steel with changing TA concentrations in 3.5 % NaCl saturated with CO_2.

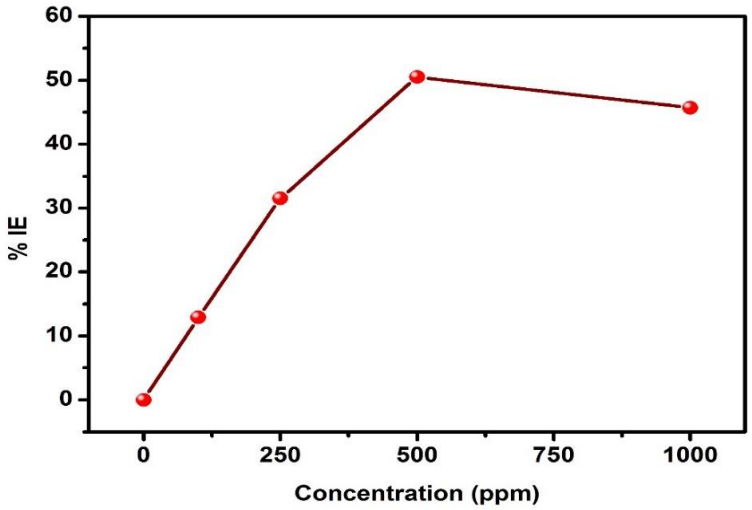

Figure 4.24: EIS result for the effect of tannic acid on the corrosion of mild steel in CO_2-saturated 3.5% NaCl at 25°C and pH = 4.

4.2.2. Synergistic effect

Addition of 2g/L of potassium iodide to 250ppm and 500ppm has synergistically raised their performances as it can be seen in Table 4.14.

Table 4.14: Synergistic effect of addition of KI on TA for corrosion inhibition of X60 mild steel in CO_2-saturated 3.5% NaCl from LPR

Concentration (ppm)	Rp (Ω cm2)	CR (mpy)	% IE
Blank	142.6	69.5	0
250	255.3	38.8	44.1
500	281.7	35.2	49.4
250 + 2g/L KI	468.1	21.2	69.5
500 + 2g/L KI	322.1	30.8	55.7

The Nyquist plot according to Figure 4.25 (a) revealed that addition of KI has raised the charge transfer resistance and hence improved the efficiency of the inhibitor compared to KI-free formulations. The Fitted parameters in table 4.15 also agree well with the behavior observed in the Plot. This result is consistent with what was observed in LPR studies.

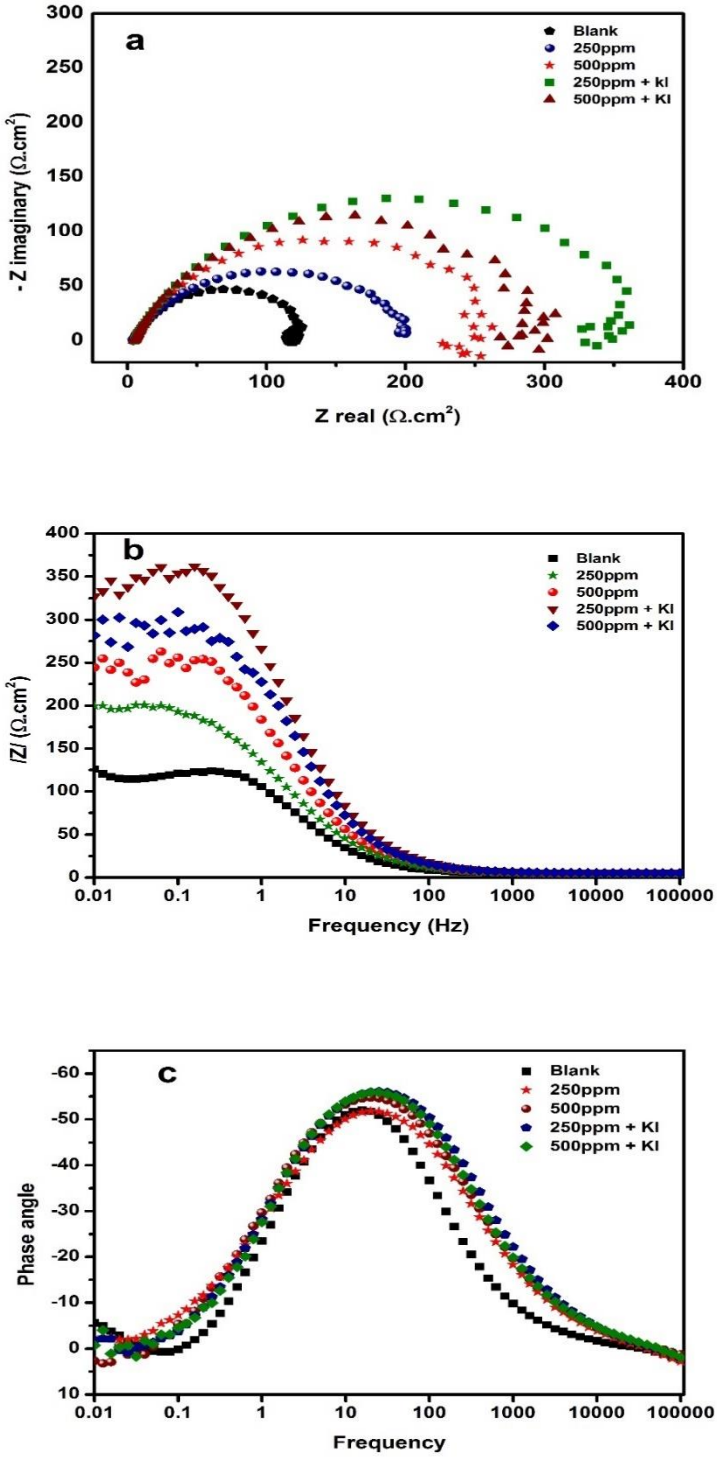

Figure 4.25: EIS results for the synergistic effect of KI addition on TA for corrosion protection of X60 mild steel in sweet environment at pH 4 and 25°C

Table 4.15: EIS parameters for the synergistic addition of KI to TA at 25°C and pH 4

Concentration (ppm)	Rs (Ω cm^2)	Rct (Ω cm^2)	Cdl (μF.cm^2)	X^2 (10^{-4})	%IE
Blank	4.9	135.4	588	5.4	…
250.0	4.0	200.8	499	2.7	31.5
500.0	4.3	280.3	358	6.3	50.5
250 + KI	5.2	386.2	260	3.0	64.2
500 + KI	5.0	314.2	320	7.8	56.0

4.2.3. Effect of immersion time on TA inhibition

Table 4.16 presents the results for the variation of TA performance on corrosion inhibition of X60 mild steel in CO_2 saturated 3.5% NaCl at 25°C and pH 4.

Table 4.16: Effect of immersion time on TA performance on corrosion inhibition of X60 mild steel in CO2 saturated 3.5% NaCl at 25°C and pH 4.

	Blank	250ppm		500ppm		250ppm + 2g/L KI		500ppm + 2g/L KI	
Time (Hrs)	Rp (Ω.cm^2)	Rp (Ω.cm^2)	% IE	Rp (Ω.cm^2)	% IE	Rp (Ω.cm^2)	% IE	Rp (Ω.cm^2)	% IE
2	142.6	255.5	44.1	281.6	49.4	470	69.6	322.9	55.7
12	111.2	321.8	65.4	385.7	71.1	918	87.9	981.4	88.7
24	105.8	406.2	73.9	456.8	76.8	1271	91.6	1321.6	92.1

Figure 4.26 gives a representation of the change in corrosion rate of X60 mild steel exposed in 3.5% NaCl saturated with CO_2 in the presence and absence of TA and TA+ KI with time.

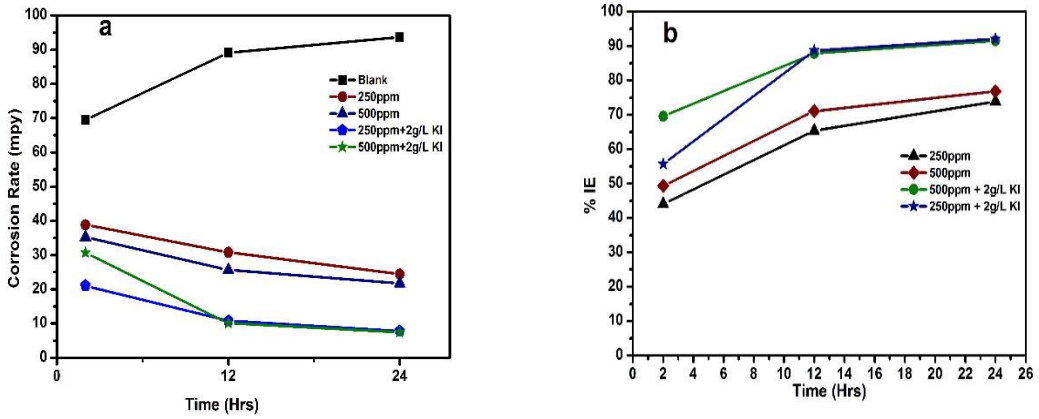

Figure4.26: Effect of time on blank TA at pH 4 and 25°C (a) Corrosion rate (b) %IE

The immersion time dependence on the effect of TA on the sweet corrosion of X60 mild steel was conducted using EIS and presented in Figure 4.27. According to Figure 4.27(a), the inductive loop appears and reduces with time. Furthermore, the charge transfer resistance has decreased with time. On the other hand, the charge transfer the inductive loop almost disappeared in the TA and TA+KI containing formulations. Moreover, the charge transfer resistance has increased with time in all the solutions containing TA and TA+KI compared to the blank solution.

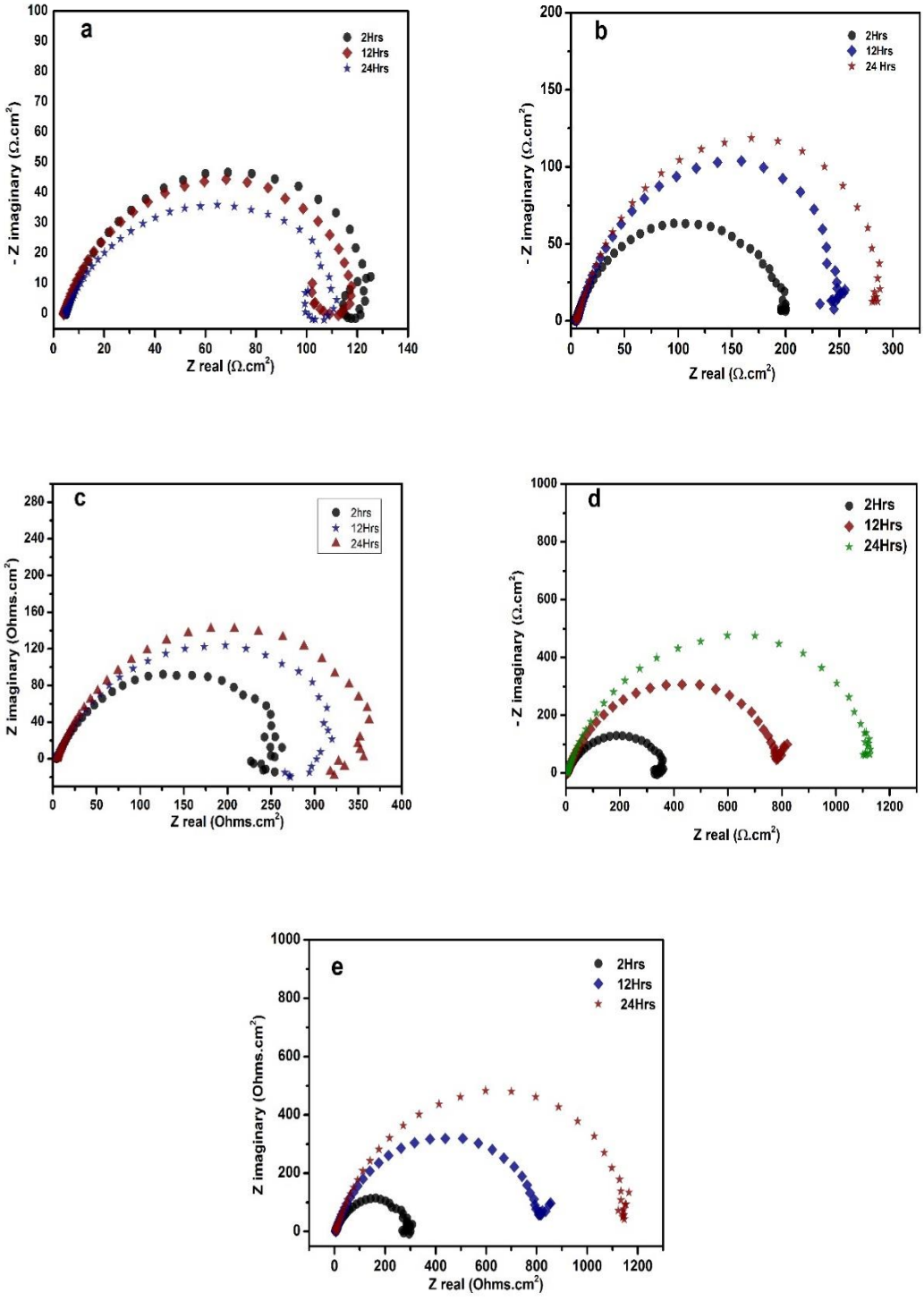

Figure 4.27: Effect of immersion time on TA (a) Blank (b) 250ppm (c) 500ppm (d) 250ppm + KI (e) 500ppm + KI at 25°C and pH 4

Table 4.17: EIS parameter for the effect of time onTA at pH 4 and 25°C

Solution	Time (Hrs)	R_s (Ω cm^2)	R_{ct} (Ω cm^2)	Cdl ($\mu F.cm^2$)	X^2 (10^{-4})	% IE
Blank	2	4.9	135.4	588	5.4	…
	12	4.9	125.3	902	6.4	…
	24	4.9	117.1	1002	4.5	….
250ppm	2	4.0	200.8	499	2.7	31.5
	12	5.4	324.4	491	5.6	60.5
	24	5.4	345	462	6.9	65.2
500ppm	2	4.3	280.3	358	6.3	50.7
	12	4.3	360.1	300	4.6	64.3
	24	4.5	411.4	291	4.0	70.7
250 + KI	2	5.2	386.2	260	3.0	64.2
	12	5.2	875.5	134	5.6	85.2
	24	5.2	1177	109	15	89.7
500 + KI	2	5.0	314.2	320	7.8	56.0
	12	5.2	847.7	129	7.3	84.7
	24	5.2	1207	104	15	90.0

Table 4.17 displays the EIS based results for the effect of time on TA on carbon dioxide corrosion of mild steel. We observe that the performance of TA is strongly time dependent

process both in the absence and presence of KI. We also note that the inhibition is better in the presence of KI compared to the solutions containing only TA. LPR and EIS measurements are in good agreement

4.2.4. Effect of temperature

The variation of the performance of tannic acid inhibitor with temperature in CO_2 saturated 3.5% NaCl is presented in Table 4.18. It was observed that the resistance of both blank and the inhibited solution decreases with temperature rise which jointly causes the efficiency of the inhibitor decrease.

Table 4.18: Effect of temperature on TA at 500ppm

	Blank	**500ppm**	
Temperature (C)	**Rp (Ω.cm^2)**	**Rp (Ω.cm^2)**	**%IE**
25	142.6	281.6	49.3
40	93.4	126.8	26.3
60	64.5	92.3	24.7
80	56.6	71.7	21.1

This behavior for the effect of temperature on the sweet corrosion of TA is presented in Figure 4.28.

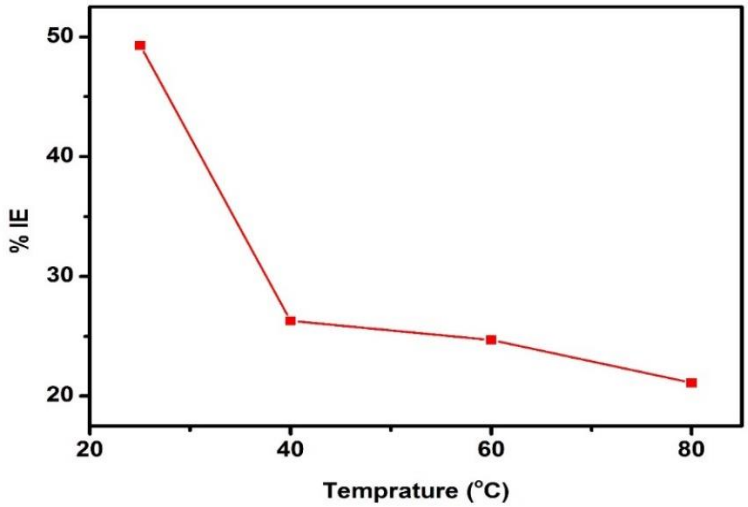

Figure 4.28: Effect of temperature on the sweet corrosion of X60 mild steel in the presence and absence of 500ppm TA at 25°C and pH = 4

Figure 4.29 (a and b) shows the Nyquist plots for the effect of temperature on the sweet corrosion of X60 mild steel in absence and presence of 500ppm TA respectively. We not in both situations that the rise in temperature significantly reduce the charge transfer resistance.

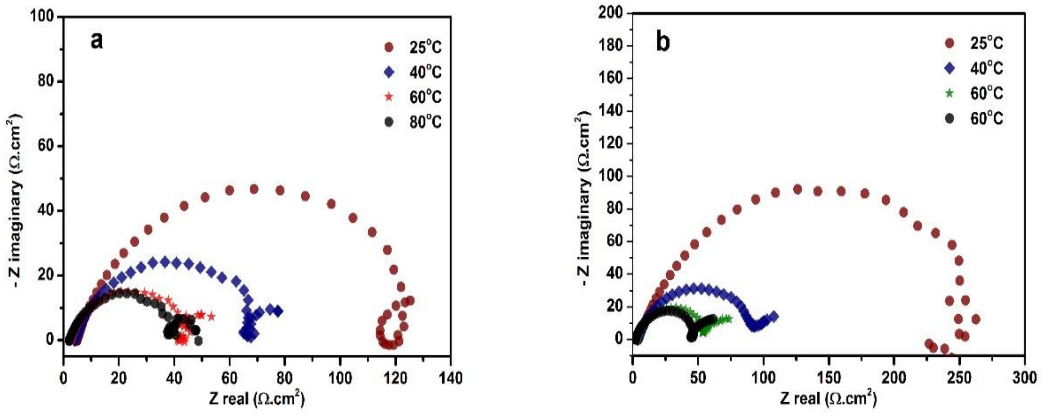

Figure 4.29: Behavior of sweet corrosion of X60 mild steel in 3.5% NaCl (a) without inhibitor (b) with 500ppm TA

The studies of LPR and EIS in this case indicate that TA's inhibition character depreciates with temperature.

4.2.5. Surface Characterization

SEM

The images in Figure 4.30 represent the specimens before immersion and after immersion CO_2-saturated 3.5% NaCl with and without 500ppm TA + 2000ppm KI addition. We observe a clear damage for inhibitor-free sample compared to the sample inhibited with 500ppm + KI. There is no much change in morphology for the sample inhibited with TBA compared to the sample before immersion.

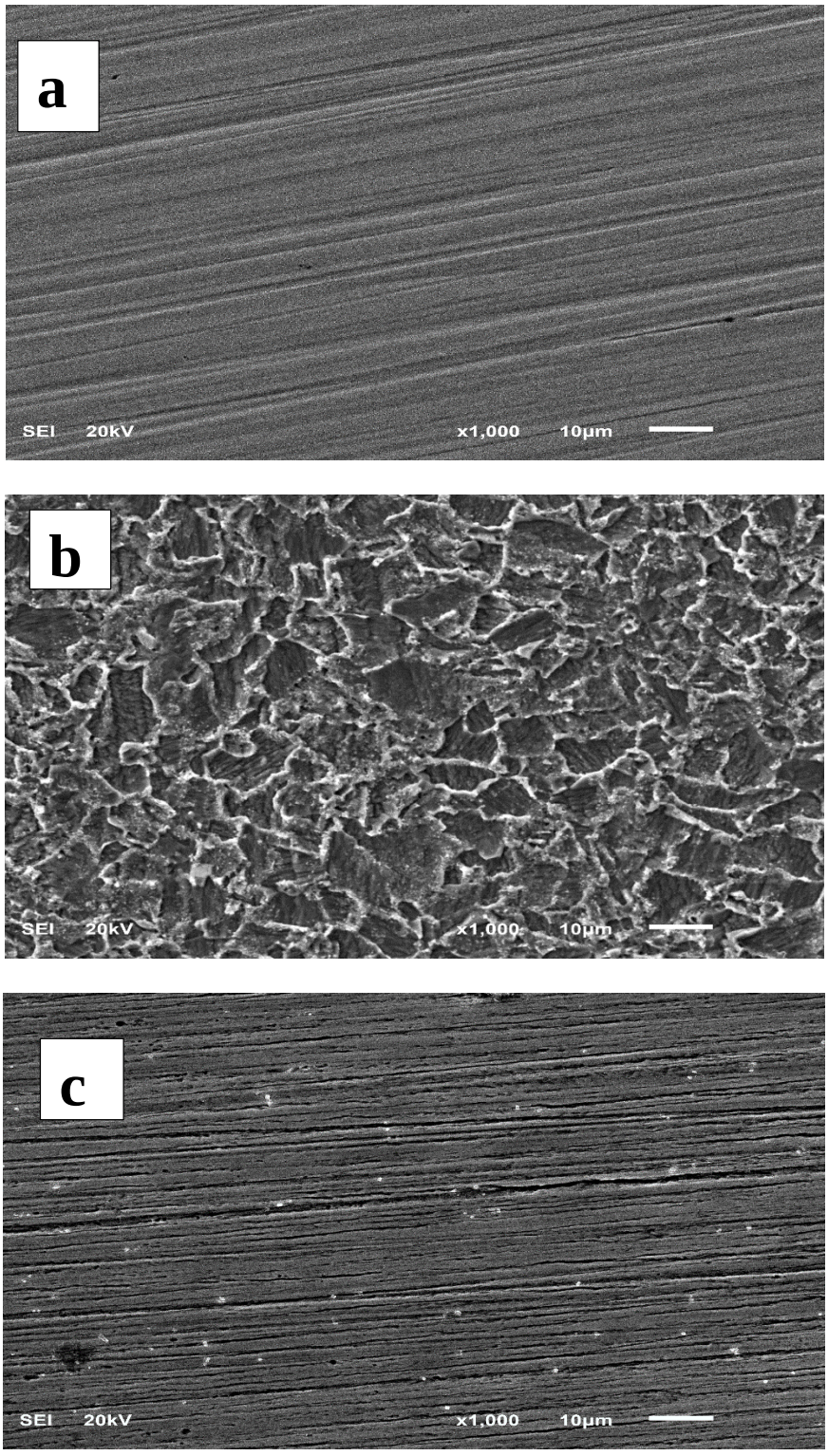

Figure 4.30: SEM images for X60 mild steel (a) before immersion (b) after immerstion in CO_2 –saturated 3.5% NaCl without inhibitor (c) with 500 ppm TA

XPS

XPS analysis for both wide and narrow scans were carried out in absence and presence of 500ppm TA at 25^{o}C and pH = 4. In the wide scan, majorly peaks for C1s, O1s and Fe2p have been detected for both the inhibited and blank specimen according to Figure 4.31. Sulfur and nitrogen were not detected. We also observed that the peaks for iron, oxygen and carbon are more intense in TA contained samples than in blank samples.

In the narrow scan of the O1s and C1s according Figure 4.32 and 4.33 we noted more peaks in the inhibited than the blank specimen. However, the peaks for Fe2p are not much different in the two samples.

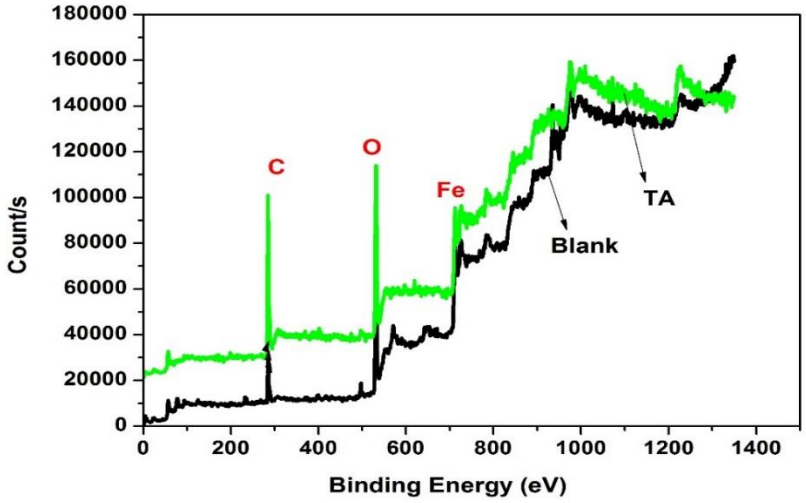

Figure 4.31: Survey scan spectra for mild steel surface product obtained after 24 hours immersion time in 3.5 % NaCl at 25^{o}C with and without 500ppm TA

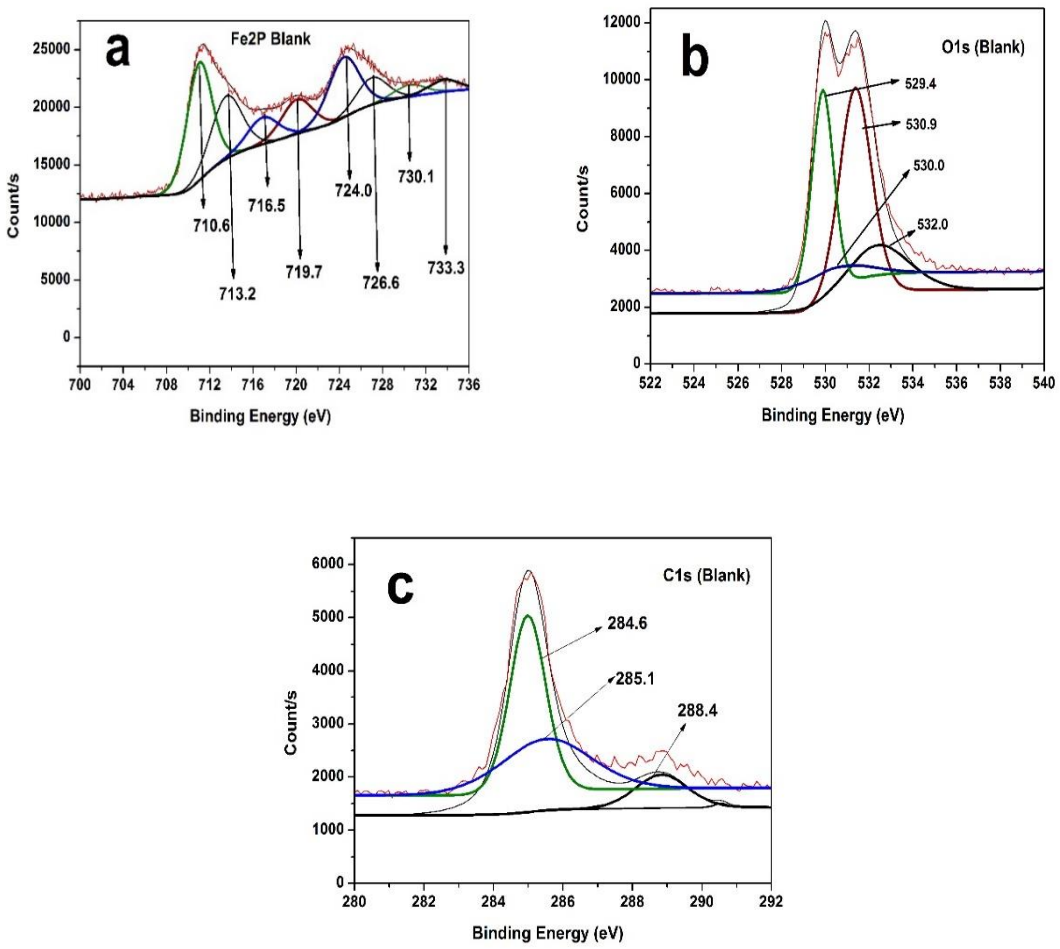

Figure 4.32: High Resolution XPS Spectra for mild steel after 24 hours immersion at 25°C in CO_2 - saturated 3.5 % NaCl: (a) Fe2p (b) O1s (c) C1s

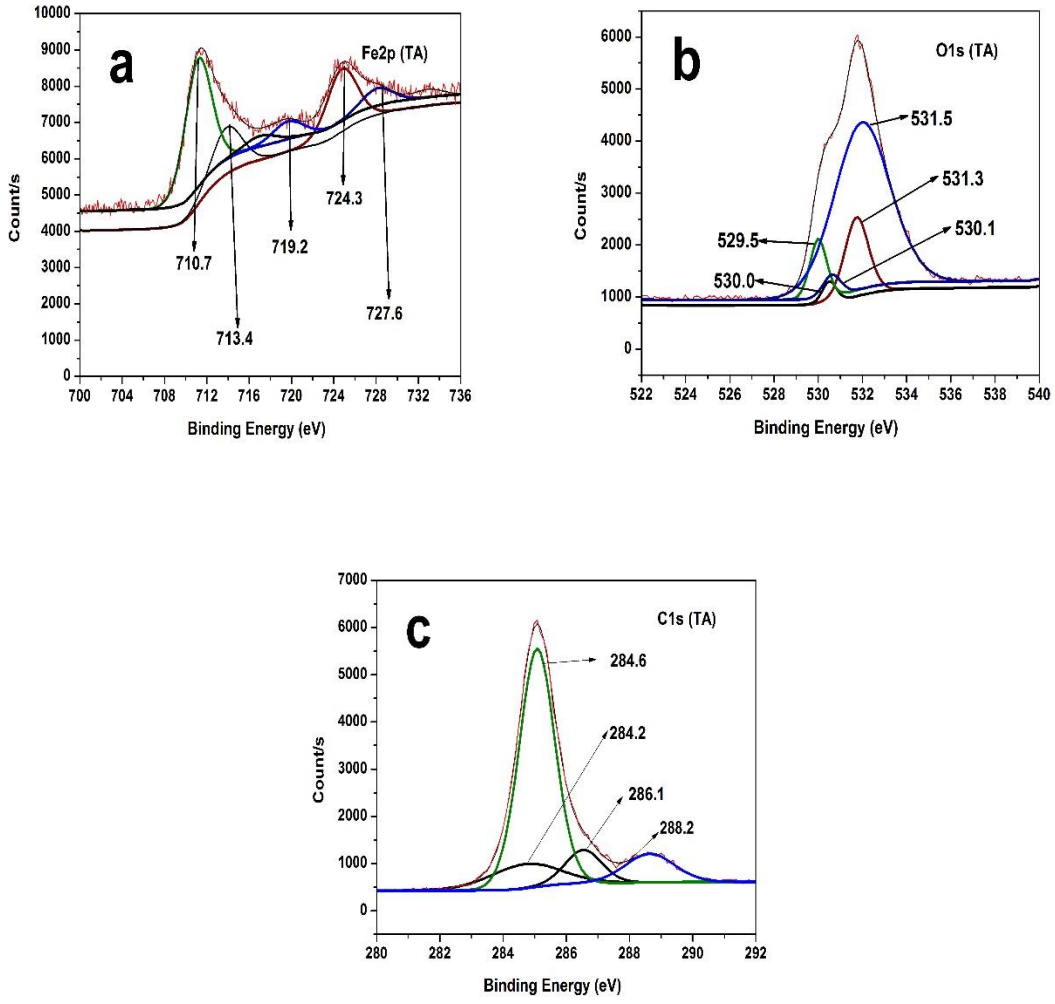

Figure 4.33: High Resolution XPS Spectra for mild steel after 24 hours immersion at 25°C in CO_2 - saturated 3.5 % NaCl with 500ppm TA: (a) Fe2p (b) O1s (c) C1s

The binding energy of the XPS peaks, proportions (in atomic weight %) and their corresponding possible assignments are listed in Table 4.19

Table 4.19: XPS spectral analysis for the surface products on mild steel after 24-hours immersion in CO_2 -saturated 3.5 % NaCl in the absence and presence of 500ppm.

Concentration (ppm)	Peak	Energy (eV)	Atomic Weight (%)	Possible Assignment
Blank	Fe2p	710.6	28.84	FeO, $FeCO_3$, Fe_2O_3, $FeCl_2$
		713.2	18.92	Fe_2O_3, FeOOH
		724.0	18.26	$FeCO_3$, Fe_3O_4, Fe_2O_3
	O1s	529.4	30.29	Fe_2O_3, FeO
		530.0	7.74	Fe_2O_3, FeO
		530.9	42.97	FeOOH, $FeCO_3$
		531.9	18.99	C=O
	C1s	284.6	50.16	C-C
		285.1	37.08	C-O-C
		288.4	12.77	O-C=O or CO_3
500ppm	Fe2p	710.7	45.42	FeO, $FeCO_3$, Fe_2O_3, $FeCl_2$
		713.4	17.13	Fe_2O_3, FeOOH,
		724.3	23.21	$FeCO_3$, Fe_3O_4, Fe_2O_3
	O1s	529.5	7.65	Fe_2O_3, FeO
		530.1	2.92	Fe_2O_3, FeO
		531.3	15.65	FeOOH, $FeCO_3$
		531.5	71.37	C=O
	C1s	284.2	13.04	C=C
		284.6	66.24	C-C
		286.1	9.65	C-O-C, C=N
		287.8	6.57	C=O, C-N
		288.2	9.65	O-C=O or CO_3

FTIR

Figure 4.34 represents an FTIR peaks and their corresponding wavenumbers for X60 mild steel in 3.5% NaCl with and without 500ppm TA inhibitor. Both inhibited and uninhibited specimens show peaks with almost same intensity at 3407 cm^{-1}. Contrary, peaks with

numbers 710, 1467, 1729, 2029 and 2915 cm^{-1} were observed to be present in TA+ KI immersed mild steel but absent in the uninhibited specimen.

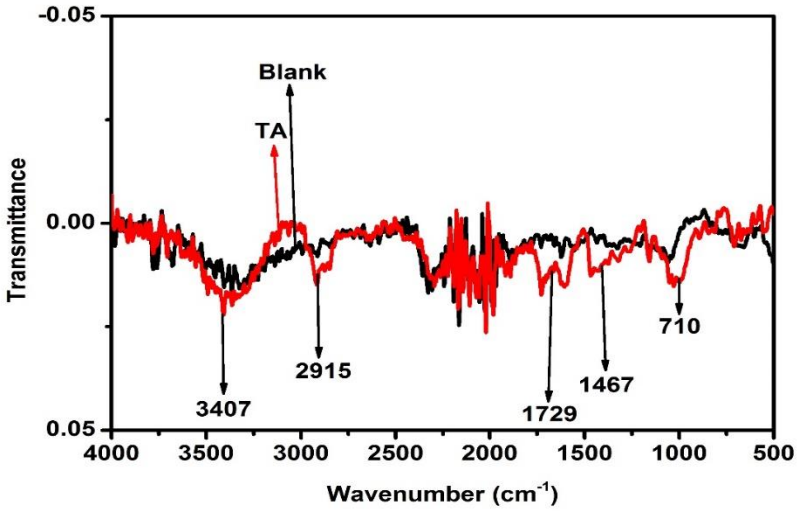

Figure 4.34: FTIR Spectra for the X60 Mild Steel immersed in CO_2-saturated 3.5% NaCl in the absence and presence of 50ppm TA inhibitor at 25°C after 24 hours.

Table 4.20 shows the noted FTIR bands with the possible functional groups responsible for such absorptions.

Table 4.20: FTIR Bands for TA+KI adsorbed on X60 mild steel in CO_2 saturated 3.5% NaCl.

FTIR Band (cm^{-1})	Assignment
710	C-H out of plane bending
1467	Aromatic C=C stretching
1729	C=O Stretching
2915	Symmetric CH_2 Stretching
3407	H-O-H Stretching (adsorbed water)

CHAPTER 5

DISCUSSIONS

5.1. Thiobarbituric acid

5.1.1. Effect of concentration at pH 4

The inhibitor has shown the optimum inhibition concentration between 50 and 75ppm. At 100 ppm the performance has declined slightly. This kind of behavior where the inhibitor manifests peak performance as a function of concentration was reported by several researchers [86,77,133-135]. There is parallel adsorption of inhibitor molecules at lower concentrations up to 75ppm which tend to block the active surface sites of the metal and drives away water from the metal surface. The higher the concentration the higher the adsorption of the inhibitor on the metal surface and the less the number of the active surface sites. The surface of the metal covered by the adsorbed inhibitor becomes protected, the corrosion rate therefore decreased up to 75ppm. On the other hand, when the inhibitor concentration was raised to 100ppm its molecules tend to adsorb perpendicularly because of strong mutual electrostatic repulsion of the molecules. The inhibitor molecules occupy a smaller surface on the metal surface as a result of intermolecular repulsion. The corrosion rate therefore increased at 100ppm and the efficiency slightly decreased.

Appearance of capacitive semicircle as observed in all Nyquist plots for both inhibited and uninhibited specimen is believed to be because of charge transfer resistance and double layer capacitance. Typically impedance spectra with a form of depressed semicircle in the complex plane with center under the real axis is believed to be the behavior for solid

electrodes [3,10], although it can also be attributed to surface roughness and inhomogeneity [59].

The appearance of inductive loop at lower frequencies in the blank solution is related to the adsorption of intermediate products ($FeOH_{ads}$). Usually there is formation of $FeOH_{ads}$ intermediates during dissolution of iron in acidic media according to Bockris et. al. [135] and in CO_2 saturated environment [136]. This behavior which indicates active dissolution of electrode was observed by previous researchers in CO_2 environment [3,72,83,86].

The mechanism for intermediate product formation can be described as follows [3]:

$$Fe + H_2O \leftrightarrow FeOH_{ads} + H^+ + e^- \quad 5.1$$

$$FeOH_{ads} \rightarrow FeOH^+_{(sol)} + e^- \quad 5.2$$

$$FeOH^+_{(sol)} + H^+ \leftrightarrow Fe^{2+} + H_2O \quad 5.3$$

Furthermore, it is observed that the semicircle diameter which is ascribed to charge transfer resistance and double layer capacitance increases with TBA addition and is dependent on concentration up to 75ppm. This indicates increases in the resistance of the metal against corrosion and hence increases in efficiency [74]. At 100 ppm, the semicircle decreases which signifies drop in inhibition efficiency compared to 50 and 75ppm.

The increase in absolute impedance in Bode plot (Figure 4.3b) at lower frequencies with addition of TBA compared to the blank solution is another evidence which indicates inhibition character for TBA [132]. The absolute impedance was observed to have increased with increase in concentration reaching its peak at 75ppm and then dropped at 100ppm. This confirms efficiency trend observed in Nyquist plot.

The phase angle versus frequency plot further corroborated the TBA's inhibition behavior. The more negative the phase angle at high frequency the more the inhibitors performance. The phase angle is more negative with addition of TBA concentration up to 75ppm and then increased at 100ppm. This suggests superior protection at 75 ppm as noted previously in other studies. Furthermore, the depression of phase angle at relaxation frequency was observed with decreasing the concentration of the inhibitor which occur as a result of decrease in capacitive response. This kind of process suggests higher corrosion process at lower TBA concentrations [132]. This trend of inhibitor performance is consistent with what was noted previously in the LPR measurements.

5.1.2. Effect of Concentration at pH = 6

As studied in pH = 4, the same behavior was observed at pH = 6. The inhibitor performance increased from 25 up to 75ppm then decreased at 100ppm. The reason for this behavior was already mentioned in the previous section.

Figure 4.9 exhibited comparison for the corrosion rates and corresponding efficiency changes in pH 4 and 6. Obviously, the corrosion rates for both blank and inhibited solutions at pH = 4 are higher than the corrosion process at pH 6. This can be attributed to the effect of pH on the cathodic reaction because anodic reaction is not affected by a change in the pH [74]. The predominant cathodic reaction at pH 4 is hydrogen reduction and at pH 6, the cathodic reaction turns to be reduction of carbonates [40,49,50]. The overall performance of the inhibitor however remains the same.

The decrease in C_{dl} values for inhibited specimens compared to blank samples noted in Table 4.2 and 4.4 for pH 4 and 6, respectively, indicates that the thickness of double layer

increases and/or local dielectric constant decreases. This is because C_{dl} is inversely proportional to the double layer thickness and directly proportional to the dielectric constant according to equation 5.4 [56,84]. Even though a decrease in C_{dl} can be attributed to an increase in the amount of inhibitor which may reduce the surface area responsible for charging [137].

$$C_{dl} = \frac{\varepsilon A}{d} \qquad 5.4$$

Where A is the area, ε is dielectric constant and d is the thickness of the double layer.

This increase in thickness arises because of the adsorption of inhibitor molecules on the metal surface [65,74].

5.1.3. Temperature Effect

The effect of temperature on the metal-inhibitor system is a complex one since a lot of changes are involved on the metal surface such as inhibitor desorption and rapid corrosion. As reported by Singh et. al. [138], chemical behavior of inhibitor molecules may change with a rise in temperature, which leads to an increase in its electron densities at the adsorption centers thereby reducing the corrosion rate. In some cases, the inhibitor itself may be subjected to decomposition and/or rearrangement [139]. The change in corrosion process was studied in CO_2 saturated 3.5 % NaCl both in absence and presence of 50ppm of TBA inhibitor. It was observed an increase in inhibitor efficiency with increase in temperature from 25-80^{o}C as reflected in Table 4.5 and Figure 4.10. Interpretation of this behavior with rise in temperature is a subject of discussions. The earlier works by Riggs and Hurds [140] suggests that by comparing the activation energies of the blank and

inhibited systems, corrosion reaction and heat of adsorption of the inhibitor molecules may be obtained. At constant concentration, when IE decreases with rise in temperature, it shows that the activation energy (E_a) in the presence of inhibitor is higher than that of the blank solution. This is an indication of physical adsorption. On the other hand, situations where IE increases with temperature increase, it is believed that Ea in the inhibited system is lower than uninhibited solution and this suggests chemical adsorption [65,137,141]. In TBA case, we noted increase in IE with temperature and jointly according to Table 5.3 thermodynamics investigations have shown that IE in in CO_2 saturated 3.5% NaCl is higher than that obtained for the inhibited system. This suggests that chemical interaction which involves charge transfer or charge sharing have taken place between the lone pairs of electrons in the inhibitor and charge on the metal surface. The value of ΔG^o_{ads} obtained from adsorption isotherm in section 5.1.5 also indicates that the inhibitor has chemically adsorbed on the metal surface. Surface characterization tools like XPS, SEM and FTIR are employed to furnish further details on the mechanism of inhibition of the inhibitor.

Activation Parameters

It can be well understood from Arrhenius equation that logarithm of corrosion rate is a linear function of inverse of kelvin temperature. This relationship was used by many researchers to explain the dependence of corrosion rate and hence inhibitor efficiency on temperature [145-148]:

$$\boldsymbol{logC_R = \frac{-Ea}{2.303RT} + logA} \qquad 5.5$$

Where E_a is the apparent activation energy, R is molar gas constant and A is the Arrhenius pre-exponential factor. The value of E_a extracted from the slope of the plot ($-E_a/2.303R$) is presented in Table 5.3.

To obtain the heat of adsorption (ΔH) and Entropy (ΔS), slope and intercept of formulation of Arrhenius equation which is based on transition state theory were used respectively. The equation is otherwise known as Eyering's equation [145]:

$$C_R = \frac{RT}{Nh} exp\left(\frac{\Delta S}{R}\right) exp\left(-\frac{\Delta H}{RT}\right) \quad 5.6$$

Where N is the Avogadro's number, h is plank's constant ΔS is the apparent entropy of activation, and ΔH is the apparent enthalpy of activation. The slope and intercept of log (C_R/T) versus 1/T are respectively $-\Delta H/2.303R$ and $[\log(R/Nh) + \Delta S/2.303R$ from which ΔH and ΔS are obtained. Figure 5.1 shows the plots of adsorption isotherms and the extracted values of Ea, ΔH and ΔS are shown in table 5.3.

The value of apparent activation energy obtained for the corrosion process in 3.5% NaCl was 37.08 $kJmol^{-1}$ which is very close to the value obtained by Desimone et. al [76] and comparable to that obtained by Okafor et. al [74]. By comparing E_a for both inhibited and uninhibited solutions, it is possible to find some relevant information about the adsorption behavior. It becomes apparent from the Table 5.3 that E_a decreased on addition of TBA compared to the blank solution. The decrease in the apparent activation energy is interpreted as the increase in the performance of the inhibitor with temperature [83]. Furthermore, it has always been reported in literature that the decrease in Ea in the presence of inhibitor compared to the blank solution and jointly increase in efficiency with temperature is believed to be as a result of chemical adsorption [65,76,141].

Table 5.1: Parameters for plotting thermodynamic relations of TBA.

	Blank			50ppm				
Temperature(K)	C_R (mpy)	$LogC_R$ (mpy)	$LogC_R/T$	C_R (mpy)	$LogC_R$ (mpy)	$LogC_R/T$	Θ	Log(Θ/1-Θ)
298	69.5	1.84	-0.64	2.1	0.32	-2.15	0.969	1.49
313	106.1	2.03	-0.48	2.5	0.40	-2.10	0.976	1.61
333	153.7	2.19	-0.34	3.3	0.51	-2.00	0.979	1.67
353	175.2	2.24	-0.3	3.5	0.54	-2.00	0.980	1.69

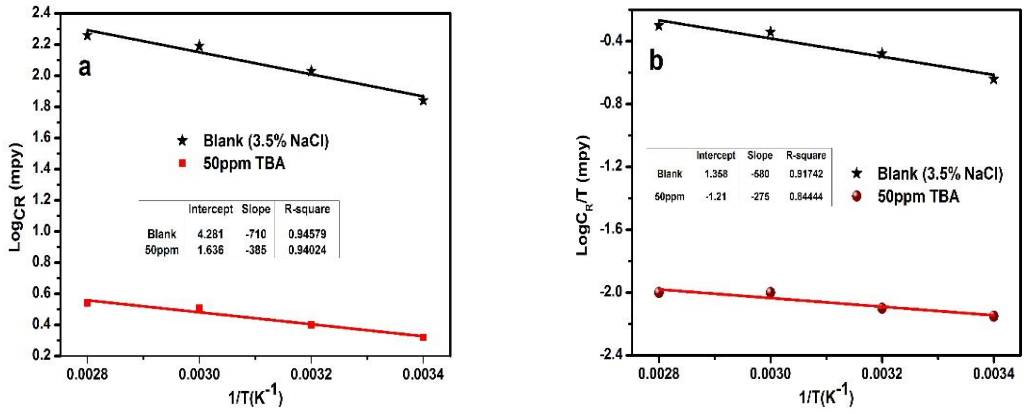

Figure 5.1: Plots for thermodynamics behavior in absence and presence of 50ppm TBA in 3.5% NaCl (a) Arrhenius plot (b) log (CR/T) versus 1/T

The positive value of ΔH in both systems is a clear indication that the anodic dissolution of iron is an endothermic process [139]. The positive value of ΔH (endothermic reaction) is unambiguously attributable to chemical adsorption [139,149]. However, exothermic process (ΔH < 0) is attributed to chemisorption [150] or physisorption [125] or both processes (comprehensive adsorption) [151].

The negative values for ΔS^o in the inhibited and uninhibited systems implies that the activation complex in the rate determining step represents association rather than dissociation step, meaning that a decrease in disorder takes place on going from reactant to the activated complex [152].

Table 5.2: Thermodynamic parameters for X60 mild steel in 3.5% NaCl and 50ppm TBA

Concentration (ppm)	Ea ($kJmol^{-1}$)	ΔH ($kJmol^{-1}$)	ΔS (J/k)
Blank	37.08	30.29	- 171
50	20.11	14.36	- 221

5.1.4. Effect of Immersion Time

According to the Nyquist plot displayed on Figure 4.12(a), all the spectra are characterized by appearance of a depressed semicircle with center under the real axis from higher to medium frequencies. At lower frequencies, the inductive loop appears after 2 hours because of active dissolution of the working electrode which is as a result of formation of intermediate products according to equation 5.1-5.3 [3]. The diameter of semicircle which signifies charge transfer resistance becomes smaller with time as well the magnitude of inductive loop. This indicates that the charge transfer phenomenon assumed to be hydrogen evolution cathodic reaction is more favorable because of the presence of Fe_3C which is part of the X60 mild steel [3]. Galvanic effect resulting from cementite regions is considerable in carbon steels with higher than 0.15% carbon content. In this work, the steel used for this investigation has a carbon content of about 0.16-0.2% wt. Since Fe_3C is an electric conductor, it is believed that there is galvanic effect between the Fe_3C (cathode) and ferrite

(anode) [143]. Therefore, continuous dissolution of ferrite as a result of higher cementite to ferrite surface area was noticed. Bode plot in Figure 4.12(b) reveals that the absolute impedance decreased continuously with respect to time. The decreased absolute impedance shows that the mild steel is more corroded at longer immersion time. Likewise in Phase angle plot in Figure 4.12(c) has shown decrease in negative value continuously. In agreement with LPR results, this suggests continuous sweet corrosion process for X60 mild steel.

According to Figure 4.13(a), the addition of TBA has increased capacitive semicircles which increase with increase in time. The Bode plot in Figure 4.13(b) revealed an increased absolute impedance with TBA introduction compared to the uninhibited samples. The absolute impedance continuously increased with time up to 72 hours. The more negative values at medium frequencies assumed to be reason for corrosion inhibition process were observed at longer time in phase angle plot according to Figure 4.13(c). Moreover, appearance of the second peak at the intermediate frequencies at longer immersion times indicates the presence of an adsorbed inhibitor film on the metal surface which is responsible for enhanced corrosion protection. The continuous increase in charge transfer resistance in the Nyquist plot, increased absolute impedance at lower frequencies in the Bode plot as well as more negative angles at medium frequencies in the phase angle plot collectively indicates a continuous inhibition process.

Increased corrosion rate for the blank sample and jointly its decrease for the inhibited specimen with longer immersion time suggests an effective inhibition process. This is in line with what Riggs [144] have reported. The metal dissolution in the presence of a

particular concentration of an inhibitor is a function of two rates; first, corrosion rate in the absence of inhibitor and second the process taking place in the presence of the inhibitor.

5.1.5. Adsorption Isotherm

It is generally accepted that organic inhibitors adsorb either physically or chemically on the surface of the metal in the process of arresting corrosion reaction. This adsorption process can be viewed as quasi-substitution process of water molecules ($H_2O_{(ads)}$) adsorbed on the metal surface by the inhibitor molecules ($Org_{(sol)}$) in aqueous solution [64];

$$Org(sol) + nH_2O(ads) \rightarrow Org(ads) + nH_2O(sol) \quad 5.7$$

To study the metal adsorption character, surface coverage (Θ) is the most important tool and is calculated as [92];

$$\theta = {}^{IE}/_{100} \quad 5.8$$

The value of Θ, is also used to identify the appropriate adsorption isotherm which provides an insight about the inhibitor interaction of the inhibitor molecules themselves and with metal surface. Langmuir adsorption isotherm was found to best describe the interaction of inhibitor with metal [73],[83]. This isoterm states that [92]:

$$\Theta/(1 - \Theta) = K_{ads}C \quad 5.9$$

It can also be simply can be rearranged and represented as:

$$C/\Theta = 1/K_{ads} + C \quad 5.10$$

Where Θ, is the surface coverage, C is concentration in mol/L. Slope of C/Θ versus C is straight line and the intercept is $1/K_{ads}$.

Table 5.3: Parameters for plotting Isotherm of TBA Corrosion Inhibition of X60 mild steel in 3.5% NaCl saturated with CO_2

Concentration (ppm)	Concentration (M) x 10^{-4}	Θ	C/Θ (M) x 10^{-4}
25	1.73	0.92	1.90
50	3.46	0.97	3.57
75	5.19	0.98	5.30
100	6.92	0.93	7.44

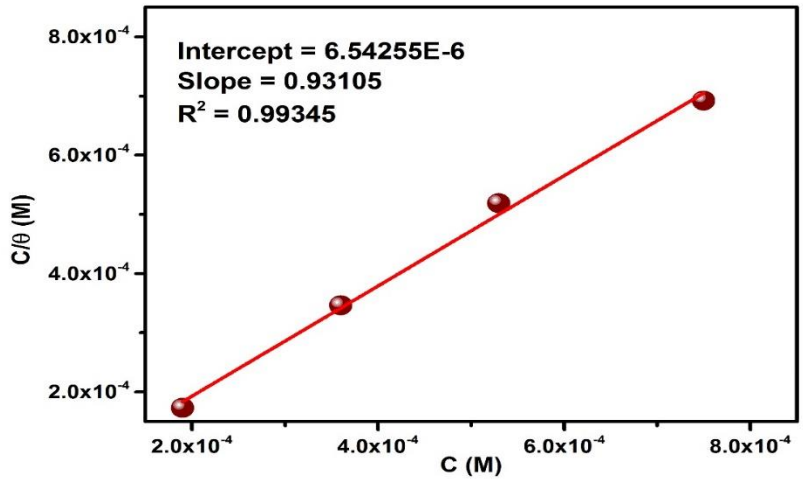

Figure 5.2 Isotherm of TBA Corrosion Inhibition of X60 mild steel in 3.5% NaCl saturated with CO_2

From the above figure, it can be seen that Langmuir adsorption isotherm is obeyed. The intercept is 6.54255 x 10^{-6} and K_{ads} is reciprocal of the intercept, 152846

Thermodynamically, standard free energy of adsorption (ΔG^{o}_{ads}) can be calculated using the relationship below;

$$\Delta G^{o}_{ads} = -RT\ln(55.5K_{ads}) \qquad 5.11$$

Where T is the absolute temperature and R is the gas constant.

$\Delta G^{o}_{ads} = -40 Kjmol^{-1}k^{-1}$

It is usually agreed that the ΔG^{o}_{ads} value of $-20 kJmol^{-1}k^{-1}$ or less negative indicates physical electrostatic interaction between charged metal surface and charged inhibitor molecules. When the value is about $-40 kJmol^{-1}k^{-1}$ or more negative is regarded as a chemical adsorption. The adsorption process is considered a combination of both physical and chemical types if the values of ΔG^{o}_{ads} is between -20 $kJmol^{-1}k^{-1}$ and $-40 kJmol^{-1}k^{-1}$ [30,79,84]. It can therefore be said in this work that at 25ºC TBA has adsorbed on X60 mild steel surface through both coulombic interaction between charged metal surface and charged inhibitor molecules and chemical bonding. This may be well supported from the thermodynamic analysis in section 5.1.6 and more evidenced in surface characterization studies to be presented in section 5.1.7

The higher the value of K_{ads} and negative value of ΔG^{o}_{ads} the higher is the spontaneity of the interaction of molecules with the metal surface [83]. Therefore, TBA molecules are believed to have strongly adsorbed on the X60 mild steel electrode through both physical and chemical modes.

5.1.7 Surface Characterizations

The influence of the TBA inhibitor can be vividly seen in Figure 4.14. SEM images for X60 mild steel before immersion and after immersion in 3.5% NaCl in the absence and presence of the inhibitor was presented. The surface of the mild steel before immersion was smooth with polishing lines (600 grit size). After 24 hours of immersion, the surface was seriously damaged and roughened due to the rapid and aggressive corrosion attack of mild steel in CO_2 saturated solution. The corrosion was relatively uniform with no sign of localized corrosion. In the presence of 50ppm TBA the steel surface remains relatively unchanged because of the formation of adsorbed inhibitor film which protects the metal from corrosion. This confirms the excellent inhibition process by TBA as studied in the electrochemical measurements.

XPS wide scan results (Figure 4.17) showed the presence of majorly peaks for N, C and Fe for both inhibited and blank specimen. However the peaks for O and C are more intense in the inhibited compared to the blank specimen because they are the basic component of the inhibitor structure. This is a clear evidence that the inhibitor has adsorbed on the metal surface. In the narrow scan, the deconvoluted profiles for Fe2p, O1s, C1s, N1s and S2p are presented Figure 4.18 and 4.19 for inhibited and uninhibited samples, respectively. The presence of sulfur peak at 162 eV for specimen containing TBA is a clear indication that there is a chemical interaction between sulfur electron donating group in the inhibitor and charge on the metal surface. This binding energy usually corresponds to that of Fe-S. For the charge effects the binding energies were corrected by taking C1s to the peak at 284.6 eV. The peaks, binding energies atomic weight and their possible assignments are displayed in Table 4.10.

Figure 4.21 displayed the FTIR bands for the X60 mild steel immersed in CO_2 saturated 3.5% NaCl with and without TBA. At 3408 cm^{-1} both the specimens have exhibited a peak assumed to be for O-H stretching vibration in water. Contrary, the inhibited sample have shown some distinct peaks that must have been from the adsorbed TBA molecules. These peaks and their possible assignments are presented in Table 4.11.

5.2. Tannic acid

5.2.1. Effect of concentration

Table 4.12 as well as Figure 4.22 show that tannic acid can mitigate corrosion rate of X60 steel in CO_2 saturated (sweet) environment. The employed range of concentration was between 100 – 1000ppm (5.9×10^{-5} - 5.9×10^{-4}M). It is clear from Figure 4.22 that corrosion rates decrease as the amount of TA is added to the solution up to 500ppm, which leads to increase in efficiency. However, when the concentration reaches 1000ppm, the corrosion rate rises and as a result, the efficiency drops. This kind of behavior where the inhibitor manifests peak performance as a function of concentration was reported by previous researchers [77,133,134,153] and in this work, section 5.1.

According to Nyquist plot, introduction of TA has changed the behavior of uninhibited electrode by increasing charge transfer resistance which indicates increase in inhibition. At 1000ppm, there is inductive loop again just like it appeared in the blank solution which shows another way of diminishing efficiency compared to lower concentrations. Similarly, the C_{dl} decreased with addition of TA and increased with increase in concentration up to 500ppm. At 1000ppm, however, the C_{dl} parameter has risen to a higher number. The decrease in C_{dl} value indicates enhanced adsorption of TA inhibitor and therefore the

thickness of the double layer increased. Therefore, consistent with LPR measurements, all EIS parameters showed increase in inhibition with increase in concentration up to 500ppm and its depreciation at 1000pppm.

5.2.2. Synergistic effect

The improvement of the performance of TA in sweet corrosion of X60 mild steel with addition of KI was presented in Table 4.14 and Figure 4.25. The charge transfer increase when KI was added compared to KI free samples indicates synergistic effect between TA and KI. The double layer capacitance has also decreased considerably compared to when there is no KI addition. This suggests improved adsorption of TA molecules on the metal surface and consequently increase in the double layer thickness [73]. This is consistent with LPR measurements.

5.2.3. Effect of immersion Time

From LPR results, there is a significant increase in Rp values with time which suggests lower corrosion rates and consequently enhanced inhibition. Much more, the KI based TA formulation has exhibited better performance with time. EIS measurements have also revealed higher charge transfer resistance and hence better inhibition as time increases. C_{dl} decreases with time as well which suggests increase in local double layer thickness due to enhanced adsorption of TA molecules on the metal surface.

5.2.4. Effect of Temperature

Unfortunately, both LPR and EIS observations have proved that TA is not a suitable corrosion inhibitor at elevated temperatures. As the temperature increases, the inhibitor

performance drops to a lower value. This usually suggests physical adsorption of the inhibitor on the steel surface [65]. Even though it is difficult to single out only one type of adsorption for a particular inhibitor. This was previously discussed in section 5.1.4. More detailed explanation on this to come in the next section.

Activation Parameters

The adsorption parameters like activation energy, heat of adsorption and entropy is calculated to give further understanding of the inhibition process. Table 5.5 gives the necessary parameters for plotting the required plots.

Table 5.4: Parameters for plotting thermodynamic studies of TA

	Blank			50ppm				
T (K)	C_R (mpy)	LogC_R (mpy)	Log(C_R/T)	C_R (mpy)	LogC_R (mpy)	Log(C_R/T)	Θ	Log(Θ/1-Θ)
298	69.5	1.84	-0.64	35.2	1.55	-0.93	0.49	0.96
313	106.1	2.03	-0.48	78.2	1.89	-0.60	0.26	0.35
333	153.7	2.19	-0.34	107.4	2.03	-0.49	0.25	0.33
353	175.2	2.24	-0.3	138.2	2.14	-0.41	0.21	0.27

Figure 5.4 presents the Arrhenius and Eyering's plot for X60 mild steel corrosion of mild steel in the absence and presence of TA. Ea, ΔH and ΔS of the corrosion process in the inhibited and blank system are calculated and presented in Table 5.6

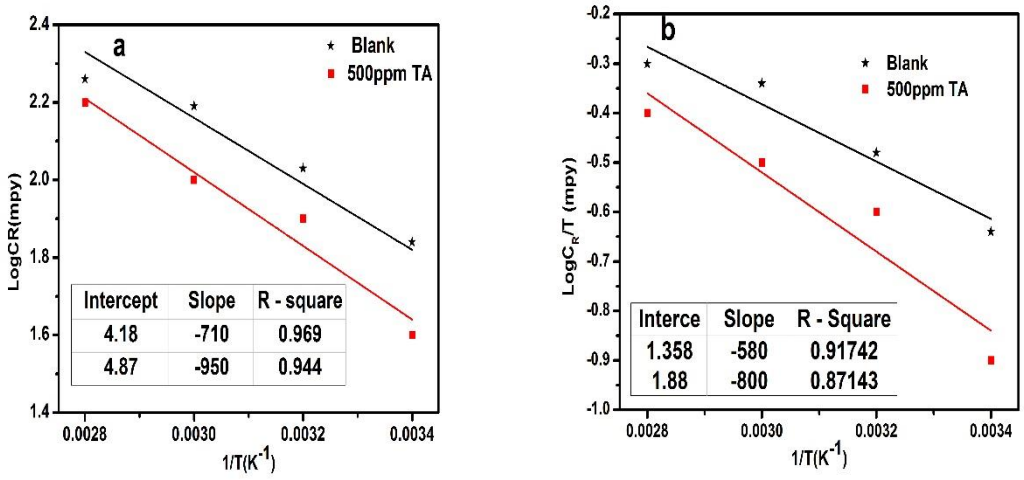

Figure 5.3: Plots for thermodynamics behavior in absence and presence of 500ppm TA in 3.5% NaCl (a) Arrhenius plot (b) Eyering's Plot.

The increase in the apparent activation energy from blank to the inhibited system is interpreted as a decrease in the performance of the inhibitor with temperature [83]. Furthermore, it has always been reported in literature that the inecrease in Ea in the presence of inhibitor compared to the blank solution and jointly decrease in efficiency with temperature is believed to be as a result of physical adsorption [65,76,141].

Table 5.5 Thermodynamic parameters for X60 mild steel in 3.5% NaCl and 500ppm TA

Concentration (ppm)	Ea ($kJmol^{-1}$)	ΔH ($kJmol^{-1}$)	ΔS (J/k)
Blank	37.08	30.29	-171
500	49.62	41.78	- 162

The positive value of ΔH in both systems is a clear indication that the anodic dissolution of iron is an endothermic process [139]. The positive value of ΔH (endothermic reaction) is unambiguously attributable to chemical adsorption [139,149]. However, exothermic process ($\Delta H < 0$) is attributed to chemisorption [150] or physisorption [125] or both processes (comprehensive adsorption) [151].

The negative values for ΔS^o in the inhibited and uninhibited systems implies that the activation complex in the rate determining step represents association rather than dissociation step, meaning that a decrease in disorder takes place on going from reactant to the activated complex [152].

5.2.5. Surface Characterization

The influence of the TA inhibitor can be vividly seen in Figure 4.30. SEM images for X60 mild steel before immersion and after immersion in 3.5% NaCl in the absence and presence of the TA+KI inhibitor are presented. The surface of the mild steel before immersion was smooth with polishing lines (600 grit size) After 24 hours of immersion, the surface was seriously damaged and roughened due to the rapid and aggressive corrosion attack of mild steel in CO_2 saturated solution. The corrosion was relatively uniform with no sign of localized corrosion. In the presence of 500ppm TA + KI the steel surface remains relatively unchanged because of the formation of adsorbed inhibitor and still with polishing lines observed. This confirms the excellent inhibition process by TA as studied in the electrochemical measurements.

XPS wide scan results (Figure 4.31) showed the presence of major peaks for N, C and Fe for both inhibited and blank specimen. However the peaks for O and C are more intense in

the inhibited compared to the blank specimen because they are the basic component of the inhibitor structure. This is a clear evidence that the inhibitor has adsorbed on the metal surface. In the narrow scan, the deconvoluted profiles for Fe2p, O1s, C1s, N1s and S2p are presented in Figure 4.32 and 4.33 for inhibited and uninhibited samples respectively. For the charge effects the binding energies were corrected by taking C1s to the peak at 284.6 eV. The peaks, binding energies atomic weight and their possible assignments are displayed in table 4.19.

Figure 4.34 displayed the FTIR bands for the X60 mild steel immersed in CO_2 saturated 3.5% NaCl with and without TA. At 3407 cm^{-1} both the inhibited and blank specimens have exhibited a peak assumed to be for O-H stretching vibration in water. Contrary, the inhibited sample have shown some distinct peaks that must have been from the adsorbed TA molecules. These peaks and their possible assignments are presented in Table 4.20.

CHAPTER 6

CONCLUSIONS

The following conclusions were made:

Thiobarbituric acid:

- TBA efficiently inhibited CO_2 corrosion of X65 mild steel in the range of sweet oilfield conditions of temperature (25-80^{o}C) and pH (4 and 6).
- The Inhibition efficiency increased with concentration showing its peak at between 50 and 75ppm in both pH 4 and 6.
- The inhibitor showed excellent inhibition effect with time of immersion up to 72 hours.
- TBA obeyed Langmuir adsorption isotherm with standard free energy of –40 KJmol $^{-1}$ at 25^{o}C.
- According to thermodynamic considerations, the inhibitor interacted with the metal surface mainly through chemical adsorption mode. This was supported by XPS and FTIR
- PDP results indicated that TBA acted as a mixed type corrosion inhibitor, interfering with both anodic and cathodic reactions.

Tannic acid:

- Electrochemical investigations indicated that tannic acid is an inhibitor for mild steel in CO_2 saturated 3.5% NaCl.

- The optimum concentration is 500ppm at 25^{o}C and pH 4. The inhibitor efficiency decreased at higher temperature.
- Addition of KI had a synergistic effect and raised the performance of the inhibitor to a very excellent value.
- Surface characterization and thermodynamic studies have shown that the inhibitor adsorbed on the metal surface through both physical mode and chemical bonding between lone pairs of electrons of the TA molecules with d – orbital electrons of the metal.

REFERENCES

[1] M. Finšgar and J. Jackson, “Application of corrosion inhibitors for steels in acidic media for the oil and gas industry: A review,” *Corros. Sci.*, vol. 86, no. 0, pp. 17–41, 2014.

[2] Z. Zhang, Y. Zhao, Q. Gong, Z. Li, and J. Li, “MOFs for CO2 capture and separation from flue gas mixtures: the effect of multifunctional sites on their adsorption capacity and selectivity.,” *Chem. Commun. (Camb).*, vol. 49, no. 7, pp. 653–61, Jan. 2013.

[3] F. Farelas, M. Galicia, B. Brown, S. Nesic, and H. Castaneda, “Evolution of dissolution processes at the interface of carbon steel corroding in a CO 2 environment studied by EIS,” *Corros. Sci.*, 2010 vol. 52, pp. 509-517.

[4] L. Popoola, A. Grema, G. Latinwo, B. Gutti, and A. Balogun, “Corrosion problems during oil and gas production and its mitigation,” *Int. J. Ind. Chem.*, vol. 4, p. 35, 2013.

[5] O. N. Sylyester, O. N. Celestine, I. G. Reuben, and C. E. Okechukwu, “Review of Corrosion Kinetics and Thermodynamics of CO2 and H2S Corrosion Effects and Associated Prediction / Evaluation on Oil and Gas Pipeline System .,” *Int. J. Sci. Technol. Res.*, vol. 1, no. 4, pp. 156–162, 2012.

[6] A. Al-Hasami, S. Ren, and B. Tohidi, “CO2 Injection for Enhanced Gas Recovery and Geo-Storage: Reservoir Simulation and Economics,” in *SPE Europec/EAGE Annual Conference*, 2013.

[7] D. A. López, T. Pérez, and S. N. Simison, “The influence of microstructure and chemical composition of carbon and low alloy steels in CO2 corrosion. A state-of-the-art appraisal,” *Mater. Des.*, vol. 24, no. 8, pp. 561–575, Dec. 2003.

[8] H. El-Lateef and V. Abbasov, “Corrosion Protection of Steel Pipelines Against CO2 Corrosion-A Review,” *Chem*, vol. 02, no. 02, pp. 52–63, 2012.

[9] C. Li, “Effect of corrosion inhibitor on water wetting and carbon dioxide corrosion in oil-water two-phase flow,” Ph.D dissertation Ohi State University 2009.

[10] G. Zhang, C. Chen, M. Lu, C. Chai, and Y. Wu, “Evaluation of inhibition efficiency of an imidazoline derivative in CO2-containing aqueous solution,” *Mater. Chem. Phys.*, vol. 105, no. 2–3, pp. 331–340, Oct. 2007.

[11] M. B. Kermani and A. Morshed, “Carbon Dioxide Corrosion in Oil and Gas Production—A Compendium,” *Corrosion*, vol. 59, no. 8, pp. 659–683, Aug. 2003.

[12] W. Villamizar, “CO2 corrosion inhibition by hydroxyethyl, aminoethyl, and amidoethyl imidazolines in water–oil mixtures,” *J. Solid State*, 2007 Vol. 11, pp. 619.

[13] A. Ikeda, “CO_2 Corrosion Behavior and Mechanism of Carbon and Alloy Steel,” *CORROSION/83*, 1983.

[14] A. Dugstad, L. Lunde, and S. Nesic, “Control of internal corrosion in multi-phase oil and gas pipelines,” *Pipeline Corros. Gulf Publ. Co*, 1994.

[15] D. a. López, W. H. Schreiner, S. R. De Sánchez, and S. N. Simison, “The influence of carbon steel microstructure on corrosion layers: An XPS and SEM characterization,” *Appl. Surf. Sci.*, vol. 207, pp. 69–85, 2003.

[16] J. Han, B. N. Brown, and S. Nešić, “Investigation of the Galvanic Mechanism for Localized Carbon Dioxide Corrosion Propagation Using the Artificial Pit Technique,” *Corrosion*, vol. 66, no. 9, pp. 095003–095003–12, Sep. 2010.

[17] K. VIDEM and A. DUGSTAD, “Corrosion of carbon steel in an aqueous carbon dioxide environment. I: Solution effects,” *Mater. Perform.*, vol. 28, no. 3, pp. 63–67.

[18] B. Kermani and L. Smith, “A Working Party Report on CO2 Corrosion Control in Oil and Gas Production: Design Considerations,” 1997.

[19] V. Garcia-Arriaga, J. Alvarez-Ramirez, M. Amaya, and E. Sosa, “H2S and O2 influence on the corrosion of carbon steel immersed in a solution containing 3M diethanolamine,” *Corros. Sci.*, vol. 52, no. 7, pp. 2268–2279, Jul. 2010.

[20] E. McCafferty, “Introduction to corrosion science,” *Springer New York, USA (*2010).

[21] R. W. Revie, *Uhlig’s Corrosion Handbook: Third Edition*. John Wiley and Sons New York, USA (2011).

[22] M. G. Fontana, “Corrosion,” *McGraw-hill New York, USA (1967)*.

[23] D. Jones, “Principles and prevention of corrosion,” Macmilan New York, USA 1992.

[24] S. Ramachandran and V. Jovancicevic, “Molecular Modeling of the Inhibition of Mild Steel Carbon Dioxide Corrosion by Imidazolines,” *Corrosion*, vol. 55, no. 3, pp. 259–267, Mar. 1999.

[25] S. Webster, D. Harrop, A. McMahon, and G. Partridge, “Corrosion inhibitor selection for oilfield pipelines,” *, D. Harrop, AJ McMahon, GJ* 1993.

[26] F. S. de Souza and A. Spinelli, “Caffeic acid as a green corrosion inhibitor for mild steel,” *Corros. Sci.*, vol. 51, no. 3, pp. 642–649, Mar. 2009.

[27] P. Agarwal and D. Landolt, “Effect of anions on the efficiency of aromatic carboxylic acid corrosion inhibitors in near neutral media: Experimental investigation and theoretical modeling,” *Corros. Sci.*, 1998.

[28] D. Horsup, J. Clark, and B. Binks, “The fate of oilfield corrosion inhibitors in multiphase systems,” *Corrosion*, 2010.

[29] N. Vaszilcsin, V. Ordodi, and A. Borza, “Corrosion inhibitors from expired drugs,” *Int. J. Pharm.*, vol. 431, no. 1–2, pp. 241–244, 2012.

[30] M. Özcan, R. Solmaz, G. Kardaş, and İ. Dehri, "Adsorption properties of barbiturates as green corrosion inhibitors on mild steel in phosphoric acid," *Colloids Surfaces A Physicochem. Eng. Asp.*, vol. 325, no. 1–2, pp. 57–63, Jul. 2008.

[31] N. O. Eddy and E. E. and Ebenso, "Adsorption and inhibitive properties of ethanol extracts of Musa sapientum peels as a green corrosion inhibitor for mild steel in H2SO4," *African J. Pure Appl. Chem.*, 2008.

[32] S. Ghareba and S. Omanovic, "Interaction of 12-aminododecanoic acid with a carbon steel surface: Towards the development of 'green' corrosion inhibitors," *Corros. Sci.*, vol. 52, no. 6, pp. 2104–2113, Jun. 2010.

[33] M. Ko, B. Ingham, N. Laycock, and D. E. Williams, "In situ synchrotron X-ray diffraction study of the effect of chromium additions to the steel and solution on CO2 corrosion of pipeline steels," *Corros. Sci.*, vol. 80, pp. 237–246, 2014.

[34] D. Lide, "DR 2003–2004 CRC Handbook of Chemistry and Physics," *Boca Raton, FL, itd CRC Press.*

[35] P. L. Fosbøl, K. Thomsen, and E. H. Stenby, "Review and recommended thermodynamic properties of FeCO3," *Corros. Eng. Sci. Technol.*, vol. 45, no. 2, pp. 115–135, 2010.

[36] D. Clover, B. Kinsella, B. Pejcic, and R. De Marco, "The influence of microstructure on the corrosion rate of various carbon steels," *J. Appl. Electrochem.*, vol. 35, pp. 139–149, 2005.

[37] M. Ueda and H. Takabe, "Effect of environmental factor and microstructure on morphology of corrosion products in CO{sub 2} environments," Nov. 1999.

[38] A. Dugstad, "The importance of FeCO 3 supersaturation on the CO 2 corrosion of carbon steels," *A. Dugstad, Pap.*, 1992.

[39] C. de Waard, U. Lotz, and D. E. Milliams, "Predictive Model for CO 2 Corrosion Engineering in Wet Natural Gas Pipelines," *Corrosion*, vol. 47, no. 12, pp. 976–985, Dec. 1991.

[40] S. Nešić, "Key issues related to modelling of internal corrosion of oil and gas pipelines – A review," *Corros. Sci.*, vol. 49, no. 12, pp. 4308–4338, Dec. 2007.

[41] P. M. Gil, J. Manuel, R. Domínguez, I. Mexicano, and R. Lindsay, "Corrosion Inhibition Performance of 2-Mercaptobenzimidazole in Sweet Oilfield Conditions," *Corros. 2014*, vol. 2, no. 4109, pp. 1–9, 2014.

[42] S. Nešić and L. Lunde, "Carbon Dioxide Corrosion of Carbon Steel in Two-Phase Flow," *Corrosion*, vol. 50, no. 9, pp. 717–727, Sep. 1994.

[43] C. DE WAARD and D. E. MILLIAMS, "Carbonic Acid Corrosion of Steel," Jan. 2013.

[44] A. Dugstad, “Mechanism of Protective Film Formation During CO2 Corrosion of Carbon Steel.” NACE International, 01-Jan-1998.

[45] K. George and S. Nešic, “Investigation of carbon dioxide corrosion of mild steel in the presence of acetic acid-part 1: basic mechanisms,” *Corrosion*, no. February, pp. 178–186, 2007.

[46] L. D. Paolinelli, T. Pérez, and S. N. Simison, “The effect of pre-corrosion and steel microstructure on inhibitor performance in CO2 corrosion,” *Corros. Sci.*, vol. 50, pp. 2456–2464, 2008.

[47] S. Nešić and K.-L. J. Lee, “A Mechanistic Model for Carbon Dioxide Corrosion of Mild Steel in the Presence of Protective Iron Carbonate Films—Part 3: Film Growth Model,” *Corrosion*, vol. 59, no. 5, pp. 616–628, 2003.

[48] M. Honarvar Nazari, S. R. Allahkaram, and M. B. Kermani, “The effects of temperature and pH on the characteristics of corrosion product in CO2 corrosion of grade X70 steel,” *Mater. Des.*, vol. 31, no. 7, pp. 3559–3563, 2010.

[49] M. Nordsveen, S. Nešić, R. Nyborg, and A. Stangeland, “A Mechanistic Model for Carbon Dioxide Corrosion of Mild Steel in the Presence of Protective Iron Carbonate Films—Part 1: Theory and Verification,” *Corrosion*, vol. 59, no. 5, pp. 443–456, May 2003.

[50] H. M. Ezuber, “Influence of temperature and thiosulfate on the corrosion behavior of steel in chloride solutions saturated in CO2,” *Mater. Des.*, vol. 30, no. 9, pp. 3420–3427, Oct. 2009.

[51] U. Lotz and T. Sydberger, “CO 2 Corrosion of Carbon Steel and 13Cr Steel in Particle-Laden Fluid,” *Corrosion*, vol. 44, no. 11, pp. 800–809, Nov. 1988.

[52] J. K. Heuer and J. F. Stubbins, “An XPS characterization of FeCO3 films from CO2 corrosion,” *Corros. Sci.*, vol. 41, no. 7, pp. 1231–1243, Jul. 1999.

[53] S. Nešić, K. J. Lee, and V. Ruzic, “A Mechanistic Model of Iron Carbonate Film Growth and the Effect on CO2 Corrosion of Mild Steel,” *Corros. 2002*, no. 02237, pp. 1–35, 2002.

[54] a. H. Mustafa, B. Ari-Wahjoedi, and M. C. Ismail, “Inhibition of CO2 corrosion of X52 steel by imidazoline-based inhibitor in high pressure CO2-water environment,” *J. Mater. Eng. Perform.*, vol. 22, no. June, pp. 1748–1755, 2013.

[55] D. Brondel, R. Edwards, A. Hayman, D. Hill, and T. Semerad, “Corrosion in the Oil Industry,” *Oilf. Rev.*, pp. 4–18, 1994.

[56] S. K. Shukla, M. A. Quraishi, and E. E. Ebenso, “Adsorption and Corrosion Inhibition properties of Cefadroxil on mild steel in hydrochloric acid,” *Int. J. Electrochem. Sci.*, vol. 6, pp. 2912–2931, 2011.

[57] P. Rajeev, “Corrosion mitigation of the oil well steels using organic inhibitors–a review,” *J. Mater. Environ.*, 2012.

[58] J. Cruz, R. Martínez, J. Genesca, and E. García-Ochoa, “Experimental and theoretical study of 1-(2-ethylamino)-2-methylimidazoline as an inhibitor of carbon steel corrosion in acid media,” *J. Electroanal. Chem.*, vol. 566, no. 1, pp. 111–121, May 2004.

[59] K. F. Khaled, “The inhibition of benzimidazole derivatives on corrosion of iron in 1 M HCl solutions,” *Electrochim. Acta*, vol. 48, no. 17, pp. 2493–2503, Jul. 2003.

[60] A. Popova, M. Christov, S. Raicheva, and E. Sokolova, “Adsorption and inhibitive properties of benzimidazole derivatives in acid mild steel corrosion,” *Corros. Sci.*, vol. 46, no. 6, pp. 1333–1350, 2004.

[61] G. Trabanelli, “Corrosion inhibitors,” *F. Mansfeld (New York, NY Marcel Dekker, 1987)*, 1987.

[62] F. Bentiss, C. Jama, B. Mernari, H. El Attari, L. El Kadi, M. Lebrini, M. Traisnel, and M. Lagrenée, “Corrosion control of mild steel using 3,5-bis(4-methoxyphenyl)-4-amino-1,2,4-triazole in normal hydrochloric acid medium,” *Corros. Sci.*, vol. 51, no. 8, pp. 1628–1635, Aug. 2009.

[63] E. Noor and A. Al-Moubaraki, “Thermodynamic study of metal corrosion and inhibitor adsorption processes in mild steel/1-methyl-4 [4′(-X)-styryl pyridinium iodides/hydrochloric acid systems,” *Mater. Chem. Phys.*, 2008 vol. 110, pp. 145-154.

[64] A. Singh, Y. Lin, W. Liu, D. Kuanhai, J. Pan, B. Huang, C. Ren, and D. Zeng, “A study on the inhibition of N80 steel in 3.5% NaCl solution saturated with CO2 by fruit extract of Gingko biloba,” *J. Taiwan Inst. Chem. Eng.*, vol. 45, no. 4, pp. 1918–1926, 2014.

[65] A. Popova, E. Sokolova, S. Raicheva, and M. Christov, “AC and DC study of the temperature effect on mild steel corrosion in acid media in the presence of benzimidazole derivatives,” *Corros. Sci.*, vol. 45, no. 1, pp. 33–58, 2003.

[66] A. Kokalj and S. Peljhan, “What determines the inhibition effectiveness of ATA, BTAH, and BTAOH corrosion inhibitors on copper?,” *J. Am. Chem. Soc.*, **2010**, *132* (46), pp 16657–16668, 2010.

[67] M. M. Antonijevic and M. B. Petrovic, “Copper Corrosion Inhibitors . A review,” *Rev. Lit. Arts Am.*, vol. 3, pp. 1–28, 2008.

[68] M. Finšgar, “2-Mercaptobenzimidazole as a copper corrosion inhibitor: Part I. Long-term immersion, 3D-profilometry, and electrochemistry,” *Corros. Sci.*, vol. 72, pp. 82–89, 2013.

[69] B. Sanyal, “Organic compounds as corrosion inhibitors in different environments — A review,” *Prog. Org. Coatings*, vol. 9, no. 2, pp. 165–236, Aug. 1981.

[70] R. Hogue, T. King, and R. Mitchell, “Corrosion inhibitors and processes for using the same,” *US Pat. 3,989,637*, 1976.

[71] P. B. Raja and M. G. Sethuraman, “Natural products as corrosion inhibitor for metals in corrosive media — A review,” *Mater. Lett.*, vol. 62, no. 1, pp. 113–116, Jan. 2008.

[72] B. Wang, M. Du, J. Zhang, and C. J. Gao, “Electrochemical and surface analysis studies on corrosion inhibition of Q235 steel by imidazoline derivative against CO2 corrosion,” *Corros. Sci.*, vol. 53, no. 1, pp. 353–361, Jan. 2011.

[73] M. Heydari and M. Javidi, “Corrosion inhibition and adsorption behaviour of an amido-imidazoline derivative on API 5L X52 steel in CO2-saturated solution and synergistic effect of iodide ions,” *Corros. Sci.*, vol. 61, pp. 148–155, Aug. 2012.

[74] P. C. C. Okafor, X. Liu, and Y. G. G. Zheng, “Corrosion inhibition of mild steel by ethylamino imidazoline derivative in CO2-saturated solution,” *Corros. Sci.*, vol. 51, no. 4, pp. 761–768, Apr. 2009.

[75] M. P. Desimone, G. Grundmeier, G. Gordillo, and S. N. Simison, “Amphiphilic amido-amine as an effective corrosion inhibitor for mild steel exposed to CO2 saturated solution: Polarization, EIS and PM-IRRAS studies,” *Electrochim. Acta*, vol. 56, no. 8, pp. 2990–2998, Mar. 2011.

[76] M. P. Desimone, G. Gordillo, and S. N. Simison, “The effect of temperature and concentration on the corrosion inhibition mechanism of an amphiphilic amido-amine in CO2 saturated solution,” *Corros. Sci.*, vol. 53, no. 12, pp. 4033–4043, Dec. 2011.

[77] X. Jiang, Y. G. Zheng, and W. Ke, “Effect of flow velocity and entrained sand on inhibition performances of two inhibitors for CO2 corrosion of N80 steel in 3% NaCl solution,” *Corros. Sci.*, vol. 47, no. 11, pp. 2636–2658, Nov. 2005.

[78] N. D. Nam, A. Somers, M. Mathesh, M. Seter, B. Hinton, M. Forsyth, and M. Y. J. Tan, “The behaviour of praseodymium 4-hydroxycinnamate as an inhibitor for carbon dioxide corrosion and oxygen corrosion of steel in NaCl solutions,” *Corros. Sci.*, vol. 80, pp. 128–138, Mar. 2014.

[79] I. Jevremović, M. Singer, S. Nešić, and V. Mišković-Stanković, “Inhibition properties of self-assembled corrosion inhibitor talloil diethylenetriamine imidazoline for mild steel corrosion in chloride solution saturated with carbon dioxide,” *Corros. Sci.*, vol. 77, pp. 265–272, Dec. 2013.

[80] N. D. Nam, Q. V. Bui, M. Mathesh, M. Y. J. Tan, and M. Forsyth, “A study of 4-carboxyphenylboronic acid as a corrosion inhibitor for steel in carbon dioxide containing environments,” *Corros. Sci.*, vol. 76, pp. 257–266, Nov. 2013.

[81] M. W. S. Jawich, G. A. Oweimreen, and S. A. Ali, “Heptadecyl-tailed mono- and bis-imidazolines: A study of the newly synthesized compounds on the inhibition of mild steel corrosion in a carbon dioxide-saturated saline medium,” *Corros. Sci.*, vol. 65, pp. 104–112, Dec. 2012.

[82] D. a. López, S. N. Simison, and S. R. De Sánchez, “Inhibitors performance in CO2 corrosion EIS studies on the interaction between their molecular structure and steel microstructure,” *Corros. Sci.*, vol. 47, pp. 735–755, 2005.

[83] Y. P. Khodyrev, E. S. Batyeva, E. K. Badeeva, E. V. Platova, L. Tiwari, and O. G. Sinyashin, “The inhibition action of ammonium salts of O,O′-dialkyldithiophosphoric acid on carbon dioxide corrosion of mild steel,” *Corros. Sci.*, vol. 53, no. 3, pp. 976–983, Mar. 2011.

[84] M. Vakili Azghandi, A. Davoodi, G. A. Farzi, and A. Kosari, “Water-base acrylic terpolymer as a corrosion inhibitor for SAE1018 in simulated sour petroleum solution in stagnant and hydrodynamic conditions,” *Corros. Sci.*, vol. 64, pp. 44–54, Nov. 2012.

[85] J. Zhao and G. Chen, “The synergistic inhibition effect of oleic-based imidazoline and sodium benzoate on mild steel corrosion in a CO2-saturated brine solution,” *Electrochim. Acta*, vol. 69, pp. 247–255, May 2012.

[86] F. Farelas and a. Ramirez, “Carbon dioxide corrosion inhibition of carbon steels through bis-imidazoline and imidazoline compounds studied by EIS,” *Int. J. Electrochem. Sci.*, vol. 5, pp. 797–814, 2010.

[87] P. Okafor, C. Liu, X. Liu, and Y. Zheng, “Corrosion inhibition and adsorption behavior of imidazoline salt on N80 carbon steel in CO2-saturated solutions and its synergism with thiourea,” *J. Solid State …*, 2010.

[88] D. A. López, S. N. Simison, and S. R. de Sánchez, “The influence of steel microstructure on CO2 corrosion. EIS studies on the inhibition efficiency of benzimidazole,” *Electrochim. Acta*, vol. 48, no. 7, pp. 845–854, Feb. 2003.

[89] X. Liu and Y. Zheng, “Effect of hydrophilic group on inhibition behaviour of imidazoline for CO2 corrosion of N80 in 3% NaCl solution,” *Corros. Eng. Sci. …*, 2008.

[90] I. Jevremović, M. Singer, M. Achour, D. Blumer, T. Baugh, V. Mišković-Stanković, and S. Nešić, “A Novel Method to Mitigate the Top-of-the-Line Corrosion in Wet Gas Pipelines by Corrosion Inhibitor within a Foam Matrix,” *Corrosion*, vol. 69, no. 2, pp. 186–192, Feb. 2013.

[91] D. Ortega-Sotelo, “CO2 corrosion inhibition of X-70 pipeline steel by carboxyamido imidazoline,” J Solid State Electrochem (2011) 15:1997–2004.

[92] X. Zhang, F. Wang, Y. He, and Y. Du, “Study of the inhibition mechanism of imidazoline amide on CO2 corrosion of Armco iron,” *Corros. Sci.*, vol. 43, no. 8, pp. 1417–1431, Aug. 2001.

[93] H. El-Lateef, “Corrosion inhibition of low carbon steel in CO2-saturated solution using Anionic surfactant,” Adv. Appl. Sci. Res., 2012, 3(2):1185-1201.

[94] F. Liu, M. Du, J. Zhang, and M. Qiu, “Electrochemical behavior of Q235 steel in saltwater saturated with carbon dioxide based on new imidazoline derivative inhibitor,” *Corros. Sci.*, Vol. 51 pp. 102 - 109 (2009).

[95] N. Negm, M. Yousef, and S. Tawfik, “Impact of Synthesized and Natural Compounds in Corrosion Inhibition of Carbon Steel and Aluminium in Acidic Media,” *Recent Patents Corros. Sci.*, vol. 3, pp. 58–68, 2013.

[96] I. Obot, N. Obi-Egbedi, and S. Umoren, “Antifungal drugs as corrosion inhibitors for aluminium in 0.1 M HCl,” *Corros. Sci.*, 2009.

[97] S. Umoren, O. Ogbobe, I. Igwe, and E. Ebenso, “Inhibition of mild steel corrosion in acidic medium using synthetic and naturally occurring polymers and synergistic halide additives,” *Corros. Sci.*, 2008.

[98] S. A. Umoren, I. B. Obot, A. Madhankumar, and Z. M. Gasem, “Performance evaluation of pectin as ecofriendly corrosion inhibitor for X60 pipeline steel in acid medium: Experimental and theoretical approaches,” *Carbohydr. Polym.*, vol. 124, pp. 280–291, Jun. 2015.

[99] I. Obot and A. Madhankumar, “Surface protection of mild steel using benzimidazole derivatives: experimental and theoretical approach,” *J. Adhes. …*, 2015.

[100] R. Bartzatt, M. Bartlett, and N. Handler, “Detection and Quantitative Analysis for 2-Thiobarbituric Acid Utilizing Uv-Visible Spectrophotometer,” *Am. J. Pharmacol. Sci.*, vol. 1, no. 1, pp. 10–14, Jan. 2013.

[101] G. Kardas, “The inhibition effect of 2-thiobarbituric acid on the corrosion performance of mild steel in HCl solutions,” *Mater. Sci.*, 2005.

[102] Y. J. Garcia, A. J. Rodríguez-Malaver, and N. Peñaloza, “Lipid peroxidation measurement by thiobarbituric acid assay in rat cerebellar slices.,” *J. Neurosci. Methods*, vol. 144, no. 1, pp. 127–35, May 2005.

[103] M. Quraishi and K. Ansari, “Corrosion Inhibition and Adsorption Studies of some Barbiturates on Mild Steel/Acid interface,” *Int. J. Electrochem. …*, 2012.

[104] G. Kardas and R. Solmaz, “Electrochemical investigation of barbiturates as green corrosion inhibitors for mild steel protection,” *Corros. Rev.*, 2006.

[105] E. Kusmierek and E. Chrzescijanska, “Tannic acid as corrosion inhibitor for metals and alloys,” *Mater. Corros.*, vol. 66, no. 2, pp. 169–174, Feb. 2015.

[106] İ. Gülçin, Z. Huyut, M. Elmastaş, and H. Y. Aboul-Enein, “Radical scavenging and antioxidant activity of tannic acid,” *Arab. J. Chem.*, vol. 3, no. 1, pp. 43–53, Jan. 2010.

[107] N. S. Khan, A. Ahmad, and S. . Hadi, “Anti-oxidant, pro-oxidant properties of tannic acid and its binding to DNA,” *Chem. Biol. Interact.*, vol. 125, no. 3, pp. 177–189, Mar. 2000.

[108] A. A. Rahim, E. Rocca, J. Steinmetz, M. J. Kassim, R. Adnan, and M. Sani Ibrahim, “Mangrove tannins and their flavanoid monomers as alternative steel corrosion inhibitors in acidic medium,” *Corros. Sci.*, vol. 49, no. 2, pp. 402–417, Feb. 2007.

[109] Z. Rahman, A. S. Zidan, S. R. Khan, I. K. Reddy, and M. A. Khan, “Cholorpheniramine tannate complexes: physicochemical, chemometric, and taste masking evaluation.,” *Int. J. Pharm.*, vol. 436, no. 1–2, pp. 582–92, Oct. 2012.

[110] S. Saha, J. Wang, B. Buckley, Q. Wang, B. Lilly, M. Chernov, and A. Kashina, “Small molecule inhibitors of arginyltransferase regulate arginylation-dependent protein degradation, cell motility, and angiogenesis.,” *Biochem. Pharmacol.*, vol. 83, no. 7, pp. 866–73, Apr. 2012.

[111] D. B. Smith and B. H. Jacobson, “Effect of a blend of comfrey root extract (Symphytum officinale L.) and tannic acid creams in the treatment of osteoarthritis of the knee: randomized, placebo-controlled, double-blind, multiclinical trials.,” *J. Chiropr. Med.*, vol. 10, no. 3, pp. 147–56, Sep. 2011.

[112] S.-C. Chen and K.-T. Chung, “Mutagenicity and antimutagenicity studies of tannic acid and its related compounds,” *Food Chem. Toxicol.*, vol. 38, no. 1, pp. 1–5, Jan. 2000.

[113] S. Maqsood and S. Benjakul, “Preventive effect of tannic acid in combination with modified atmospheric packaging on the quality losses of the refrigerated ground beef,” *Food Control*, vol. 21, no. 9, pp. 1282–1290, Sep. 2010.

[114] S. M. Burkinshaw and N. Kumar, “The mordant dyeing of wool using tannic acid and FeSO4, Part 1: Initial findings,” *Dye. Pigment.*, vol. 80, no. 1, pp. 53–60, Jan. 2009.

[115] P. S. Vankar, R. Shanker, and A. Verma, “Enzymatic natural dyeing of cotton and silk fabrics without metal mordants,” *J. Clean. Prod.*, vol. 15, no. 15, pp. 1441–1450, Oct. 2007.

[116] J. Iglesias, E. De Saldaña, and J. Jaén, “On the tannic acid interaction with metallic iron,” *Hyperfine Interact.*, 2001.

[117] H. Winkelmann and E. Badisch, “Corrosion behaviour of tool steels in tannic acids,” *... Corros.*, 2009.

[118] V. Pugsley, G. Korn, and S. Luyckx, “The influence of a corrosive wood-cutting environment on the mechanical properties of hardmetal tools,” *Int. J. ...*, 2001.

[119] P. Hazlewood, P. Singh, and J. Hsieh, “Role of wood extractives in black liquor corrosiveness,” *Corrosion*, Vol 62 (2006).

[120] H. MacLean and J. Gardner, “Pulp & Paper Mag,” *Can*, 1953.

[121] S. Kannan and R. Kelly, “The role of dihydroxybenzenes and oxygen on the corrosion of steel in black liquor,” *Corros. Sci.*, 1996.

[122] P. Singh and A. Anaya, “Effect of wood species on corrosion behavior of carbon steel and stainless steels in black liquors,” *Corros. Sci.*, 2007.

[123] S. Zelinka and D. Stone, “The effect of tannins and pH on the corrosion of steel in wood extracts,” *Mater. Corros.*, 2011.

[124] G. Matamala, W. Smeltzer, and G. Droguett, “Comparison of steel anticorrosive protection formulated with natural tannins extracted from acacia and from pine bark,” *Corros. Sci.*, 2000.

[125] E. Oguzie, “Evaluation of the inhibitive effect of some plant extracts on the acid corrosion of mild steel,” *Corros. Sci.*, 2008.

[126] I. Radojčić, K. Berković, S. Kovač, and J. Vorkapić-Furač, “Natural honey and black radish juice as tin corrosion inhibitors,” *Corros. Sci.*, 2008.

[127] M. Stern and A. Geary, “Electrochemical polarization I. A theoretical analysis of the shape of polarization curves,” *J. Electrochem. Soc.*, 1957.

[128] R. Skold and T. Larson, “Measurement of the instantaneous corrosion rate by means of polarization data,” *Corrosion*, 1957.

[129] S. Wu, Z. Cui, G. Zhao, and M. Yan, “EIS study of the surface film on the surface of carbon steel from supercritical carbon dioxide corrosion,” *Appl. Surf. …*, 2004.

[130] M. A. J. Mazumder, H. A. Al-Muallem, and S. A. Ali, “The effects of N-pendants and electron-rich amidine motifs in 2-(p-alkoxyphenyl)-2-imidazolines on mild steel corrosion in CO2-saturated 0.5M NaCl,” *Corros. Sci.*, vol. 90, pp. 54–68, Jan. 2015.

[131] M. A. J. Mazumder, H. A. Al-Muallem, M. Faiz, and S. A. Ali, “Design and synthesis of a novel class of inhibitors for mild steel corrosion in acidic and carbon dioxide-saturated saline media,” *Corros. Sci.*, vol. 87, pp. 187–198, Oct. 2014.

[132] M. Mahdavian and S. Ashhari, “Corrosion inhibition performance of 2-mercaptobenzimidazole and 2-mercaptobenzoxazole compounds for protection of mild steel in hydrochloric acid solution,” *Electrochim. Acta*, vol. 55, no. 5, pp. 1720–1724, Feb. 2010.

[133] J. Wang, “Inhibition mechanism and desorption behavior of organic inhibitor,” Ph.D. Dissertation, Institute of Corrosion and Protection of Metals, Chinese Academy of Sciences, 1990.

[134] V. V. Torres, V. A. Rayol, M. Magalhães, G. M. Viana, L. C. S. Aguiar, S. P. Machado, H. Orofino, and E. D’Elia, “Study of thioureas derivatives synthesized from a green route as corrosion inhibitors for mild steel in HCl solution,” *Corros. Sci.*, vol. 79, pp. 108–118, Feb. 2014.

[135] J. Bockris, D. Drazic, and A. Despic, “The electrode kinetics of the deposition and dissolution of iron,” *Electrochim. Acta*, 1961.

[136] S. Nesic, J. Postlethwaite, and S. Olsen, “An electrochemical model for prediction of corrosion of mild steel in aqueous carbon dioxide solutions,” *Corrosion*, 1996.

[137] F. Bentiss, M. Traisnel, and M. Lagrenee, “The substituted 1 , 3 , 4-oxadiazoles : a new class of corrosion inhibitors of mild steel in acidic media,” *Corros. Sci.*, vol. 42, pp. 127–146, 2000.

[138] D. Singh and R. Chaudhary, “Inhibitive efficiency of some substituted thioureas for the corrosion of aluminium in nitric acid,” *Br. Corros. ...*, 1979.

[139] F. Bentiss, M. Lebrini, and M. Lagrenée, “Thermodynamic characterization of metal dissolution and inhibitor adsorption processes in mild steel/2,5-bis(n-thienyl)-1,3,4-thiadiazoles/hydrochloric acid system,” *Corros. Sci.*, vol. 47, no. 12, pp. 2915–2931, Dec. 2005.

[140] O. R. Jr and R. Hurd, “Temperature coefficient of corrosion inhibition,” *Corrosion*, 1967.

[141] A. Popova, “Temperature effect on mild steel corrosion in acid media in presence of azoles,” *Corros. Sci.*, 2007.

[142] E. Ivanov, “Inhibitors for metal corrosion in acid media,” *Metall. Moscow*, 1986.

[143] P. Li, T. Tan, and J. Lee, “Impedance spectra of the anodic dissolution of mild steel in sulfuric acid,” *Corros. Sci.*, 1996.

[144] O. R. Jr and C. Nathan, “Corrosion inhibitors,” *NACE, Houston, Texas*, 1973.

[145] S. K. Shukla, A. K. Singh, and M. a Quraishi, “Corrosion Inhibition and Adsorption Properties of N-Phenylhydrazine-1 , 2-Dicarbothioamide on Mild Steel in Hydrochloric Acid,” *Int. J. Electrochem. Sci.*, vol. 6, pp. 5779–5791, 2011.

[146] M. Schorr and J. Yahalom, “The significance of the energy of activation for the dissolution reaction of metal in acids,” *Corros. Sci.*, 1972.

[147] S. Umoren, M. Solomon, I. Udosoro, and A. Udoh, “Synergistic and antagonistic effects between halide ions and carboxymethyl cellulose for the corrosion inhibition of mild steel in sulphuric acid solution,” *Cellulose*, 2010.

[148] M. Khedr and A. Lashien, “The role of metal cations in the corrosion and corrosion inhibition of aluminium in aqueous solutions,” *Corros. Sci.*, 1992.

[149] W. Durnie, R. De Marco, B. Kinsella, a. Jefferson, and B. Pejcic, “Predicting the Adsorption Properties of Carbon Dioxide Corrosion Inhibitors Using a Structure-Activity Relationship,” *J. Electrochem. Soc.*, vol. 152, no. 1, p. B1, 2005.

[150] S. Ali, A. El-Shareef, R. Al-Ghamdi, and M. Saeed, “The isoxazolidines: the effects of steric factor and hydrophobic chain length on the corrosion inhibition of mild steel in acidic medium,” *Corros. Sci.*, 2005.

[151] L. Tang, G. Mu, and G. Liu, “The effect of neutral red on the corrosion inhibition of cold rolled steel in 1.0 M hydrochloric acid,” *Corros. Sci.*, 2003.

[152] E. a. Noor and A. H. Al-Moubaraki, “Corrosion behavior of mild steel in hydrochloric acid solutions,” *Int. J. Electrochem. Sci.*, vol. 3, pp. 806–818, 2008.

[153] I. Singh, “Inhibition of steel corrosion by thiourea derivatives,” *Corrosion*, Vol 49, Issue 6 1993.

VITAE

BACKGROUND

- DATE OF BIRTH: 09 DECEMBER, 1986
- PLACE OF BIRTH: BUNZA
- MARITAL STATUS: MARRIED
- STATE OF ORIGIN: SOKOTO
- NATIONALITY: NIGERIAN
- RELIGION: ISLAM

EDUCATION

- Masters in Materials Science and Engineering August 2014-May 2016

King Fahad University of Petroleum and Minerals

- Applied Chemistry, Bachelor of Science January 2007-May 2011

  Usmanu Danfodiyo University Sokoto, Nigeria

EXPERIENCE

- Chemistry Teacher May 2011-November 2013

  (Government Secondary School Bunza)

- Graduate Assistant November 2013-August 2014

Pure and Applied Chemistry Department,

Kebbi State University of Science and

Technology Aliero, Nigeria.

AWARDS AND SCHOLARSHIPS

- King Fahd University of Petroleum and Minerals Full Packaged Masters Scholarship Awarded by the Ministry of Higher Education of Saudi Arabia August 2013.
- Kebbi State University of Science and Technology Masters Fellowship Award, July 2013
- Federal Government of Nigeria Award for Undergraduate Studies 2009
- Sokoto State Scholarship Award for Undergraduate Studies 2008